Smart structures based on piezoceramics 5

Irschik, H.[1]; Krommer, M.[1]; Nader, M.[2]; Schöftner, J.[1]; Zehetner, Ch.[2]; Vetyukov, Yu.[2] 5

[1]Institute for Technical Mechanics, Johannes Kepler University Linz, Linz, Austria
[2]Linz Center of Mechatronics GmbH, Linz, Austria

1. Accurate Electromechanically Coupled Modeling of Smart Structures 5
2. Dynamic Shape Control and Displacement Tracking by Piezoelectric Actuation and Sensing 5
3. Piezoelectric Sensor Networks for Measuring Structural Behavior and Damage 6
4. Acknowledgement 7

Future perspectives for multi-material-systems 11

Schneebauer, M.; Würtele, M. 11

KraussMaffei Technologies GmbH, Munich, Germany

Fabrication and characterization of a form- and force-locked piezo-metal sensor module 23

Neugebauer, R.[1,3]; Schubert, A.[1,3]; Richter, F.[2]; Koriath, H.-J.[3]; Peter, S.[2]; Berg, S.[2]; Jahn, S. F.[1]; Müller, B.[1]; Müller, M.[1] 23

[1]Institute for Machine Tools and Production Processes, Chemnitz University of Technology, Chemnitz, Germany
[2]Institute of Physics, Chemnitz University of Technology, Chemnitz, Germany
[3]Fraunhofer Institute for Machine Tools and Forming Technology, Chemnitz, Germany

1. Introduction 23
2. Fabrication of the piezo-metal sensor module 24
   - *2.1 Design 24*
   - *2.2 Aluminium Sheet Carrier 24*
   - *2.3 Insulation of the Aluminium Sheet 25*
   - *2.4 Piezoceramic Rods width Center Electrodes 25*
   - *2.5 Assembly of the Piezo-Metal Module 25*
3. Characterization of the piezo-metal sensor module 26
4. Conclusion 27
5. Acknowledgement 28

CNT-filled PP compound for in-situ bonding and connection of piezoelectric ceramics by using multi-component micro injection molding 29

Heinrich, M.; Kroll, L.; Walther, M.; Elsner, H. 29

Chemnitz University of Technology, Department of Lightweight Structures and Polymer Technology, Chemnitz, Germany

1. Introduction 29
2. Experimental part 31
   - *2.1 Materials 31*
   - *2.2 Compounding 31*
   - *2.3 Tensile test 31*
3. Results 31
   - *3.1 Mass temperature 31*
   - *3.2 Injection speed 32*
4. Discussion 32
5. Conclusion 33
6. Acknowledgement 33

Multifunctional components in vehicle space frames - Cast parts for prototypes and small series 35

Kretz, R.; Khalil, Z.; Simon, P. 35

AIT Austrian Institute of Technology, Light Metals Technologies Ranshofen, Ranshofen, Austria

1. Introduction and history 35
2. Aluminium frames 36
3. LKR prototype frames 36
4. Design and prototyping process selection 37
5. Summary and outlook 40
6. Acknowledgement 40

Energy harvesting by means of integrated piezoelectrics 41

Juuti, J.; Sobocinski, M.; Palosaari, J.; Leinonen, M.; Jantunen, H. 41

University of Oulu, Microelectronics and Materials Physics Lab, Oulu, Finland

1. Introduction 41
2. Experimental 41
3. Results and discussions 42
4. Summary 43
5. Acknowledgement 44

Integration of piezoceramic sensors and actuators into structural components via high pressure die casting 45

Klassen, A.[1]; Rübner, M.[1]; Ilg, J.[2]; Rupitsch, S. J.[2]; Lerch, R.[2]; Körner, C.[1]; Singer, R. F.[1] 45

[1]Friedrich-Alexander Universität Erlangen-Nürnberg, Chair of Metals Science and Technology, Erlangen, Germany
[2]Friedrich-Alexander Universität Erlangen-Nürnberg, Chair of Sensor Technology, Erlangen, Germany

1. Introduction 45
2. Experimental procedures 46
   - *2.1 Fabrication 46*
   - *2.2 Characterization 46*
   - *2.3 Simulation of the infiltration process 47*
3. Results and discussion 47
4. Conclusions 50
5. Acknowledgement 50

Piezo-metal-composites in structural parts: Technological design, process simulation and material modelling 51

Neugebauer, R.[1]; Ihlemann, J.[2]; Lachmann, L.[1]; Drossel, W.-G.[1]; Hensel, S.[1]; Nestler, M.[1]; Landgraf, R. [2]; Rudolph, M. [2] 51

[1]Fraunhofer Institute for Machine Tools and Forming Technology IWU, Chemnitz, Germany
[2]Chemnitz University of Technology, Chair of Solid Mechanics, Chemnitz, Germany

1. Introduction 51
2. Experimental Research 51
   - *2.1 Forming of Piezo-Metal-Composites 51*
   - *2.2 Selection of Adhesive 52*
3. Numerical Investigation 53
   - *3.1 Forming Simulations 53*
   - *3.2 Phenomenological material model for the adhesive including curing 54*
4. Summary and Outlook 56
5. Acknowledgement 56

Fiber reinforced polymers in automotive applications – History - state-of-the-art - future trends 57

Deinzer, G. H.; Haverkamp, C. 57

Audi AG Neckarsulm, Neckarsulm, Germany

1. Introduction 57
2. History and state-of-the-art in the sue of CFRP 57
3. Light Weight Potential of CFRP 58
4. Commercial Issues 58
5. Conclusion 58

Process development for high volume manufacture of thermoplastic composites with integrated piezoceramic modules 59

Gude, M.[1]; Hufenbach, W.[1]; Modler, N.[1]; Schmidt, M.[2,3]; Geiger, M.[2]; Heber, T.[1]; Winkler, A.[1]; Pfeiffer, C.[2]; Albert, F.[2]; Roth, S.[2] 59

[1]Technische Universität Dresden, Institute of Lightweight Engineering and Polymer Technology (ILK), Dresden, Germany
[2]Bayerisches Laserzentrum GmbH, Erlangen, Germany
[3]Friedrich-Alexander-Universität Erlangen-Nürnberg, Chair of Photonic Technologies, Erlangen,Germany

1. Introduction 59
2. Process chain 59
3. Manufacture of thermoplastic-compatible piezoceramic modules 60
4. Laser contacting of the piezoceramic modules 61
5. Composite manufacture and integration process 62
6. Conclusions 63
7. Acknowledgement 63

Integration of piezoceramic and electronic functional elements in glass fibre-reinforced polyurethane composite structures 65

Hufenbach, W.[1]; Fischer, W.-J.[2]; Michaelis, A.[3,4]; Gebhardt, S.[4]; Geller, S.[1]; Tyczynski, T.[1]; Heinig, A.[2]; Weder, A.[2]; Hohlfeld, K.[3] 65

[1]Technische Universität Dresden, Institute of Lightweight Engineering and Polymer Technology (ILK), Dresden, Germany
[2]Technische Universität Dresden, Institute of Semiconductors and Microsystems (IHM), Dresden, Germany
[3]Technische Universität Dresden, Institute of Material Science, Dresden, Germany
[4]Fraunhofer Institute for Ceramic Technologies and Systems IKTS, Dresden, Germany

1. Introduction 65
2. Process development of the Multi-Fibre-Injection technology 66
3. Development and fabrication of piezoceramic components 66
4. Processing studies on embedded piezoceramic and electronic functional elements 67
5. Conclusions 69
6. Acknowledgements 69

Methods for reliable modeling of piezoceramic materials 71

Rupitsch, S. J.[1]; Nicolai, M.[2]; Wolf, F.[1]; Ilg, J.[1]; Schönecker, A.[2]; Lerch, R.[1] 71

[1]Friedrich-Alexander Universität Erlangen-Nürnberg, Chair of Sensor Technology, Erlangen, Germany
[2]Fraunhofer Institute for Ceramic Technologies and Systems IKTS, Dresden, Germany

1. Introduction 71
2. Small Signal Behavior 72
3. Large Signal Behavior 73
   - *3.1 Phenomenological approach 73*
   - *3.2 Viscoplastic approach 74*
4. Conclusion 76
5. Acknowledgement 76

Pyroelectric response as a sensitive tool for the characterization of piezoelectrics 77

Movchikova, A. A.[1]; Malyshkina, O. V.[1]; Suchaneck, G.[2], Gerlach, G.[2]; Steinhausen, R.[3]; Langhammer, H. T.[3]; Beige, H.[3] 77

[1]Tver State University, Dep. of Ferroelectric and Piezoelectric Physics, Tver, Russia
[2]Technische Universität Dresden, Solid State Electronics Lab, Dresden, Germany
[3]Martin-Luther-Univ. Halle-Wittenberg, Department of Physics, Halle, Germany

1. Introduction 77
2. Direct and inverse methods 77
3. Investigation of piezoelectric materials by TSWM 77
4. Conclusions 78

Pulsed magnetron sputtered AlN thin films - a lead-free material for piezoelectric applications 81

Glöß, D.[1]; Bartzsch, H.[1]; Gittner, M.[1]; Barth, S.[1]; Frach, P.[1]; Herzog, T.[2]; Walter, S.[2]; Heuer, H.[2] 81

[1]Fraunhofer Institute for Electron Beam and Plasma Technology (FEP), Dresden, Germany
[2]Fraunhofer Institute for Non-Destructive Testing (IZFP, Dresden branch), Dresden, Germany

1. Introduction 81
2. Experimental 81
3. Structural, electrical and mechanical properties 82
4. Characterization of piezoelectric properties 83
   4.1 Pulse Echo Mode 84
   4.2 Berlincourt-Meter 84
5. Investigation of suitability for energy harvesting 85
6. Conclusions 85
7. Acknowledgment 85

Evaluation of the polarization state of integrated piezoelectrics using thermal waves 87

Suchaneck, G.; Hu, W.; Gerlach, G. 87

Technische Universität Dresden, Solid-State Electronics Lab, Dresden, Germany

1. Introduction 87
2. Theory 87
3. Experimental 88
4. Results and discussion 88
5. Conclusions 89

Novel approaches for the determination of the process specific polarization of piezoceramic modules embedded in thermoplastic composites.....91

Brückner, B. W.[1]; Gerlach, G.[2]; Winkler, A.[3]; Hu, W.[2]; Hufenbach, W. A.[3]; Michaelis, A.[1]; Modler, N.[3]; Schönecker, A. J.[1]; Suchaneck, G.[2] 91

[1]Fraunhofer Institute for Ceramic Technologies and Systems IKTS, Dresden, Germany
[2]Technische Universität Dresden, Institute of Solid-State Electronics Lab (IFE), Dresden, Germany
[3]Technische Universität Dresden, Institute of Lightweight Engineering and Polymer Technologies (ILK), Dresden, Germany

1. Motivation 91
2. State of the Art 91
3. Measurement Setup 92
4. Measurement System Analysis 93
5. Measurement - Hot Pressing Process 94
6. Thermal Wave Methods 95
7. Conclusion 95
8. Acknowledgement 95

Smart structures based on piezoceramics

Irschik, H.[1]; Krommer, M.[1]; Nader, M.[2]; Schöftner, J.[1]; Zehetner, Ch.[2]; Vetyukov, Yu.[2]

[1]*Institute for Technical Mechanics, Johannes Kepler University Linz, Linz, Austria*
[2]*Linz Center of Mechatronics GmbH, Linz, Austria*

Abstract

Structures equipped with firmly attached piezoceramic actuators and sensors, which are connected by an automatic control system, represent most prominent members of the class of so-called smart structures. Various physical effects similar to piezoelectricity are under discussion also for actuation and sensing, but piezoceramic devices are on the leading edge, from both, their versatility and applicability. These devices represent an important current topic of interest in Mechatronics, since electrical and mechanical fields are involved in an interdisciplinary manner, and since the efficiency of piezoceramic materials has increased dramatically in the last years.

The present paper gives a review on the research on smart structures based on piezoceramics, which has been performed at the Institute of Technical Mechanics of the Johannes Kepler University Linz, Austria, during the last twenty years. Particularly, own contributions in the following fields are reviewed subsequently: Accurate electromechanically coupled structural modeling; dynamic shape control by piezoelectric actuation and sensing; sensor networks for measuring structural behaviour and damage. The present paper represents a condensed version of the reviews [1] and [2], however including more recent works also.

1. Accurate Electromechanically Coupled Modeling of Smart Structures

From the point of computational efficiency, complicating effects in smart multi-layered structures, like the direct piezoelectric effect, or the pyroelectric effect, should be taken into account in a sufficiently accurate manner, but without the need of solving the partial differential equations of electrostatics directly. Having this goal in mind, the influence of the direct piezoelectric effect on free transverse vibrations of smart beams was treated by Krommer and Irschik [3]. A Reissner-Mindlin-type plate theory including the direct piezoelectric and the pyroelectric effect was presented in [4]. An electromechanically coupled plate theory taking into account the influence of shear, rotatory inertia and electric field is due to Krommer in [5]. Non-local constitutive relations were studied by Krommer in Refs. [6-10]. These formulations for an accurate modeling were taken as a basis in many of the subsequently cited works. For a recent contribution, see Vetyukov et al. [11].

2. Dynamic Shape Control and Displacement Tracking by Piezoelectric Actuation and Sensing

The piezoelectric actuation effect (the converse piezoelectric effect) can be used to control the shape of composite structures, i.e. their displacements. This is denoted as shape control. For a state-of-the-art review on static and dynamic shape control of structures by piezoelectric actuation, see [12]. In order to control more complex displacement fields, a spatially varying piezoelectric actuation is needed. The first suggestion of shaping piezoelectric actuators in order to suppress displacements of beams that vibrate in a certain natural mode was due to Lee and Moon [13]. Motivated by this contribution, our group has systematically treated dynamic shape control of forced vibrations of smart elastic beams by spatially shaped, properly distributed piezoelectric actuators, see Refs. [14-21]. In short, we have introduced the following novel solution: Assume that the beam motion starts from rest and is produced by an imposed system of forces, which is separable in space and time, with a given spatial distribution and a given time-evolution. Then it is sufficient to spatially shape the piezoelectric actuation according to the distribution of quasi-static bending moments and normal forces due to the imposed spatial force distribution. Assigning this spatially distributed piezoelectric actuation with the negative of the time-evolution of the forces, no displacements

are produced in total by the forces and the piezoelectric actuation. In the course of the latter studies, our group was also the first to identify inappropriate or so-called nilpotent piezoelectric actuator shapes, which do not produce any deformation in the structure under consideration, and which thus can be superimposed without changing the displacements. Our group also has studied more complex effects in Refs. [14]-[21], such as shear-actuation, the question of sensor distributions that are collocated to the actuator shapes, self-sensing actuators, and, last but not least, superimposed rigid-body motions. Shape control of force induced vibrations of thin circular plates were treated by Nader et al. in [22]. For the case that the time-evolution of the force loading is unknown, an automatic feedback-control was implemented involving piezoelectric sensing, Gattringer and Nader [23]. A fundamental part of our studies was concerned with dynamic shape control in the framework of the three-dimensional linear theory of elasticity in the presence of eigenstrains, such as produced by the electric field in piezoelectric bodies, or by a temperature change in thermoelastic bodies. These theoretical studies extended previous 3D static results derived by Irschik and Ziegler in [24], see also Nyashin et al. [25]. A first dynamic study involving convolution integral formulations and thermal expansion was presented by Irschik and Pichler in [26], while a solution involving general types of eigenstrains was presented in [27], where an extended Neumann formulation was utilized. The results presented in [27] were as follows: Assume the body to be loaded by transient forces, the motion starting from rest. Assume that the forces are separable in space and time. Compute the quasi-static stress tensor due to the spatial force distribution, and shape the eigenstrain actuation accordingly throughout the body. Apply the negative time-evolution of the forces to the eigenstrain actuation. Then, the total displacements vanish everywhere at all times. In Refs. [26] and [27], inappropriate eigenstrain distributions, which do not produce displacements, were identified as stress distributions due to any imposed eigenstrain acting upon the structure under consideration. Krommer and V.V. Varadan established a new branch of shape control, namely to suppress displacements in sub-domains of force-loaded structures by piezoelectric actuation, Refs. [28]-[32]. In a next step, our group introduced the novel problem of producing desired displacement fields by piezoelectric actuation, be there imposed force loadings present or not. We have termed this problem as displacement tracking problem, since we could not find an adequate notion in the literature for it. A first fundamental 3-D study was presented in Ref. [33], where we considered also visco-elastic constitutive relations involving the general Boltzmann convolution formulation. Various structural applications of increasing complexity were treated in Refs. [34]-[40]. As studies concerning structures of rather complex geometrical shapes, we mention the work of our group on vibration suppression in the shell-type funnels of magnetic resonance tomographs (MRT), see Refs. [41]-[43]. Various automatic control strategies were implemented and experimentally tested in these studies as well, see [43]. The necessity of using plate theory in wide beam-type structures has been demonstrated by Huber et al. in [44] and [45]. Piezoelectric shape control in the presence of torsional motions was treated in a series of papers by Zehetner et al., [46]-[51]. Recently, methods for passive damping and exact annihilation of beam vibrations using shaped piezoelectric layers and tuned inductive networks have been developed by Schöftner and Irschik [52]-[55].

3. Piezoelectric Sensor Networks for Measuring Structural Behavior and Damage

Assume that a flat patch made of piezoelectric material is deformed through an external action, such as imposed forces, temperature changes or imposed displacements. When the patch is electroded on both sides, it is possible to detect an electric voltage or charge, respectively, at the electrodes, due to the direct piezoelectric effect. Now, when such a patch is firmly bonded to a surface of a primary structure, or when it is firmly integrated within a primary structure, then the patch intends to follow the deformation of this structure, and the deformation induced in the patch can be used for sensing purposes. Our group has particularly followed the idea of finding spatially shaped distributed sensors for measuring structural entities, such as displacements and slopes, see e.g. [14], [15], [17], [19], [34] for various structural applications. A general method for computing properly distributed continuous sensors was presented Krommer and Irschik in [37], see also [2]. In short, it was shown that strain type sensors measure the virial of a set of auxiliary static forces with respect to the actual transient displacements, when the sensors are spatially

shaped according to the static stresses produced by the auxiliary forces. From this, distributed sensors that measure transient structural entities, such as displacements or slopes, can be developed in a straightforward manner. Nilpotent sensors, which cannot measure any output, can also be easily derived. Krommer, Zellhofer and Heilbrunner [56] studied sensor networks for structural monitoring of beam-type structures using integral equation methods. An optimization technique was presented for accurately replacing continuous sensors by sparse sensor networks made of piezoceramic patches. Recently, Krommer and Vetyukov [57] studied piezoelectric sensing of kinematically meaningful entities, such as displacements and slopes, in the vicinity of a time-dependent geometrically nonlinear pre-deformed state. Optimal continuous strain-type sensors for finite deformations of shell structures were presented by Vetyukov and Krommer in [58].

4. Acknowledgement

Support of the authors in the framework of the Kplus "Linz Center of Competence in Mechatronics (LCM)" and the K2 "Austrian Center of Competence in Mechatronics (ACCM)" is gratefully acknowledged. We also appreciate the support by the Austrian Science Fund FWF (Project P11993-TEC: "Mechanics of Smart Structures" and Translational Project L441-N14 "Sensor Systems for Structural and Health Monitoring"). Moreover, we thank our co-authors Dr. Uwe Pichler and Dr. Daniel Huber, and we appreciate the work of our master and doctoral students Matthias Hörl and Markus Zellhofer. We are very grateful to our industrial partners, Prof. H. Meixner, Dr. G. Lugert, Dr. H.-G. v. Garßen and Dr. Randolf Mock from Siemens Corporate Technology, Munich, for stimulating cooperation in this field.

Literature

[1] *H. Irschik, M. Krommer, M. Nader, Ch. Zehetner: "Mechatronics – The Innovation Request", Advances in Science and Technology, Vol. 56 (2008), p. 1.*

[2] *H. Irschik, M. Krommer, Yu. Vetyukov: "On the Use of Piezoelectric Sensors in Structural Mechanics: Some novel strategies", Sensors, Vol. 10(6) (2010), p. 5626.*

[3] *M. Krommer, H. Irschik: "On the Influence of the Electric Field on Free Transverse Vibrations of Smart Beams", Smart Materials and Structures, Vol. 8 (1999), p. 401.*

[4] *M. Krommer, H. Irschik: "A Reissner-Mindlin-Type Plate Theory Including the Direct Piezoelectric and the Pyroelectric Effect", Acta Mechanica, Vol. 141 (2000), p. 51.*

[5] *M. Krommer: "An Electromechanically Coupled Plate Theory Taking into Account the Influence of Shear, Rotatory Inertia and Electric Field", Mech. Res. Comm., Vol. 27 (2000), p. 197.*

[6] *M. Krommer: "On the correction of the Bernoulli-Euler beam theory for smart piezoelectric beams", Smart Materials and Structures, Vol. 10 (2001), p. 668.*

[7] *M. Krommer, H. Irschik: "An electro-mechanically coupled theory for piezoelastic beams taking into account the charge equation of electrostatics", Acta Mechanica, Vol. 154 (2002), p. 141.*

[8] *M. Krommer: "Piezoelastic Vibrations of Composite Reissner - Mindlin - type Plates", Journal of Sound and Vibration, Vol. 263 (2003), p. 871.*

[9] *M. Krommer: "The Significance of Non-Local Constitutive Relations for Composite Thin Plates Including Piezoelastic Layers with Prescribed Charge", Smart Mat. Struct., Vol. 12 (2003), p. 318.*

[10] *M. Krommer: "On the influence of pyroelectricity upon thermally induced vibrations of piezothermoelastic plates", Acta Mechanica, Vol. 171 (2004), p. 59.*

[11] *Yu. Vetyukov, A. Kuzin, M. Krommer: "Asymptotic splitting in the three-dimensional problem of elasticity for non-homogeneous piezoelectric plates", International Journal of Solids and Structures, Vol. 48 (2011), p. 12.*

[12] *H. Irschik: "A review on static and dynamic shape control of structures by piezoelectric actuation", Engineering Structures, Vol. 24 (2002), p. 5.*

[13] *C.-K. Lee, F.C. Moon: "Modal sensors/ actuators", J. Applied Mech., Vol. 57 (1990), p. 434.*

[14] *H. Irschik, M. Krommer, A.K. Belyaev, K. Schlacher: "Shaping of Piezoelectric Sensors/Actuators for Vibrations of Slender Beams: Coupled Theory and Inappropriate Shape Functions", Journal of Intelligent Materials Systems and Structures, Vol. 9 (1998), p. 546.*

[15] *H. Irschik, M. Krommer, U. Pichler: "Shaping Distributed Piezoelectric Self-Sensing Layers for Static Shape Control of Smart Structures", Journal of Structural Control, Vol.7 (2000) p. 173.*

[16] *M. Krommer, H. Irschik: "Shape Control of Timoshenko Beams by Shear-Based Piezoelectric Actuation", In: CD-ROM Proc. ASME Design Eng. Tech. Conf./Biennial Conference on Mechanical Vibration and Noise (Am. Soc. Mech. Eng., New York 2001).*

[17] *H. Irschik, M. Krommer, U. Pichler: "Collocative Control of Beam Vibrations with Piezoelectric Self-Sensing Layers", In: Proceedings of IUTAM Symposium on Smart Structures and Structronic Systems (U. Gabbert and H.S. Tzou, eds., Kluwer, Dordrecht, 2001, p. 315.)*

[18] *U. Pichler, H., Irschik, M. Krommer: "Dynamic shape control of flexural beam vibrations: an experimental setup", In: Proceedings of SPIE, Modeling, Signal Processing, and Control for Smart Structures (SPIE Vol. 4326, 2001, p. 408).*

[19] *H. Irschik, M. Krommer, U. Pichler: "Dynamic shape control of beam – type structures by piezoelectric actuation and sensing", International Journal of Applied Electromagnetics and Mechanics, Vol. 17 (2003), p. 251.*

[20] *Ch. Zehetner, H. Irschik: "Displacement compensation of beam vibrations caused by rigid-body motions", Smart Materials and Structures, Vol.14 (2005), p. 862.*

[21] *H. Irschik, M. Nader, Ch. Zehetner: "Exact Cancellation of Vibrations in Elastic Structures Performing Large Rigid Body Motions", In: Proc. 10th Int. Sound and Vibration (IISV, Stockholm, Vol.7, 2003, p. 3487).*

[22] *M. Nader, H. Gattringer, M. Krommer, H. Irschik: "Shape Control of Flexural Vibrations of Circular Plates by Shaped Piezoelectric Actuation", J. Vibration Acoustics, Vol 125, (2003), p. 88.*

[23] *H. Gattringer, M. Nader, M. Krommer, H. Irschik: "Collocative PD control of circular plates with shaped piezoelectric actuators / sensors", J. Vibration and Control, Vol. 9 (2003), p. 965.*

[24] *H. Irschik, F. Ziegler: "Eigenstrain without stress and static shape control of structures", AIAA Journal., Vol. 39 (2001), p. 1985.*

[25] *Y. Nyashin, V. Lokhov, F. Ziegler: "Stress-free displacement control of structures", Acta Mechanica Vol. 175 (2005), p. 45.*

[26] *H. Irschik, U. Pichler: "Dynamic shape control of solids and structures by thermal expansion strains", Journal of Thermal Stresses, Vol. 24 (2001), p. 565.*

[27] *H. Irschik, U. Pichler: "An extension of Neumann's method for shape control of force-induced elastic vibrations by eigenstrains", Int. Journal Solids and Structures, Vol. 41 (2004), p. 871.*

[28] *M. Krommer, V.V. Varadan: "Dynamic shape control of conformal antennas", In: Proc. of SPIE, Modeling, Signal Processing, and Control for Smart Structures (SPIE Vol. 5049, 2003, p. 622).*

[29] *M. Krommer: "Dynamic shape control of sub – regions of linear elastic beams by self – stress actuation", In: Proc. of 2nd MIT Conference on Computational Fluid and Solid Mechanics (K.J. Bathe, ed., Elsevier, Amsterdam, 2003, Vol. 2, p. 2308).*

[30] *M. Krommer: "Shape Control of Sub - Domains of Structures", In: Proc. of the 3rd European Conference on Structural Control, Vienna, Austria 2004 (R. Flesch, H. Irschik and M. Krommer, eds., Vienna, Austria, 2005, Vol. 2, pp. S1-151).*

[31] *M. Krommer, V.V. Varadan: "Control of Bending Vibrations Within Subdomains of Thin Plates – Part I: Theory and Exact Solution", Journal of Applied Mechanics, Vol. 72 (2005), p. 432.*

[32] *M. Krommer, V.V. Varadan: "Control of Bending Vibrations Within Subdomains of Thin plates – Part II: Piezoelectric Actuation and Approximate Solution", J. of Appl. Mech., Vol. 73 (2006), p. 259.*

[33] *H. Irschik, M. Krommer: "Dynamic Displacement Tracking of Force-Loaded Linear Elastic or Viscoelastic Bodies by Eigenstrain-Induced Actuation Stresses", In: in CD-Rom Proc. of ASME-IDETC/CIE 2005 (Am. Soc. Mech. Eng., New York 2005).*

[34] *M. Krommer, H. Irschik, U. Pichler: "Design of Sensors/Actuators for Structural Control of Continuous CMA Systems", In: Proceedings of SPIE, Sensors and Smart Structures Technologies for Civil, Mechanical, and Aerospace Systems (SPIE-Vol. 5765, 2005, p. 130).*

[35] *H. Irschik, M. Nader, Ch. Zehetner: "Tracking of Displacements in Smart Elastic Beams Subjected to Rigid Body Motions", In: CD-Rom Proc. of III European Conf. Comp. Mech., Solids, Struct. and Coupled Problems in Eng. (C.A. Mota Soares, ed., Springer-Verlag, Heidelberg, 2006).*

[36] *H. Irschik, M. Krommer: "Tracking of transient displacements in solids and structures", In: Proceedings 4th World Conference on Structural Control and Monitoring (S. Masri, ed., San Diego, Cal., 2006).*

[37] *M. Krommer, H. Irschik: "Sensor and actuator design for displacement control of continuous systems", Smart Structures and Systems, Vol. 3 (2007), p. 147.*

[38] *M. Krommer, H. Irschik, D. Huber: "Dynamic Displacement Tracking of a Frame Structure by Piezoelectric Patches: Analytical Solution and Comparison to Coupled FE-Computations", In: Computational Methods for Coupled Problems in Science and Engineering II. (Onate, E., Papadrakakis, M., Schrefler, B., eds., CIMNE, 2007, p. 491).*

[39] *M. Krommer, M. Nader, H. Irschik: "Tracking of transient displacements of plates with support excitations", In: Proc. of SPIE, Modeling, Signal Processing, and Control for Smart Structures (SPIE-Vol. 6523, 2007).*

[40] *M. Krommer, H. Irschik, M. Zellhofer: "Design of actuator networks for dynamic displacement tracking of beams", Mechanics of Advanced Materials and Structures 15(3&4), Special Issue - Design, Modelling and Experiments of Adaptive Structures and Smart Systems (2008), p. 235.*

[41] *M. Nader, M. Krommer, H.-G. von Garßen, H. Irschik: "Piezoelectric actuation of thin shells with support excitation", In: Proceedings of SPIE, Modeling, Signal Processing, and Control for Smart Structures (SPIE-Vol. 5049, 2003, p. 180).*

[42] *M. Nader, H.-G. von Garßen, H. Irschik: "Application of Distributed Piezoelectric Patches for Active Noise and Vibration Control", In: CD-Rom Proceedings of III European Conference on Computational Mechanics Solids, Structures and Coupled Problems in Engineering (C.A. Mota Soares et.al., eds., Springer-Verlag, Heidelberg, 2006).*

[43] *M. Nader: "Compensation of Vibrations in Smart Structures: Shape Control, Experimental Realization and Feedback Control", (Doctoral Thesis, Schriften der Johannes Kepler Universität Linz, Reihe C, Vol. 54, Trauner Verlag Universität, Linz, Austria 2008).*

[44] *D. Huber, M. Krommer, H. Irschik: "Dynamic Displacement Tracking for Frame Structures with a Piezoelectric Patch Network based on Plate Theory", Advances in Science and Technology, Vol. 56 (2008), p. 64.*

[45] *D. Huber, M. Krommer, H. Irschik: "Dynamic dicplacement tracking of a one-storey frame structure using patch actuator networks: Analytical plate solution and FE validation", Journal of Smart Structures and Systems, Vol. 5 (6) (2009), p. 613.*

[46] *Ch. Zehetner: "Compensation of torsional vibrations in rods by piezoelectric actuation", Acta Mechanica, Vol. 207 (2009), p. 121.*

[47] *Ch. Zehetner, J. Gerstmayr: "Control of flexible vibrations in a two-link robot by piezoelectric actuation, In: Proceedings MATHMOD 2009 Vienna - Full Papers CD Volume (Vienna, Austria, 11-13 Februray 2009, I. Troch, F. Breitenecker, eds., 2009, p. 988).*

[48] *Ch. Zehetner, M. Krommer: "Control of torsional vibrations by piezoelectric sensors and actuators", In: Proc. of ECCOMAS Thematic Conference on Computational Methods in Structural Dynamics and Earthquake Engineering (M. Papadrakakis, N.D. Lagaros, M. Fragiadakis, eds., COMPDYN 2009, Rhodes, Greece, June 22-24, 2009).*

[49] *Ch. Zehetner, H. Irschik: "Compensation of flexural and torsional vibrations of piezo-laminated beams performing rigid-body motions", In: Proceedings of IV European Conference on Computational Mechanics, ECCM 2010, May 16-21, Paris, France, 2010.*

[50] *Ch. Zehetner, M. Krommer: "Control of torsional vibrations in rods by piezoelectric sensors and actuators", Structural Control and Health Monitoring (2011), DOI: 10.1002/stc.455*

[51] *Ch. Zehetner, M. Zellhofer, M. Krommer: "Piezoelectric torsional sensors and actuators: A computational study", In: ECCOMAS Thematic Conference on Computational Methods in Structural Dynamics and Earthquake Engineering (M. Papadrakakis, N.D. Lagaros, M. Fragiadakis, eds., COMPDYN 2011, Corfu, Greece, May 26-28, 2011).*

[52] *J. Schoeftner, H. Irschik: "Passive damping and exact annihilation of vibrations of beams using shaped piezoelectric layers and tuned inductive networks", Smart Materials and Structures, Vol. 18 (2009), p. 125008-1-9*

[53] *J. Schoeftner, H. Irschik: "Piezoelastic structures interacting with electric networks: vibration canceling and shape control", In: Proc. Fifth World Conference on Structural Control and Monitoring (published on http://wcscm5.com, Tokyo, Japan, 2010).*

[54] *J. Schoeftner, H. Irschik: "A comparative study of smart passive piezoelectric structures interacting with electric networks: Timoshenko beam theory versus finite element plane stress calculations", Smart Mater. Struct., Vol. 20 (2011), p. 025007-1-13.*

[55] *J. Schoeftner, H. Irschik: "Passive shape control of force-induced harmonic lateral vibrations for laminated piezoelastic Bernoulli-Euler beams- theory and practical relevance", Smart Mater. Struct., Vol. 7(5) (2011), p. 417.*

[56] *M. Krommer, M. Zellhofer, K.-H. Heilbrunner: "Strain-type Sensor Networks for Structural Monitoring of Beam-type Structures", Journal of Intelligent Material Systems and Structures, Vol. 20 (2009), p. 1875.*

[57] *M. Krommer, Yu. Vetyukov: "Adaptive sensing of kinematic entities in the vicinity of a time-dependent geometrically nonlinear pre-deformed state", International Journal of Solids and Structures, Vol. 46 (2009), p. 3313.*

[58] *Yu. Vetyukov, M. Krommer: "Optimal continuous strain-type sensors for finite deformations of shell structures", Mechanics of Advanced Materials and Structures, Vol. 18 (2011), p. 125.*

Future perspectives for multi-material-systems

Schneebauer, M.; Würtele, M.

KraussMaffei Technologies GmbH, Munich, Germany

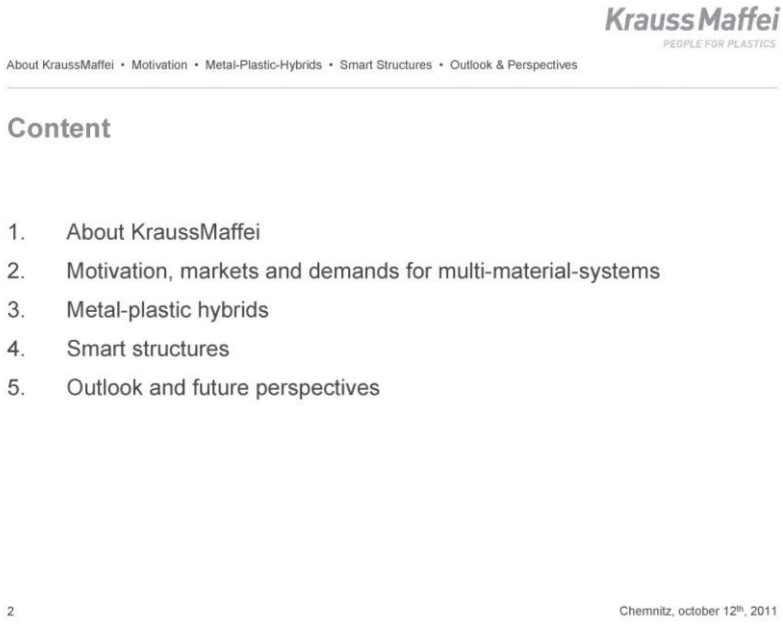

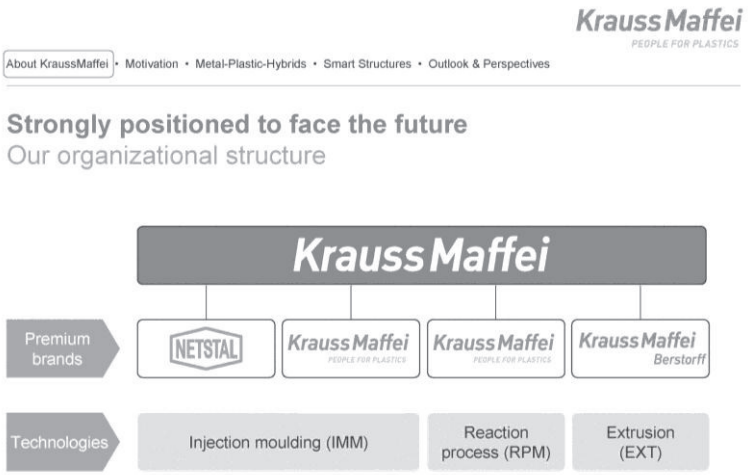
Krauss Maffei
PEOPLE FOR PLASTICS
About KraussMaffei • Motivation • Metal-Plastic-Hybrids • Smart Structures • Outlook & Perspectives
Strongly positioned to face the future
Our organizational structure
Krauss Maffei
Premium brands
NETSTAL
Krauss Maffei
PEOPLE FOR PLASTICS
Krauss Maffei
PEOPLE FOR PLASTICS
Krauss Maffei
Berstorff
Technologies
Injection moulding (IMM)
Reaction process (RPM)
Extrusion (EXT)
3
Chemnitz, october 12th, 2011

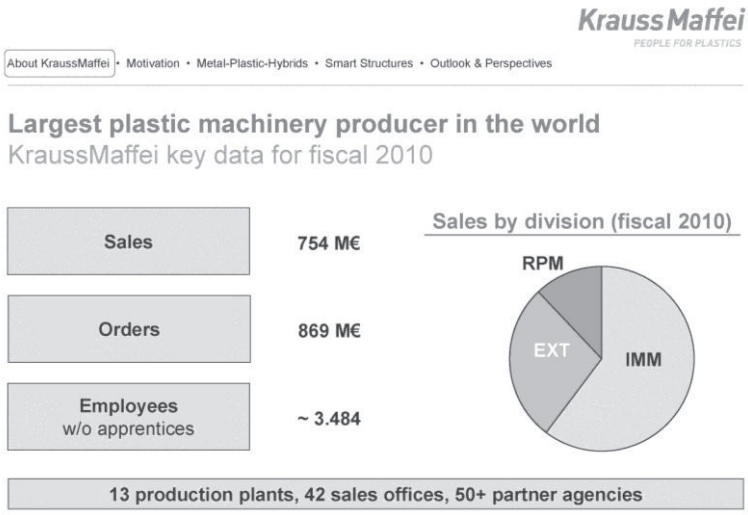
Krauss Maffei
PEOPLE FOR PLASTICS
About KraussMaffei • Motivation • Metal-Plastic-Hybrids • Smart Structures • Outlook & Perspectives
Largest plastic machinery producer in the world
KraussMaffei key data for fiscal 2010
Sales
754 M€
Orders
869 M€
Employees w/o apprentices
~ 3.484
Sales by division (fiscal 2010)
RPM
EXT
IMM
13 production plants, 42 sales offices, 50+ partner agencies
4
Chemnitz, october 12th, 2011


Krauss Maffei
PEOPLE FOR PLASTICS
About KraussMaffei • Motivation • Metal-Plastic-Hybrids • Smart Structures • Outlook & Perspectives
Global player with 42 sales offices and over 50 partner agencies
KraussMaffei Group: our worldwide network
Jönköpping (S)
Moscow (RUS)
Detroit (USA)
Devens (USA)
Florence (USA)
Okazaki (JPN)
Seoul (KOR)
Shanghai (PRC)
Taipeh (TWN)
Shenzhen (PRC)
Hong Kong
Pune (IND)
Bangkok (Thai)
Singapore
Hanover (GER)
Stone (GB)
Warrington (GB)
Harderberg/Viersen (GER)
Zaventem (B)
Genneviliers (F)
Collégien (F)
Rotkreuz (CH)
Näfels (CH)
Oyonnax (F)
Roskilde (DK)
Breda (NL)
Stuttgart (GER)
Munich (GER)
Vienna (A)
Abbiategrasso (I)
Cerro Maggiore (I)
Mexico City (MX)
Bogotá (CO)
São Paulo (BR)
Mollet del Vallés (E)
Sales and service organizations
Partner agencies
Overview for the whole group:
Krauss Maffei
Krauss Maffei Berstorff
NETSTAL
5
Chemnitz, october 12th, 2011

KraussMaffei
PEOPLE FOR PLASTICS

About KraussMaffei • Motivation • Metal-Plastic-Hybrids • Smart Structures • Outlook & Perspectives

Multi-material-systems
Carrier of innovations

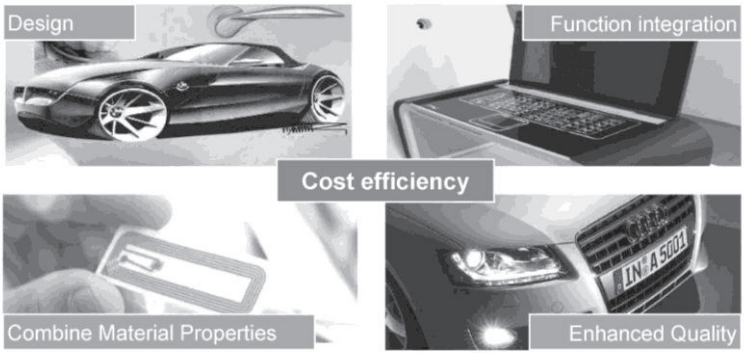

6 Chemnitz, october 12th, 2011

KraussMaffei
PEOPLE FOR PLASTICS

About KraussMaffei • Motivation • Metal-Plastic-Hybrids • Smart Structures • Outlook & Perspectives

Merging Properties for extended merits

Metals
- Isotropic
- High Young's Module
- Electric conductivity
- Good surface (class-A)
- Ductility
- …

Plastics / FRPs
- Anisotropic
- Energy absorption
- Low density
- Freedom of Design
- Damping properties
- …

Electronic Components
- Part reduction
- Cost reduction
- Functionality
- Reliability
- …

7 Chemnitz, october 12th, 2011

KraussMaffei
PEOPLE FOR PLASTICS

About KraussMaffei • Motivation • Metal-Plastic-Hybrids • Smart Structures • Outlook & Perspectives

Motivation…

…use synergies, compensate weaknesses!

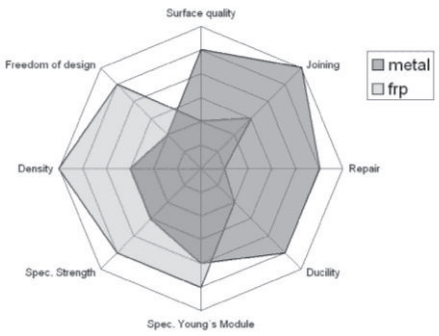

8 Chemnitz, october 12th, 2011

KraussMaffei
PEOPLE FOR PLASTICS

About KraussMaffei • Motivation • Metal-Plastic-Hybrids • Smart Structures • Outlook & Perspectives

Markets for highly integrated systems

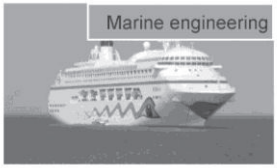

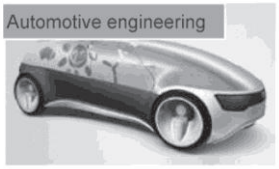

9 Chemnitz, october 12th, 2011

KraussMaffei
PEOPLE FOR PLASTICS

About KraussMaffei • Motivation • Metal-Plastic-Hybrids • Smart Structures • Outlook & Perspectives

Content

Metal-plastic hybrids Smart systems Outlook & perspectives

10 Chemnitz, october 12th, 2011

KraussMaffei
PEOPLE FOR PLASTICS

About KraussMaffei • Motivation • Metal-Plastic-Hybrids • Smart Structures • Outlook & Perspectives

History – First steps of Hybrid Technology
Example: Frontends Audi A6 and Ford Focus

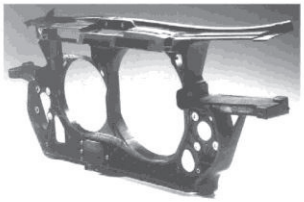

Source: Lanxess Deutschland GmbH

Material: steel-sheet with elastomer-modified nylon6 GF 30 (fibre content 30wt.%)

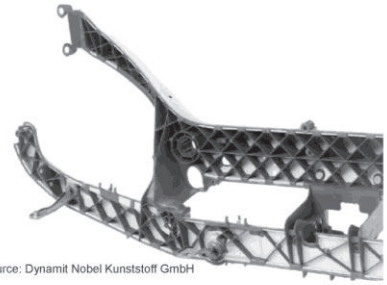

Source: Dynamit Nobel Kunststoff GmbH

11 Chemnitz, october 12th, 2011

KraussMaffei
PEOPLE FOR PLASTICS

About KraussMaffei • Motivation • Metal-Plastic-Hybrids • Smart Structures • Outlook & Perspectives

Process-chain for injection-moulded hybrid parts
Hybrid door-module

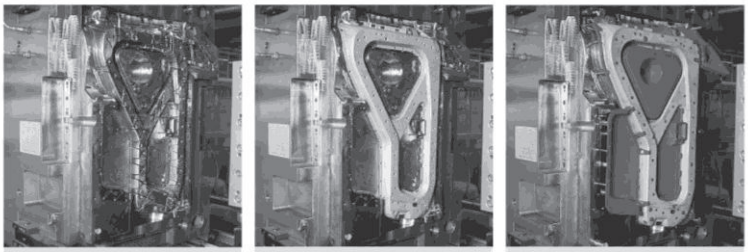

Open mould | Metal insert | Finished hybrid part

Source: Bayer AG

12 Chemnitz, october 12th, 2011

KraussMaffei
PEOPLE FOR PLASTICS

About KraussMaffei • Motivation • Metal-Plastic-Hybrids • Smart Structures • Outlook & Perspectives

Research – Hybrid structural elements
„Erlanger Träger“

- Thin-walled metal-sheets with high Young‘s modulus
- Plastic ribs (reduced sound emission)
- High structural stiffness
- Construction depends on design space

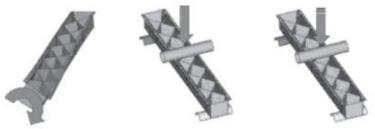

Source: M Plan GmbH/ Lanxess Deutschland GmbH

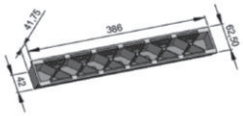

Source: LKT Universität Erlangen-Nürnberg

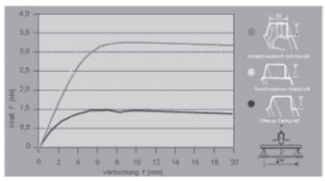

Source: Lanxess Deutschland GmbH

13 Chemnitz, october 12th, 2011

KraussMaffei
PEOPLE FOR PLASTICS

About KraussMaffei • Motivation • Metal-Plastic-Hybrids • Smart Structures • Outlook & Perspectives

Facing new challenges

- mass production joining-technologies

Source: Boellhoff

14 Chemnitz, october 12th, 2011

KraussMaffei
PEOPLE FOR PLASTICS

About KraussMaffei • Motivation • Metal-Plastic-Hybrids • Smart Structures • Outlook & Perspectives

Facing new challenges

mass production joining-technologies
Repair possibilities
Surface quality

Source: Lamborghini

15 Chemnitz, october 12th, 2011

KraussMaffei
PEOPLE FOR PLASTICS

About KraussMaffei • Motivation • Metal-Plastic-Hybrids • Smart Structures • Outlook & Perspectives

Facing new challenges

mass production joining-technologies
Repair possibilities
Surface quality
Force transmission areas

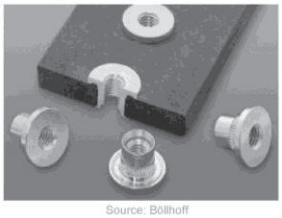

Source: Böllhoff

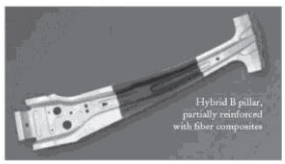

Source: Benteler SGL

16 Chemnitz, october 12th, 2011

KraussMaffei
PEOPLE FOR PLASTICS

About KraussMaffei • Motivation • Metal-Plastic-Hybrids • Smart Structures • Outlook & Perspectives

Applications for metal-plastic hybrids in structural components
Automotive industry

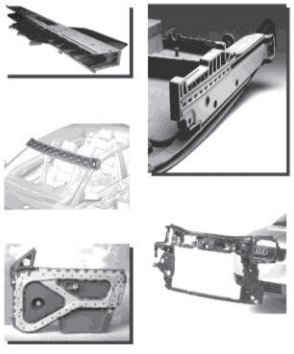

- Frontend
- Dashboard support
- Seat-structure
- Cross-beam
- Rear lid-carrier
- Door-carrier
- Roof-mechanic
- Pedals
- Door sill
- Spare wheel well

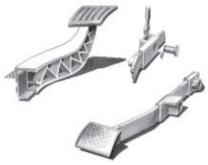

17 Chemnitz, october 12th, 2011

KraussMaffei
PEOPLE FOR PLASTICS

About KraussMaffei • Motivation • Metal-Plastic-Hybrids • Smart Structures • Outlook & Perspectives

Upcoming requirements on metal-plastic-hybrids
Extract

...
Adhesive bonds
Sealed joint areas
Resistance against climate changes
Long-term stability
Reduction of residual stress in joint areas
No interference of following steps (e.g. coating)
Process-integration of primer application (use of cheap semi-finished products)
Local primer application (cost reduction)
...

direct-plastic-to-metal, dpma

primer-plastic-to-metal, ppma

18 Chemnitz, october 12th, 2011

KraussMaffei
PEOPLE FOR PLASTICS

About KraussMaffei • Motivation • Metal-Plastic-Hybrids • Smart Structures • Outlook & Perspectives

Direct-plastic-to-metal-adhesion
dpma-technology – cost efficient and ready for mass production

Using the thermal activation of metal surfaces a direct joining is possible

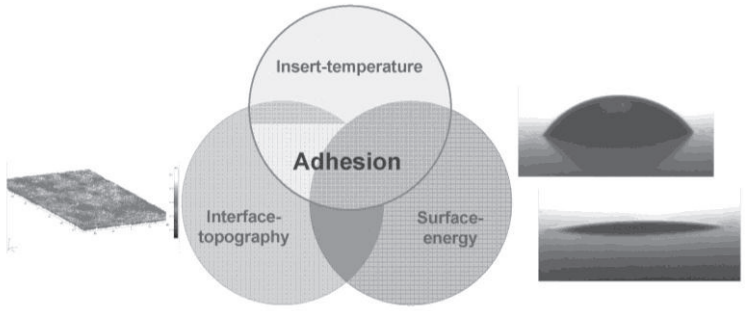

Influences of the „direct-plastic-to-metal-adhesion“ (dpma) technology

19 Chemnitz, october 12th, 2011

KraussMaffei
PEOPLE FOR PLASTICS

About KraussMaffei • Motivation • Metal-Plastic-Hybrids • Smart Structures • Outlook & Perspectives

Primer-plastic-to-metal-adhesion
ppma-technology – for high demands in the interface

- By the use of primers a much higher joining strength is reached
- Primers can represent even more functions because of an additional layer

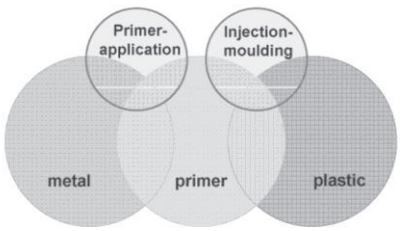

Influences on the „primer-plastic-to-metal-adhesion“ (ppma) technology

20 Chemnitz, october 12th, 2011

KraussMaffei
PEOPLE FOR PLASTICS

About KraussMaffei • Motivation • Metal-Plastic-Hybrids • Smart Structures • Outlook & Perspectives

Content

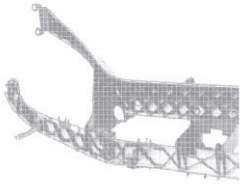

Metal-plastic hybrids | **Smart systems** | Outlook & perspectives

21 Chemnitz, october 12th, 2011

KraussMaffei
PEOPLE FOR PLASTICS

About KraussMaffei • Motivation • Metal-Plastic-Hybrids • Smart Structures • Outlook & Perspectives

State of the art – hybrid electronic parts
Example: plug

Process

- Integration of a die cutter
- Insertion of insert in IMM and demoulding of finished part with automation
- Two-component part in one process

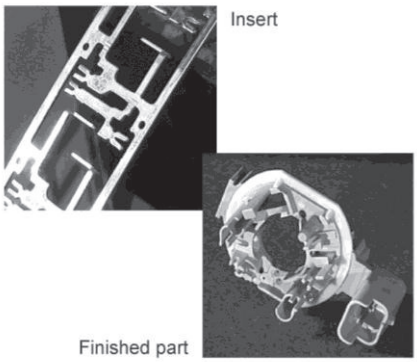

22 Chemnitz, october 12th, 2011

KraussMaffei
PEOPLE FOR PLASTICS

About KraussMaffei • Motivation • Metal-Plastic-Hybrids • Smart Structures • Outlook & Perspectives

RFID
…state of the art for logistic applications

- Nowadays there are numerous examples for integrated RFID-Chips in logistic applications
- In-mould labelling of RFIDs has been examined
- Extension and miniaturisation of memory-capacity enables new functions
  - → Protection against product piracy
  - → Process data saved on part
  - → Future: health-monitoring (in combination with piezo-sensors)
  - →…

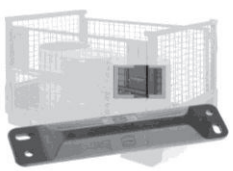

23 Chemnitz, october 12th, 2011

KraussMaffei
PEOPLE FOR PLASTICS

About KraussMaffei • Motivation • Metal-Plastic-Hybrids • Smart Structures • Outlook & Perspectives

3D MID-Technology
Energy and mass savings

1. first component: form-function
2. sec. component: metalizable
3. electroless copper

24 Chemnitz, october 12th, 2011

KraussMaffei
PEOPLE FOR PLASTICS

About KraussMaffei • Motivation • Metal-Plastic-Hybrids • Smart Structures • Outlook & Perspectives

MID-Technology – Laser Direct Structuring
control panel for steering wheel

- Substrate: PBT+PET
- Process: laser direct structuring
- Industry: automotive
- Manufacturer: TRW automotive safety systems GmbH & Co. KG

- Efficient use of expensive LDS-materials with multi-inject technology
  → Core-back
  → Turntable
  → Sliding Table
  → SpinForm

25 Chemnitz, october 12th, 2011

KraussMaffei
PEOPLE FOR PLASTICS

LED lamp with electronic encapsulation
AX C.A.S.E exhibit at K-Show

Application:
- Transparent PC Lamp Body / 2-cavities
- LED board-insert
- High Pressure PUR C.A.S.E. Encapsulation
- Cycle time: 35 seconds

Production equipment:
- AX 50-180
- LRX 50
- RimStar Nano 1,2 / 0,6

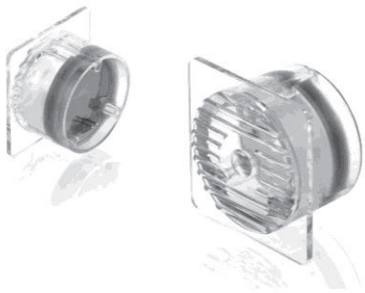

26

KraussMaffei
PEOPLE FOR PLASTICS

LED lamp with electronic encapsulation
Production cell

Application:
- Transparent PC Lamp Body / 2-cavities
- LED board-insert
- High Pressure PUR C.A.S.E. Encapsulation
- Cycle time: 35 seconds

Production equipment:
- AX 50-180
- LRX 50
- RimStar Nano 1,2 / 0,6

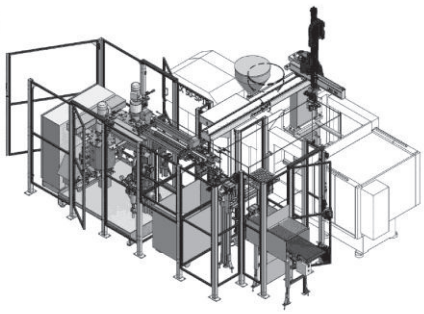

27

KraussMaffei
PEOPLE FOR PLASTICS

About KraussMaffei • Motivation • Metal-Plastic-Hybrids • Smart Structures • Outlook & Perspectives

Content

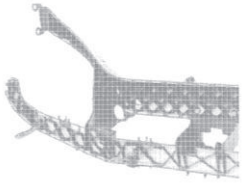

Metal-plastic hybrids

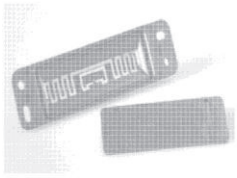

Smart systems

Outlook & perspectives

28 Chemnitz, october 12th, 2011

KraussMaffei
PEOPLE FOR PLASTICS

About KraussMaffei • Motivation • Metal-Plastic-Hybrids • Smart Structures • Outlook & Perspectives

Integrated Functions in Automotive Applications

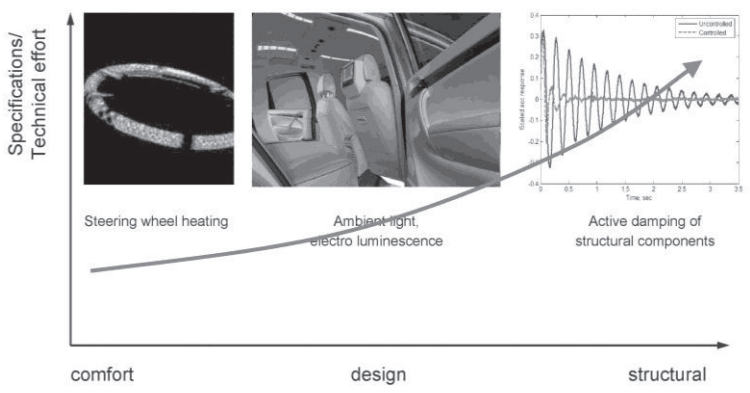

29 Chemnitz, october 12th, 2011

KraussMaffei
PEOPLE FOR PLASTICS

About KraussMaffei • Motivation • Metal-Plastic-Hybrids • Smart Structures • Outlook & Perspectives

Structural - Active damping
Sound emissions in lightweight structures

- Mass-reduction of carbody-structure promotes solid-borne-sound
- Use of materials with high stiffness leads to thin-walled structures
- Physics: $F = m \cdot a$
- Sound source localisation via beamforming (depends on frequency)

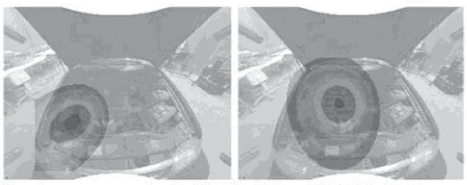

Sound sources car engine for 925 MHz (left) and 1250 MHz (right)

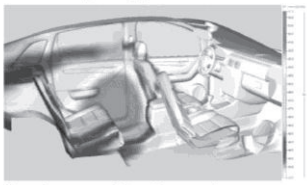

Sound sources of door trim panel

30 Chemnitz, october 12th, 2011

KraussMaffei
PEOPLE FOR PLASTICS

About KraussMaffei • Motivation • Metal-Plastic-Hybrids • Smart Structures • Outlook & Perspectives

Function integrated hybrid-parts
Piezo-electric sensors and actors

- Film-based actors and sensors are mainly used in thin-walled lightweight structures, with the objectives
  - •Closed loop control
  - •Suppress and reduce the appearance of structural deformations
  - •Active reduction of sound emission
- Integrated sensors can be used for health-monitoring of security-relevant fibre-composite parts
- Applications

  ⇒ where passive optimizations of noise reductions can't be achieved with maintainable effort in energy and material

  ⇒ for monitoring of complex fibre-composite structures

31 Chemnitz, october 12th, 2011

KraussMaffei
PEOPLE FOR PLASTICS

Your questions please!

Martin Schneebauer
Dipl.-Ing.
New Technologies / Process Engineering
KraussMaffei Technologies GmbH
Krauss-Maffei-Strasse 2
D-80997 Munich
Germany

Fabrication and characterization of a form- and force-locked piezo-metal sensor module

Neugebauer, R.[1,3]; Schubert, A.[1,3]; Richter, F.[2]; Koriath, H.-J.[3]; Peter, S.[2]; Berg, S.[2]; Jahn, S. F.[1]; Müller, B.[1]; Müller, M.[1]

[1]*Institute for Machine Tools and Production Processes, Chemnitz University of Technology, Chemnitz, Germany*
[2]*Institute of Physics, Chemnitz University of Technology, Chemnitz, Germany*
[3]*Fraunhofer Institute for Machine Tools and Forming Technology, Chemnitz, Germany*

Abstract

The direct integration of piezoceramics in sheet metal is a novel approach for production of adaptronic structural metal parts. In this paper the manufacturing process and characterization results of the first piezo-metal sensor module are described. The processes include high precision generation of micro-cavities in sheet metal, microscopic piezoceramic rods, PECVD insulating layers with high dielectric strength, micro-assembly and non-positive joining by forming. For the characterization of the module measurements of surface roughness, geometric parameters, and electrical properties were performed on the rods, the micro-structured sheet, and the insulation layer. Finally, the sensor function has been proven by a mechanical excitation resulting in a proportional measured sensor signal.

1. Introduction

Integration of functions into structural metal parts is a key technology for numerous future products aiming for increased resource efficiency and performance. The functional integration of active materials in sheet metal provides both, a reduction of product weight and cost along with superior sensor and actuator performance compared to current products. Sheet metal with integrated piezoelectric elements for actuation and sensing can be used for various applications, including collision sensing and health monitoring of joint connections in automotive components or security-related components for aircrafts.

A novel concept for the functional integration of piezoceramics in aluminium sheets has been developed. Unlike current technologies where piezoelectric modules are applied to existing structural parts, a direct integration of piezoceramics without prior packaging is proposed. In order to achieve sensor and actuator functionality, the piezoceramics require mechanical coupling to the sheet metal while not significantly deteriorating the passive mechanical properties of the base material.

In the following, the design, fabrication methods, and characterization results of the first functional prototype of a piezo-metal sensor module are described.

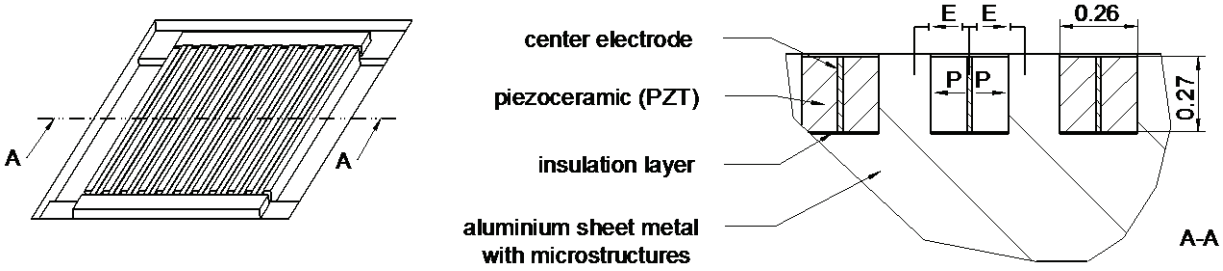

Fig. 1: *Design principle for the piezo-metal sensor module*

2. Fabrication of the piezo-metal sensor module

2.1 Design

The design principle chosen for the prototype is shown in figure 1. Piezoceramics are placed into micro cavities located on the surface of a sheet metal part. The depth of active area is less than 0.3 mm and the thickness of the sheet metal is 1.5 mm. The piezoceramic rods are therefore placed far-off the neutral axis of the sheet metal.

Within the prototype piezo-metal module ten piezoceramic rods with cross-sectional areas of 0.26×0.27 mm^2 and 10 mm length have been applied. Each of the rods consists of two piezo-ceramic layers and a center electrode for electrical contact. The rods are integrated in micro cavities with nominal dimensions of $0.3 \times 0.3 \times 10$ mm^3 resulting in a clearance between the piezoceramic rod and the cavity walls to ensure assemblability. The web between two cavities is 0.2 mm wide, which results in a pitch of 0.5 mm.

The piezoelectric d_{33} effect is used to provide for both maximum charges generated by strains resulting from deformations of the sheet metal and ease of manufacturing. Comparable to piezoelectric stack actuators, the piezoceramics are arranged in an electrical parallel circuit and mechanical series connection as it is depicted in figure 1. Thereby, the ground electrode is formed by the basis material and the signal is generated at the center electrode. Short circuits between the center electrode and the carrier sheet are prevented by the application of an insulating coating on the cavity grounds.

Mechanical and electrical coupling and therefore functional integration of the piezoceramic rods in the sheet metal is achieved by a subsequent forming process recently described in [1]. This forming process provides further an averaging of manufacturing tolerances [2] and the required pretension of the piezoceramic rods.

2.2 Aluminium Sheet Carrier

The ten micro cavities were fabricated by means of micro milling using a sheet of EN AW-5182 aluminium alloy (AlMg4.5Mn0.4), which is a common car body material. Figure 2 shows a scanning electron microscope (SEM) image of the micro-structured sheet.

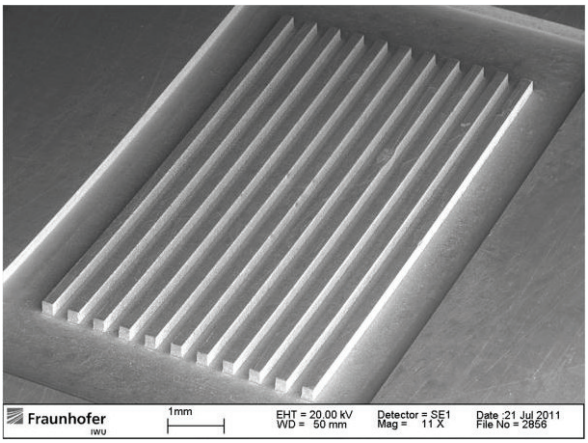

Fig. 2: *Micro-structured aluminium sheet metal*

Between the cavity sidewall and the piezo-ceramic rods a stiff mechanical coupling is necessary to transfer small strains within the sheet metal to the piezo-ceramic rods in order to sense small amplitude vibrations coupled into the carrier.

In order to allow for good transfer of the generated charges of the piezoceramics to the sheet metal, a close electrical contact is required. A prerequisite to achieve that close contact is a minimum surface roughness at the cavity walls. Figure 3 shows a close-up SEM image of the cavity walls where the surface roughness of these areas is observable. An average surface roughness of $R_a = 0.36$ µm and $R_z = 2.20$ µm has been measured on the cavity walls using a laser microscope.

The surface roughness of the cavity ground influences the properties of the subsequent insulating coating for preventing shorts and is therefore crucial for the function of the piezo-metal sensor module. The roughness of the cavity ground was determined to be in the range of $R_a = 0.22$ - 0.31 µm and $R_z = 0.29$ - 0.40 µm, which is expected to be sufficiently smooth.

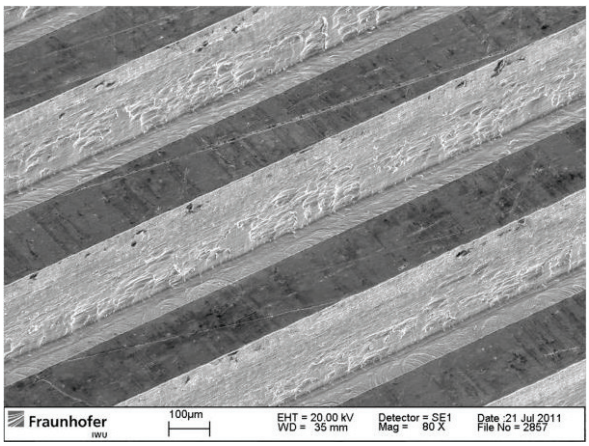

Fig. 3: *Magnification of micro cavity walls*

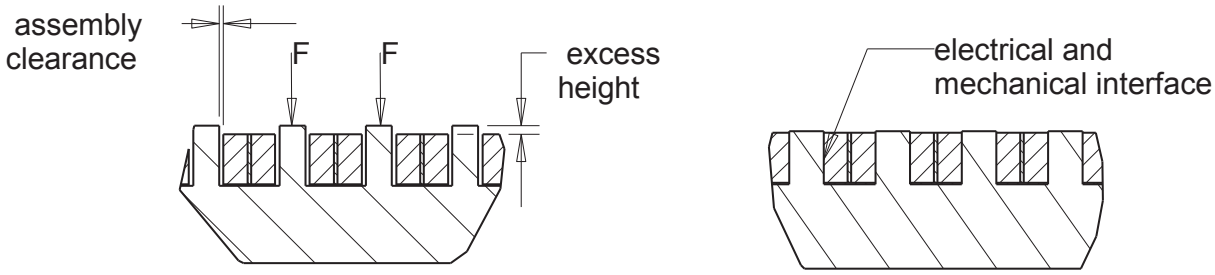

Fig. 4: *Principle of joining by forming for functional integration after assembly*

Another important parameter of the micro cavities is the depth. An average cavity depth of 312 µm with maximum deviations in the range of 3 µm has been determined from a cross-section of a sample sheet. The cavities depth therefore exceeds the 270 µm nominal height of the piezoceramic rods by more than 40 µm. This excess material is required for subsequent joining by forming.

2.3 Insulation of the Aluminium Sheet

The electrical insulation of the piezoceramic rods center electrodes against the micro-structured sheet metal is one of the most critical issues for the manufacturing of the piezo-metal sensor module. Its effectiveness depends on the chosen insulator material, the deposition parameters used [3] and the above described properties of the cavity ground.

Insulating layers were fabricated using a vacuum deposition system MicroSys400 (Roth & Rau). The insulating hydrogenated silicon carbonitride film SiCN:H was deposited in a PECVD process from trimethylsilane ($SiH(CH_3)_3$; “3MS”) in mixture with nitrogen, hydrogen and argon using 13.56 MHz RF discharge.

The performance of the insulating layer is particularly defined by the dielectric strength. Breakdown voltage measurements were conducted for numerous samples by positioning a V-shaped electrode at the center of the cavity’s ground and applying a variable voltage ranging from 0 to 1100 V in 5 V increments (voltage source Keithley 2410). Breakdown voltages in the range of 600 V have been measured at the cavity ground.

Significant differences comparing the layer thickness and resulting dielectric strength at the cavity ground and on flat areas away from the micro structure have been observed. On flat areas outside the micro cavities the insulator thickness is 4.5 µm and hence about 35 % larger than at the center of the ground of the micro cavities. Therefore, the breakdown voltage of the SiCN:H film exceeds values of 1.1 kV on flat areas.

However, a decreased dielectric strength was observed in assembled piezo-metal sensor modules. Breakdown voltages ranging from 170 to 280 V have been measured for modules with integrated piezoelectric rods. This deteriorated performance is likely to be caused by pinholes generated either due to roughness peaks in the micro cavities, inhomogeneous deposition of the insulating layer or defects resulting from the plastic deformation during the joining of the piezoceramic rods and the micro structured sheet metal by forming.

It should be noted that the measured dielectric strength is sufficient for sensor mode operation and would also be sufficient for small and large signal actuation.

2.4 Piezoceramic Rods width Center Electrodes

Piezoceramic rods with dimensions of 0.26 × 0.27 × 10 mm³ and center electrodes were cut from composite plates using a wafer dicing saw. The composite plates consist of two piezoceramic layers with an intermediate layer of Sn42Bi58 alloy. Those plates have been manufactured by joining metalized and polarized piezoceramic plates (M1100, Johnson Matthey Catalysts). Subsequent lapping and chemical mechanical polishing (CMP) of the composite plates produced the desired plate thickness of 260 µm and surface roughness of $R_a < 0.02$ µm and $R_q < 0.03$ µm.

2.5 Assembly of the Piezo-Metal Module

The piezoceramic rods were assembled into the micro cavities as shown in figure 4. The actual assembly clearances are influenced by the clearance fit and the deviations of the width of the rods and the micro cavities.

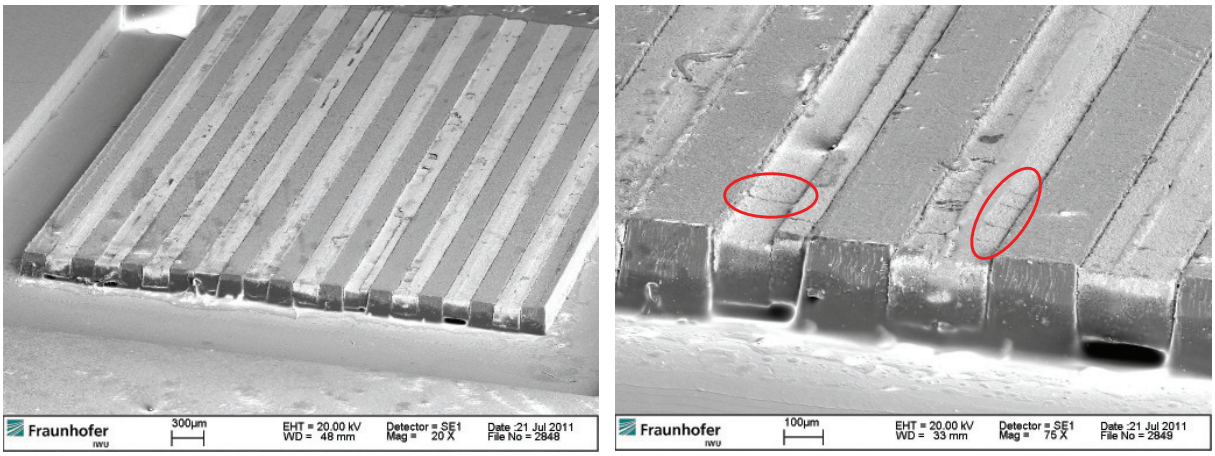

Fig. 5: *Joined piezoceramic rods in a micro-structured aluminium sheet*

Figure 4 illustrates that a non-positive coupling is achieved by a forming process, where the webs are deformed using a planar die. This results in an electrical and mechanical interface between the piezoceramic and the sheet metal.

The joining by forming process was carried out in a hydraulic force-controlled press applying a maximum load of 12 kN. Figure 5 shows a SEM image of the joined piezo-metal module. The magnification on the right image shows that the high stress during the forming process caused small fractures (circles) within the piezoceramic rods, which have been described earlier in [4]. It should be noted that eccentricities of the center electrodes result from inaccuracies due to the manual manufacturing of the piezoceramic.

Further, it can be seen from figure 5 that piezoceramic rods are clamped by the deformed webs. The close contact between the piezo rods and the cavity sidewalls is more clearly observable from figure 6, which shows a microscope image of a polished section depicting the interface between piezoceramic and metal.

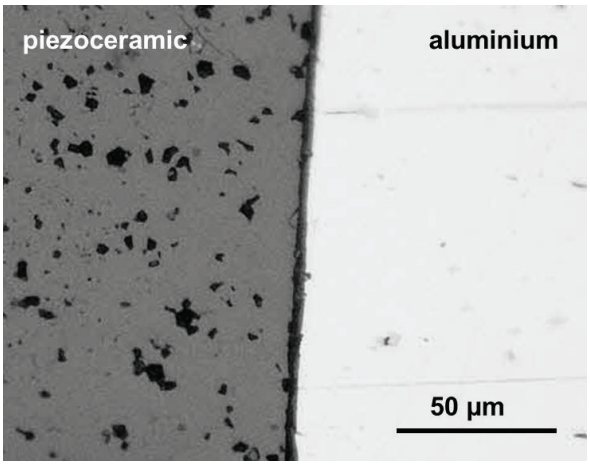

Fig. 6: *Interface between piezoceramic and metal*

The cavity widths have been measured before and after the joining by forming process using a Nikon MM400 measuring microscope. The results are shown in figure 7.

The average cavity width before joining was 312 µm and showed very little deviations in the range of 4 µm. After the joining by forming process, an average cavity width of 260 µm has been measured. Significant deviations of the cavity width occurred resulting from the varying width of the piezoceramic rods. This correlation proves the effect of averaging of dimensional errors since the variations of the width of the piezoceramic rods are reflected in the joined cavity width.

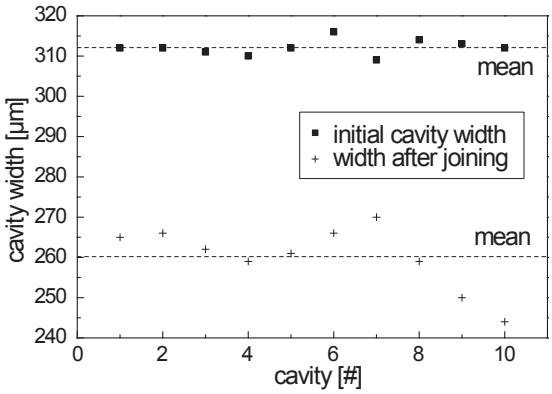

Fig. 7: *Cavity width before and after joining*

3. Characterization of the piezo-metal sensor module

In figure 8, the experimental setup for the characterization is depicted. The piezo-metal module is clamped on one side and bent on the other side by an excitation force resulting in a deflection *u* causing strains within the module.

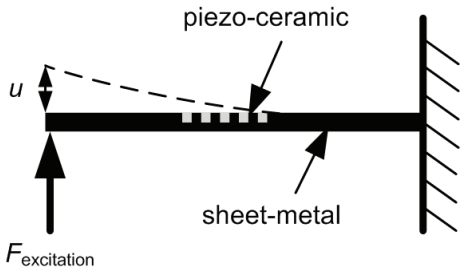

Fig. 8: *Schematic of the experimental setup*

Figure 9 is a photograph of the setup where the sheet-metal (1) and the piezoceramic rods (2) were electrically connected to a charge amplifier. The module was clamped on one side (3) and a piezo cube (PI P-611:3S Nano Cube) (4) driven by an amplified sinusoidal signal was mounted to perform periodic excitation on the other side.

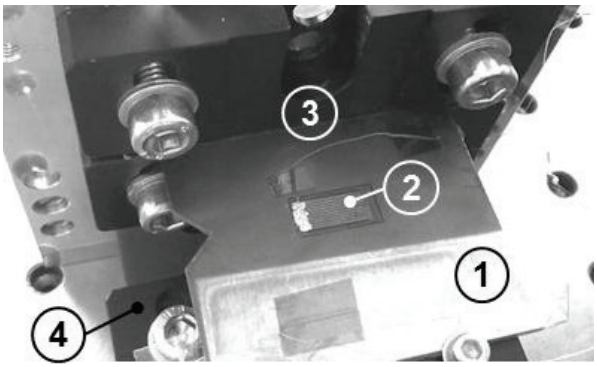

Fig. 9: *Experimental setup for characterization*

The deflection of the sheet metal causes strains in the direction of d_{33} within the piezoceramic rods and therefore generates charges due to the direct piezoelectric effect. In figure 10 the amplified charges generated by the piezo-metal sensor module are plotted in comparison to the exciting sinusoidal deflection measured by a high resolution laser triangulation sensor.

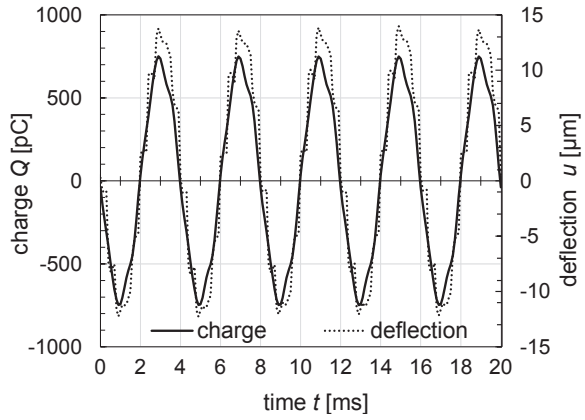

Fig. 10: *Deflection u (bending) of the piezo-metal sensor module and corresponding charge generated by the integrated piezoceramic rods (phase of signals was fitted for comparability)*

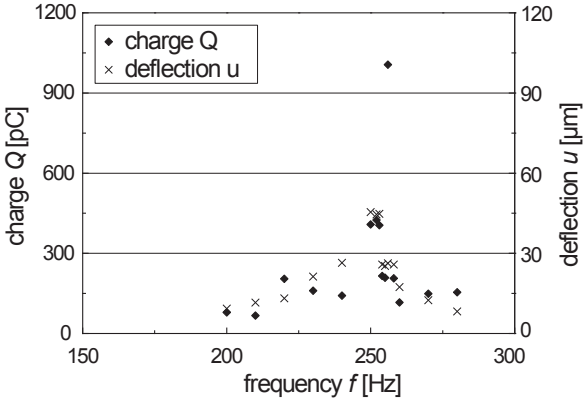

Fig. 11: *Generated charge by the piezo-metal sensor module and deflection of the piezo cube*

It can be seen from the graphs in figure 10 that the sensor signal is proportional to the mechanical excitation with high repeatability. This proves the effective electromechanical coupling of piezoceramic and sheet metal.

The charge generated by the piezo-metal sensor module is further a quantitative measure of the amplitude of the deflection *u* at the tip of the module (cf. figure 8). This was proven by measurements close to the mechanical resonance frequency (256 Hz) of the mechanical system consisting of clamped piezo-metal sensor module and exciting piezo cube.

In figure 11 the frequency response characteristics of both the generated charge and the deflection are plotted. Nearly congruent resonance responses have been observed. Therefore, the piezo-metal sensor module is capable of providing a quantitative measure of the mechanical deflection.

4. Conclusion

The feasibility of the direct functional integration of piezoceramics in micro-structured sheet metal has been demonstrated. It was shown that a configuration consisting of piezoceramic rods with center electrodes, where the sheet metal is used as ground electrode, allows for operation of piezo-metal modules as sensors.

The mechanical and electrical connection of the metal and the piezoceramic is solely achieved by a non-positive coupling generated by a forming process. This process is obviously capable of averaging dimensional errors of piezoceramic rods and micro cavities which are present due to tolerances in manufacturing. Piezoceramic rods with center electrodes can bear the mechanical stress induced by the forming process.

It was shown that the insulating coatings applied are sufficiently strong to endure assembly, joining by forming and generated electrical potentials in sensor operation in the range of 0 to 285 Hz excitation.

Further research aims for high-volume capable production technologies particularly for the manufacturing of micro cavities, the assembly and joining by forming processes. A significant reduction of the cycle times and increased repeatability and therefore reliability is expected by the use of micro impact extrusion to produce micro-formed cavities and automated micro-assembly of parallel batches of piezoceramic rods.

Further efforts are taken to increase the strength of the insulating coatings in order to increase the reliability of the piezo-metal sensor module and to enable in-situ polarization techniques and use of the module as actuator.

5. Acknowledgement

The authors thank the German Research Foundation for the financial support of the investigations within the scope of the Collaborative Research Center CRC/TR 39 PT-PIESA.

References

[1] *Schubert, A.; Drossel, W.-G.; Pohl, R.; Kranz, B.: Investigation of a force-locked connection of micro piezo elements with aluminium carrier material. In:* Production Engineering 4 (2010)*, 4, pp. 399-405.*

[2] *Neugebauer, R.; Koriath, H.-J.; Regel, J.; Müller, M.: Process chain and tolerance management for precision manufacturing of piezo-metal-modules. In:* Proc. ISEM 2011. *Available at: http://www.isem.org.za/index.php/isem/isem2011/paper/view/54/33. Date accessed 20 Sep 2011.*

[3] *Peter, S.; Günther, M.; Hauschild, D.; Richter, F.: Low temperature plasma enhanced chemical vapor deposition of thin films combining mechanical stiffness, electrical insulation, and homogeneity in microcavities. In: Journal of Applied Physics 108, 043303 (2010), pp. 1-12.*

[4] *Schubert, A.; Jahn, S. F.; Hackert, M.: Simulation of a Forming Process for Joining a Piezo Aluminium Module. In: Proc. 4th COMSOL Conference, 2010.*

CNT-filled PP compound for in-situ bonding and connection of piezoelectric ceramics by using multi-component micro injection molding

Heinrich, M.; Kroll, L.; Walther, M.; Elsner, H.

Chemnitz University of Technology, Department of Lightweight Structures and Polymer Technology, Chemnitz, Germany

Abstract

Based on an increasing demand for function integration in small components, micro injection molding offers a highly productive solution to combine plastic structures with additional electronic and mechatronic features. Particularly two-component micro injection molding allows embedding of active elements as well as the application of electric contacts in one process step by using insolating and conductive compounds, respectively. The investigations showed several typical and exceptional mechanical characteristics of the applied materials, depending on processing parameters and the concentration of the employed conductive additives. With regard to the prospective usage as contacting member of a micro injection molded piezo module, the selection of the plastics and optimization of the machine setting are significant variables to achieve the best results. The study outlines major effects on mechanical properties of compounded polypropylenes with conductive additives. By means of the two-component micro injection molding process specimens were manufactured and the influence of the micro architecture has been investigated to predict favorable composite design and processing parameters.

1. Introduction

The increasing miniaturization of products including electronic and mechatronic assemblies leads to a maximal integration of functions and developments of manufacturing technologies for very small multi-component devices. For this purpose the micro injection molding technology for plastic based micro parts is outstandingly appropriated. This technology is able to produce plastic parts with a high degree of shape-freedom in a high quantity without post processing. The flexibility of this process allows the combination of different materials and the integration of metallic and ceramic inserts as well as electronic or magnetic functional parts [1, 2].

Particularly the in the electrical industry required increase of the functional density of injection molding parts with small installation space is a specific challenge, wherein the internal stress effect and the shrinkage effect have a high weight [3]. For this purpose are basic numerical and verifying experimental analysis of the mould-filling characteristics, of the warpage as a result of thermal stress to the anisotropic mechanical structural behavior and the dependence between thermal mechanical material stress and process related parameters essential [4]. The usage of plastic based piezo ceramic modules as actuator, sensor and as energy supplier have already been discussed in theoretical and experimental studies with different objective targets [5, 6].

The ideal method for the economical bonding and integration of piezo elements in plastic based parts are compounded polymers with conductive additives, because of their cheapness in large quantities. By means of the two-component micro injection molding process it is possible to injection-mould the technical embedding and bonding of a piezo ceramic component in use of an electrical conductive thermoplastic (E-plastic), as well as to enable defined mould cavities with an electrical insulated plastic (I-plastic), so that the electrodes and piezo elements lie electrical separated. The considered piezo fiber composites are made of uni-axial piezo fibers (lead zirconate titanate (LZT), Sonox® P53), which are embedded in epoxy resin (circa 70% vol. fiber content), wherein the piezo fibers are arranged perpendicular to the rod axis. One possible example of a micro injection molding produced µIM-Piezomodule (micro injection molding piezo module) is shown in fig. 1.

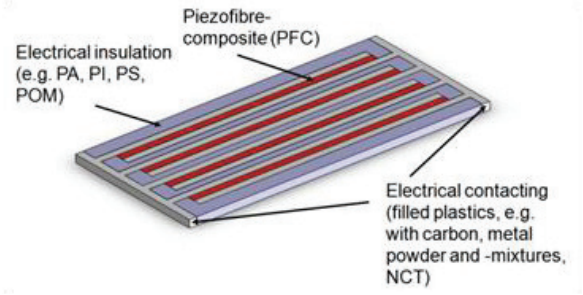

Fig. 1: *Design example of the µIM-Piezomodul*

Compared to inherent conductive plastics, filled polymers gain their electrical conductivity through additives, e.g. metals or carbon in different modifications [7]. Depending on volume fraction and filling material, the electrical resistivity can be influenced in a wide range. Especially nano carbon tubes are appropriate to build a conductive network with a low filling material concentration, the so-called percolation threshold [8]. The typical curve of electrical conductivity depending on additive volume fraction shows fig. 2.

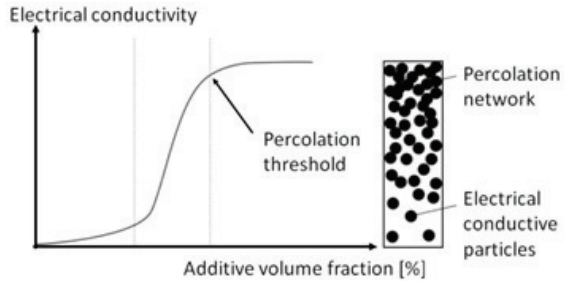

Fig. 2: *Electrical conductivity depending on additive volume fraction [9]*

Those nano composites have outstanding features compared to polymers with usual fillers: (1) low percolation threshold, (2) excellent particle-particle-interdependence, (3) high deployment density within polymer matrix, (4) very high surface to volume ratio, (5) small distance between particles and (6) small influence on the polymer structure resulting from storing into the polymer-chains, which is essential to avoid weakening the micro injection-molded piezo module.

A characteristic of the injection molding process is a distinct molecular orientation, which is caused by the flow of polymer melt induced shear and stretching forces [10]. Unlike the extrusion and compression molding processes, the process forces are high enough to align the additives accordingly [11].

With regard to a shift of the percolation threshold to higher levels of carbon nano tube with an increasing orientation of the additives in the matrix, it is important to minimize this negative influence by a process optimization [12, 13].

The first detailed results for that purpose provides Villmow et al. [12]. The focus of the investigation of the influence of injection speed, melt temperature, cavity temperature and holding pressure were on the orientation of the nano tubes within the polymer matrix. Hence mainly the injection speed and the melt temperature have decisive influence on the conductivity of the composites.

Since an increasing injection speed leads to a significant decrease in the electrical conductivity by several orders of magnitude, an increase of melt temperature leads to improved electrical conductivity. The influence of the melt temperature is significantly lower compared to the injection speed and the effect of cavity temperature as well as holding pressure is only marginal.

Based on the growing trend of miniaturization of micro-mechanical and micro-electro-mechanical parts and the resulting micro-system technology, a wide application spectrum is opened for the polymer carbon nano tube composites [14]. From industrial point of view especially the micro-injection molding plays a major role.

As with conventional injection molding, the property profile of the micro-injection molded parts is highly dependent on the process parameters used, although the transferability of the results due to the micro-technical features is only possible under certain conditions [14].

In comparison to conventional injection molding processes, a much higher injection pressure and as a consequence significantly greater shear forces are typical for micro injection-molding. In addition, a short solidification time, short molding-cycle-times and a high surface to volume ratio characterize the process [14, 15].

In this paper, we give an overview of how to prepare functionalized polypropylene and how the mechanical characteristics such as stiffness and strength can be influenced by injection speed and melt temperature due to flow behavior of carbon nano tubes.

2. Experimental part

2.1 Materials

The polypropylene used in this work is manufactured by Borealis AG and marketed under the trade name of Polypropylene HJ325MO. For the production of polypropylene nano composites the master batch of PLASTICYL PP2001 Nanocyl s.a. with a carbon nano tube volume content of 20% has been used.

2.2 Compounding

The micro injection-mold scaled nano composite pellets were prepared with a twin-screw compounder of Noris Plastic GmbH and CO KG ZSC type 25/44 D. The treatment of the melt was carried out at a constant temperature of 180 °C (356 °F) in air flow direction.

After compounding the nano composites the specimens were injection molded with the Wittmann/Battenfeld Microsystem 50.

2.3 Tensile test

All injection molded specimens were tested at room temperature (20-23 °C) according to the Standard DIN EN ISO 527 on a universal testing machine (table Inspect 50kN, Hegewald & Peschke GmbH Meß- und Prüftechnik GmbH).

The specimens are shown in fig. 3.

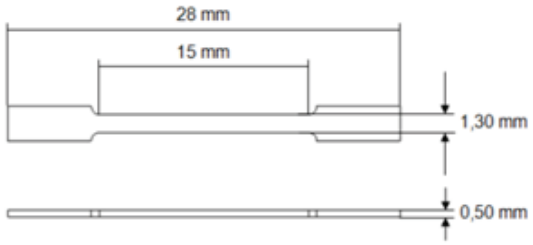

Fig. 3: *Micro injection molded tensile bar*

3. Results

3.1 Mass temperature

In the evaluation of the pure PP with mass temperatures between 240 °C and 300 °C it could be measured a decrease of Young's modulus from 1077 MPa to 901 MPa, which means a drop of 16 %. Equal to the modulus results, a decrease in yield strength with increasing melt temperature was measured. The exact results are shown in fig. 4.

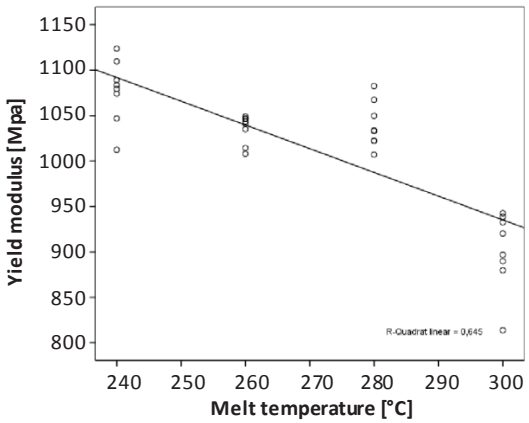

Fig. 4: *Yield strength depends on the melt temperature of pure PP*

For the PP nano composites the statistical analysis showed that with increasing carbon nano tube content, the influence of melt temperature on the elastic modulus grows. Characteristic of the collected data is a good homogeneity of the measurements, which contributes to a high correlation between mass temperature and Young's modulus, which is show exemplarily in fig. 5.

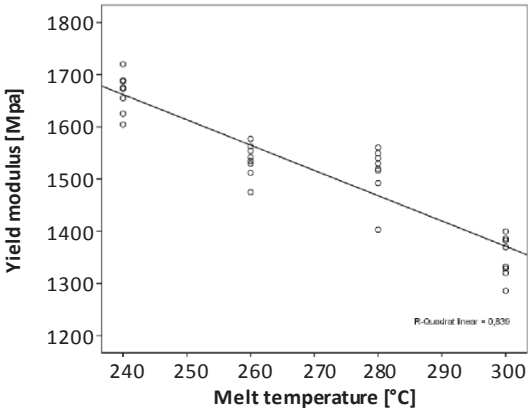

Fig. 5: *Yield strength depends on the melt temperature of PP with 5-wt% CNT*

The yield strength shows a characteristic which is shown in tab. 1. The decrease of yield strength rises with incremental volume fraction of carbon nano tubes.

Table 1: *Yield strength depends on melt temperature and CNT-content*

Volume fraction CNT [%]	***Yield strength at melt temperature [MPa]***		***Difference [%]***
	240 °C	***300 °C***	
0	*30,65*	*26,14*	*-14,71*
1	*34,44*	*32,87*	*-4,56*
2	*35,53*	*33,37*	*-6,08*
3	*37,34*	*35,1*	*-6,00*
4	*38,57*	*35,8*	*-7,18*
5	*39,36*	*36,11*	*-8,26*

3.2 Injection speed

Compared to the mass temperature, the mass injection speed has less influence on the Young's modulus of the pure PP. Between 50 mm/s and 750 mm/s, the Young's modulus decreases approximately 7 % (1077 MPa to 1004 MPa). In contrast to the mass temperature, the injection rate has no linear characteristic.

The nano composites show a more distinctive characteristic. From the box plot diagram it can be seen, that the modulus drops significantly by increasing injection speed (50 mm/s to 250 mm/s) and then remains nearly constant up to 750 mm/s, despite the relatively high scatter, see fig. 6.

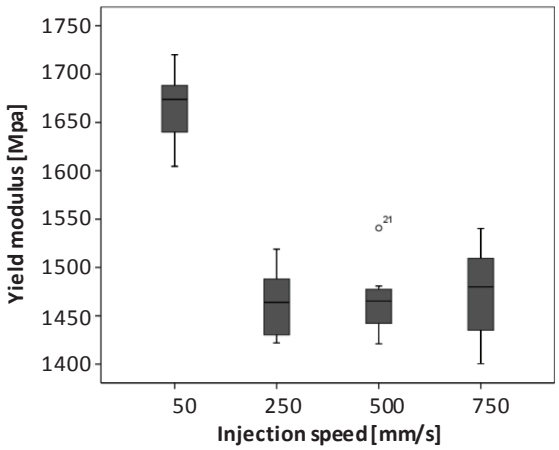

Fig. 6: *Yield strength depends on the injection speed of PP with 5-wt% CNT*

As shown in tab. 2, the influence of injection speed on the yield strength of the unfilled PP is more pronounced than for the investigated nano composites.

Table 2: *Yield strength depends on injection speed and CNT-content*

Volume fraction CNT [%]	***Yield strength at injection speed [MPa]***		***Difference [%]***
	50 mm/s	***750 mm/s***	
0	*30,65*	*28,87*	*-5,81*
1	*34,44*	*33,90*	*-1,57*
2	*35,35*	*35,03*	*-0,91*
3	*37,34*	*36,35*	*-2,65*
4	*38,57*	*37,03*	*-3,99*
5	*39,36*	*38,19*	*-2,97*

4. Discussion

The overall assessment of results indicates the following:

- increasing the injection speed leads to decreases the strength of the investigated thermoplastics (PP) and thermoplastic nano composites (PP with CNT),
- increasing the melt temperature leads to decreases the strength of the investigated thermoplastics (PP) and thermoplastic nano composites (PP with CNT).

Particularly for the PP matrix plastic, these results could be detected with high significance. They thus contradict the well-known phenomenon from the conventional injection molding of an increase in strength with increase in energy input by increasing the focus and distribution of carbon nano tubes within the polymer matrix [13].

It can therefore be assumed that the orientation and distribution of carbon nano tubes have smaller influence on the mechanical properties of the micro-injection molded nano composites. As possible causes for the progression of results in micro injection molding, there are two explanations:

1) With the increase of energy input the aspect ratio of carbon nano tubes changes.
2) By increasing the energy input the molecular structure of the matrix resins changes.

Both approaches can be justified by the increase in micro injection molding shearing effects [13, 16]. Liu et al. assumes that the morphological characteristics of the micro-injection molded nano composites differ from those produced of conventional injection molding. His studies show that the micro molded parts exhibit over the cross section from the edge to the core, a layer morphology, as it is well known from the conventional injection molding.

While in conventional injection molding the little-oriented core is trained strong, in the micro-injection molding a wide shear zone dominates the morphological structure. This observation is confirmed by several studies [17]. The shear forces acting in this area are strong enough to influence the molecular structure [17, 18]. At the same time the high shear forces lead to a shortening of the carbon nano tubes. Due to the high shear effects which break the carbon nano tubes, a decrease in aspect ratio results.

The consequence of this is that the load-bearing function of the in tensile direction oriented carbon

nano tubes decreases and thus leads to a reduction in strength.

Against this presumption, a characteristic drop in modulus and yield stress for the pure PP matrix plastic, which is equal to the evaluated nano composites, could be detected. In view of this, for the micro-injection molding the molecular structure of the matrix material, depending on injection speed and melt temperature is more important for the mechanical properties than the orientation, distribution and aspect ratio of the carbon nano tubes. It is assumed that the carbon nano tubes, even at low injection speed and melt temperature are fully oriented and therefore take no more significant influence on strength.

PP belongs to the group of semi-crystalline thermoplastics with presence of crystalline regions with a parallel orientation of the macromolecules, and amorphous regions with disordered orientation of the macromolecules, whereat the size of the crystalline regions adjacent to the structure and the length of the macromolecules depend on the crystal nucleation and crystal growth rate. These are generally influenced by the application of energy, in particular, the injection speed and mass temperature, in particular for PP. Liu et al. [16] found for in micro-injection molded PP increased crystallinity comparable to the conventional injection molding process. Those crystalline regions have an increased proportion of β-crystal phases which is shown as brightly zones on fig. 7.

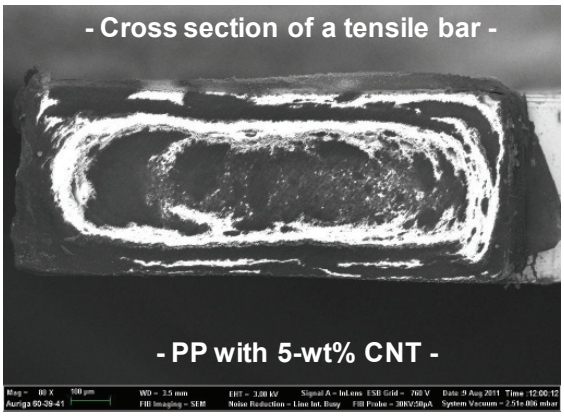

Fig. 7: *Cross section of a tensile bar (brightly zones are areas which are charging under REM cause of low electric conductivity)*

The increased degree of crystallization results from higher shear forces that favoring the alignment of the polymer chains along the flow direction.

In the shear zone then large areas of oriented structures that promote the nucleation and thus the growth of crystalline lamellae are formed. This increased molecular orientation and number of oriented crystals promote the growth of the β-crystal phases. Thus, even the increased β-crystal phase fraction is attributed to the increase in micro injection molding shear forces [19, 20]. The significance of this shows the study of Henning et al. [21]. According to its results, the crystal phases within the polypropylene matrix have different degrees of micro hardness. In the conventional injection molding the α-phase are dominant compared to considerably harder β-phase within micro injection molding. Thus it can be assumed that these results have significant influence on the mechanical properties [16, 20].

5. Conclusion

The executed investigations show the influence of mass temperature and injection speed on the mechanical properties of micro injection molded pure PP and PP-based nano composites filled with different volume shares of carbon nanotubes. Compared to conventional injection molded plastics, micro injection molded plastics have an increased degree of crystallized areas which leads to a decreased Young's modulus and the yield strength. The volume fraction of carbon nanotubes is not particularly important. Further research should therefore be performed in that direction.

6. Acknowledgement

The underlying research is gratefully supported by the German Research Foundation (DFG) as part of the special research field CRC/TR 39.

Literature

[1] Heinle, C.; Vetter, M.; Brocka-Krzeminska, Z.; Ehrenstein, G. W.; Drummer, D.: Mediendichte Materialverbunde in mechatronischen Systemen durch Montage-spritzguss. Kunststofftechnik / Journal of Plastics Technology, Nr. 6, 2009, pp. 428-450.

[2] Ehrenstein, G. W.; Drummer, D.: Hochgefüllte Kunststoffe mit definierten magnetischen, thermischen und elektrischen Eigenschaften. Springer-VDI-Verlag, 2009.

[3] Giboz, J.; Copponnex, T.; Mélé, P.: Microinjection molding of thermoplastic polymers: a review. Journal of Micromechanics and Microengineering, Nr. 17, 2007, S. R96-R109.

[4] Giboz, J.; Copponnex, T.; Mélé, P.: Microinjection molding of thermoplastic polymers: morphological comparison with conventional injection molding. Journal of Micromechanics and Microengineering, Nr. 19, 2009.

[5] Heinrich, M.; Kroll, L.; Elsner, H.; Leibelt, J.: Lightweight structures with autarchic functional piezoceramic modules for energy harvesting. 17. International Conference on Composites or Nano engineering, Honolulu: 2009.

[6] Inman, D. J.: Trans in Adaptive Structures. Neugebauer, R. (Hrsg.): 2. Wissenschaftliches Symposium des SFB/ Transregio 39, Großserienfähige Produktionstechnologien für leichtmetall- und faserverbundbasierte Komponenten mit integrierten Piezosensoren und -aktoren, 2009.

[7] Wong, Y. W.; Lo, K. L.; Shin, F. G.: Electrical and thermal properties of composite of liquid crystalline polymer filled with carbon black. In: Journal of Applied Polymer Science. Bd: 82. (2001), Nr. 6, pp. 1549-1555.

[8] Kumar, A.; Depan, D.; Singh Tomer, N.; Singh, R.: Nanoscale particles for polymer degradation and stabilization-Trends and future perspectives. In: Progress in Polymer Science. Bd: 34. (2009), Nr. 6, pp. 479-515.

[9] Domininghaus, H.; Elsner, P.; Eyerer, P.; Hirth, T.: Kunststoffe. Springer Berlin Heidelberg, 2008.

[10] Johannaber, F.; Michaeli, W.: Handbuch Spritzgießen. München. Hanser, 2002. ISBN 3446156321.

[11] Li, Z.; Narh, K. A.: Experimental determination and numerical prediction of mechanical properties of injection molded self-reinforcing polymer composites. In: Composites Part B: Engineering. Bd: 32. (2001), Nr. 2, pp. 103-109.

[12] Villmow, T.; Pegel, S.; Pötschke, P.; Wagenknecht, U.: Influence of injection molding parameters on the electrical resistivity of polycarbonate filled with multi-walled carbon nanotubes. In: Composites Science and Technology. Bd: 68. (2008), Nr. 3-4, pp. 777-789.

[13] Abbasi, S.; Carreau, P.; Derdouri, A.: Flow induced orientation of multiwalled carbon nanotubes in polycarbonate nano-composites: Rheology, conductivity and mechanical properties. In: Polymer. Bd: 51. (2010), Nr. 4, pp. 922-935.

[14] Abbasi, S.; Derdouri, A.; Carreau, P.: Properties of microinjection molding of polymer multiwalled carbon nanotube conducting composites. In: Polymer Engineering & Science. Bd: 51. (2011), Nr. 5, pp. 992-1003.

[15] Abbasi, S.; Derdouri, A.; Carreau, P.: Effect of nanotube alignment on the morphology and properties of Polycarbonate/MWCNT nanocomposites. 2009.

[16] Liu, F.; Guo, C.; Wu, X.; Qian, X.; Liu, H.; Zhang, J.: Morphological comparison of isotactic polypropylene parts prepared by micro injection molding and conventional injection molding. In: Polymers for Advanced Technologies. (2011). doi: 10.1002/pat.1946.

[17] Viana, J. C.: Development of the skin layer in injection moulding: phenomenological model. In: Polymer. Bd: 45. (2004), Nr. 3, pp. 993-1005.

[18] Narh, K.; Li, Z.: Morphological development during injection molding of self reinforcing composites. I: Experimental results. In: Polymer composites. Bd: 21. (2000), Nr. 5, pp. 751-761.

[19] Varga, J.; Ehrenstein, G.: Formation of [beta]-modification of isotactic polypropylene in its late stage of crystallization. In: Polymer. Bd: 37. (1996), Nr. 26, pp. 5959-5963.

[20] Lu, Z.; Zhang, K. F.: Crystal distribution and molecule orientation of micro injection molded polypropylene microstructured parts. In: Polymer Engineering & Science. Bd: 49. (2009), Nr. 8, pp. 1661-1665.

[21] Henning, S.; Michler, G. H.; Ania, F.; Baltá-Calleja, F. J.: Microhardness of a-and ß-modified isotactic polypropylene at the initial stages of plastic deformation: analysis of micromechanical processes. In: Colloid & Polymer Science. Bd: 283. (2005), Nr. 5, pp. 486-495.

Multifunctional components in vehicle space frames - Cast parts for prototypes and small series

Kretz, R.; Khalil, Z.; Simon, P.

AIT Austrian Institute of Technology, Light Metals Technologies Ranshofen, Ranshofen, Austria

Abstract

The development of light metal vehicle frame components is described by means of cast nodes. These nodes are the joining elements for the space frame sections and usually they have no additional functions. The need of saving weight and assembling effort leads to components which integrate additional functions in the joining elements. Wheel suspension mounts or energy absorbing elements are examples for additional functions in joining element. In this paper the prototype manufacturing methods of frames with casted nodes are discussed by means of various vehicle research projects at LKR. The integration of more functions in the components leads to the reduction of the number of parts in a system and to less tolerance adjustment for assembly. “Multifunctional castings” are clearly identified as a future trend in vehicle design.

1. Introduction and history

In the automotive development light weight construction has a long tradition, especially in the case of sports cars to be moved on public roads the weight has to be reduced even though these cars need a couple of technical equipment for fulfilling legal and safety requirements. In conjunction with high engine performance the reduced weight is responsible for good driving performance and sportive image.

In order to meet the requirements of environmental friendly technologies the vehicle designs have to change. Today the whole mobility development is challenged by demands of light weight, save road handling, crash safety, driver assistance systems, new drive train technologies and much more.

The first cars were developed from horse-drawn carriages, where the horse power was replaced by a combustion engine. For a long time the main assembly groups in a car chassis, body and engine were separated. The frame materials were wood which was later replaced by steel. Inspired by the upcoming aluminium and aircraft industry and the light weight design potential of this new material was recognized by the car manufacturers and soon the first car with an aluminium body was presented by NSU in 1913. But even this car, shown in Fig. 1, was built on a steel ladder frame.

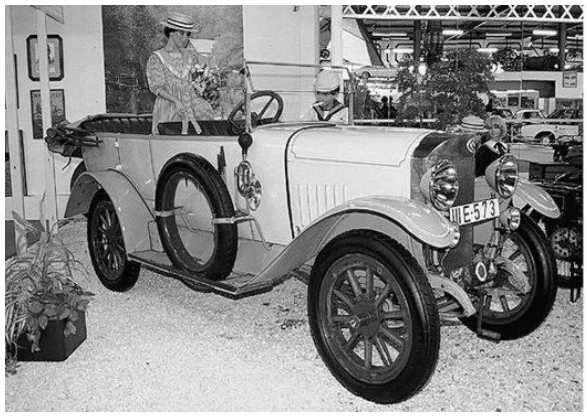

Fig. 1: *The first aluminium body car, NSU 8/24 (1913)*

In the 1920s the self-supporting steel bodies were developed using new material processing and joining technologies (Rivets, welding etc.). In Europe the Lancia, Opel Citroen developed these technique. In the United States this development was driven by General Motors [1]. At the same time sports cars with outstanding driving performance, using space frames were developed. The Mercedes Benz 300 SL and its space frame is shown in Fig. 2. This was a typical example for sports cars at the time [2].

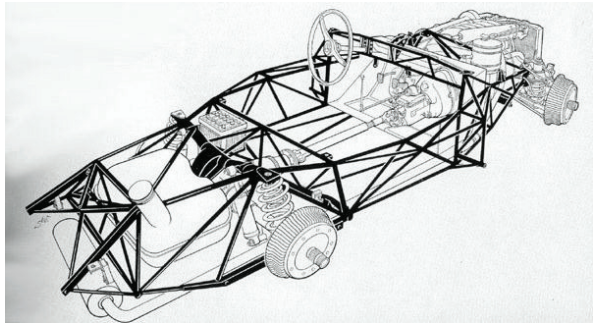

Fig. 2: *Space frame of the MB 300SL (1956) [2]*

2. Aluminium frames

In 1994 Audi launched the first A8 type, built with the ASF (Audi Space Frame) design. This design was characterised by a mix of aluminium profiles, sheets and castings. So called casted nodes were used for joining the profiles. The aim of the nodes was to join the profiles and to allow a plastic deformation in the case of a crash. Thus the castings had to provide high elongation values [3]. These mechanical proprieties could only be achieved by producing the nodes in the “Vacural” process, a special high pressure die casting method [3]. Fig. 3 shows two cast nodes of the space frame.

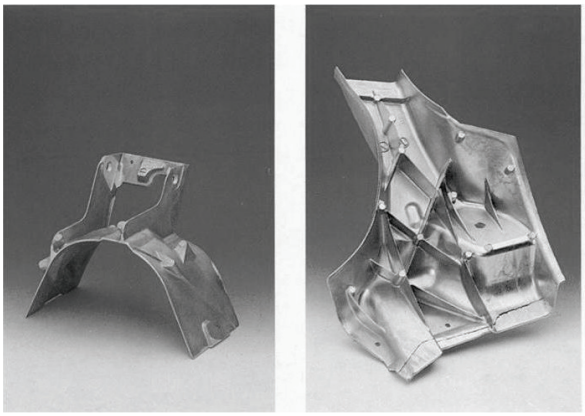

Fig. 3: *Vacural Castings [3]*

Aluminium has been rediscovered as a material for automobile production in recent time, but due to its lower Young’s Modulus compared with steel the design of aluminium vehicles had change. Various space frame and aluminium profile/sheet combinations were developed in the following years by OEMs as well as by small series car manufactures. Also in the motor bike industry the aluminium was considered for the frame design, as shown in Fig. 4. This picture shows a casted combined steering head and link bracket.

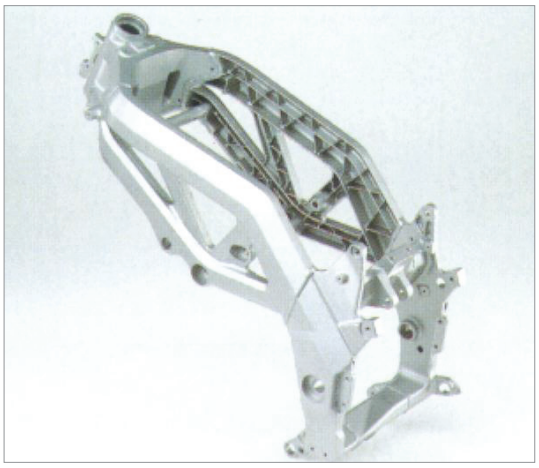

Fig. 4: *Frame – Suzuki SV 1000 from 2001*

The Suzuki frame in Fig. 4 on the one hand shows advanced lightweight design, which is typical for motorbikes and on the other hand the aluminium castings fulfil further structural support for engine components and the assembly of the bike. The frame part is thus a “multifunctional“ casting.

3. LKR prototype frames

The Clever vehicle was developed in an EC project from 2003 – 2006 [4]. The goal of the project was the development a two-seater vehicle for urban transport. Although it was a small vehicle it should meet the requirements on comfort (rain protection) styling and safety as well as on ecology and costs.

The space frame, delivered by LKR was built from standard Aluminium profiles (alloy AW 6060 T6) which were joined by aluminium nodes. The nodes were welded to the profiles. Due to high mould costs for castings the nodes for the five prototypes were made by machining, but in a series production these parts would have be produced in a casting process, like sand casting or permanent mould casting. The difference of the properties between casted and machined nodes was accepted.

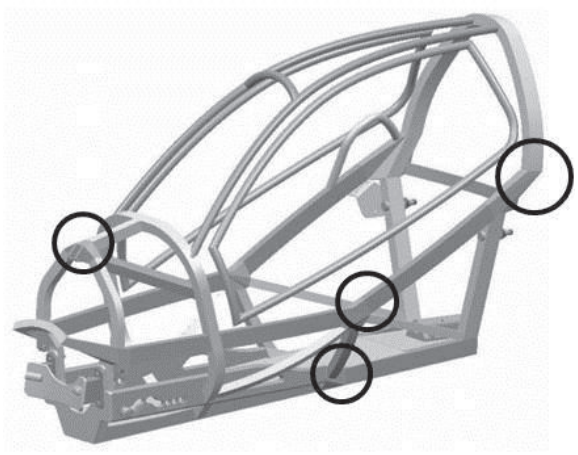

Fig. 5: *Clever space frame with machined nodes [4]*

The nodes of the Clever vehicle (see Fig. 5) had the only function to connect the aluminium profiles. But the need to additional weight savings leads to considerations about integration of various functions into the frame components. In particular, due to the proper scope for design castings are predestined for functional integration measures in a complex system like a car.

The next frame generation developed by LKR shows the first step to integration of more functions for the nodes [5]. The nodes again have to the join the aluminium frame profiles, but in addition they had to fulfil two important tasks:

a) Absorbing energy in the case of an accident

b) Wheel suspension assembly

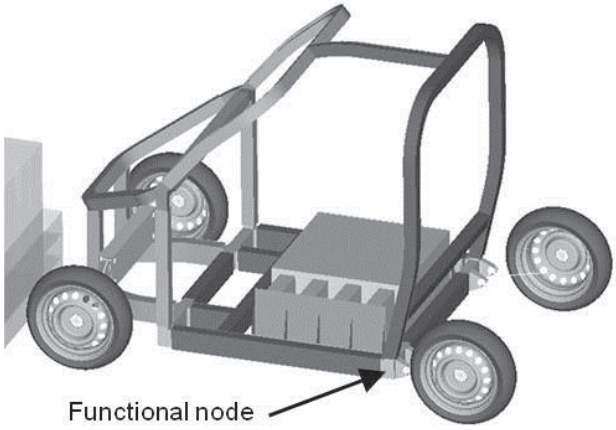

Fig. 6: *LKR „Eco-Car“ space frame [5]*

In order to ensure safe behaviour of the vehicle frame in the case of an accident, all frame components, - profiles and cast nodes as well – were designed and analyzed in compliance with the actual “state of the art” in crash structure development. Since the car was configured as an electric vehicle, the designers had to pay attention to the volume, and the weight of the batteries. In addition, the danger of electricity and battery mass had to be considered in the case of a crash because the batteries must not be any hazard for the passengers. The frame structure must be able to absorb the impact Energy and it also must ensure that the batteries are not released from their housing. Thus the frame grew to a rather stable structure.

4. Design and prototyping process selection

The process from the first sketches to the manufacturing of the frame components followed the current design and calculation paths. After definition of the possible component space, the parts were designed by CAD and subsequently transferred to the topology optimisation tool “TOSCA”. The Tosca result was a part geometry, optimised to a minimum of mass (part weight) but usually the topology optimization result is not a “cast-process-friendly” shape. Thus material shrinkage, mould incline, machining allowances and other foundry, related modifications had to be considered for the final geometry. Fig. 7 shows the sequence of the development process.

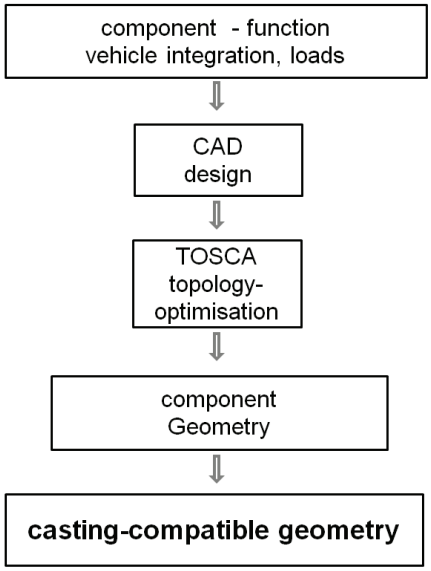

Fig. 7: *Sequence of geometry development*

After definition of the final part geometry, the mould making method and the casting process for manufacturing the nodes had to be selected. The criteria for the selection of the prototyping method were the number of required parts, the aluminium alloy, the time of delivery and the prototyping costs. A large number of possible suppliers in Austria and Germany offer the required services. After identification of potential partners a couple of moulding and casting processes, provided by eight suppliers were possibilities for making the nodes. The following process routes were considered:

- RP sand moulds from "ProMetal RCT™ printer" + low pressure die casting at LKR
- Laser sintering of moulds + casting at supplier or low pressure die casting at LKR
- Direct sand mould machining + casting at supplier
- CNC patterns, sand moulds + gravity casting at LKR
- Mild steel permanent mould + + low pressure die casting at LKR

On basis of the node "A-bottom" data (see Fig. 9) quotations were requested from the potential suppliers. As shown in Fig. 8 the most methods determine initial costs for providing the patterns or moulds, which do not depend on the number of cast parts. Just the

RP sand mould process, providing sand moulds which are directly "printed" from CAD Data by the "ProMetal RCT" printer [6] does not generate initial costs, because no patterns and moulds are necessary.

That means that this prototyping route is very economic if the number of cast parts is very low. As it can be seen in Fig. 8 the break even with conventional prototyping methods (patterns/sand moulds) lies approximately between ten and fifteen pieces.

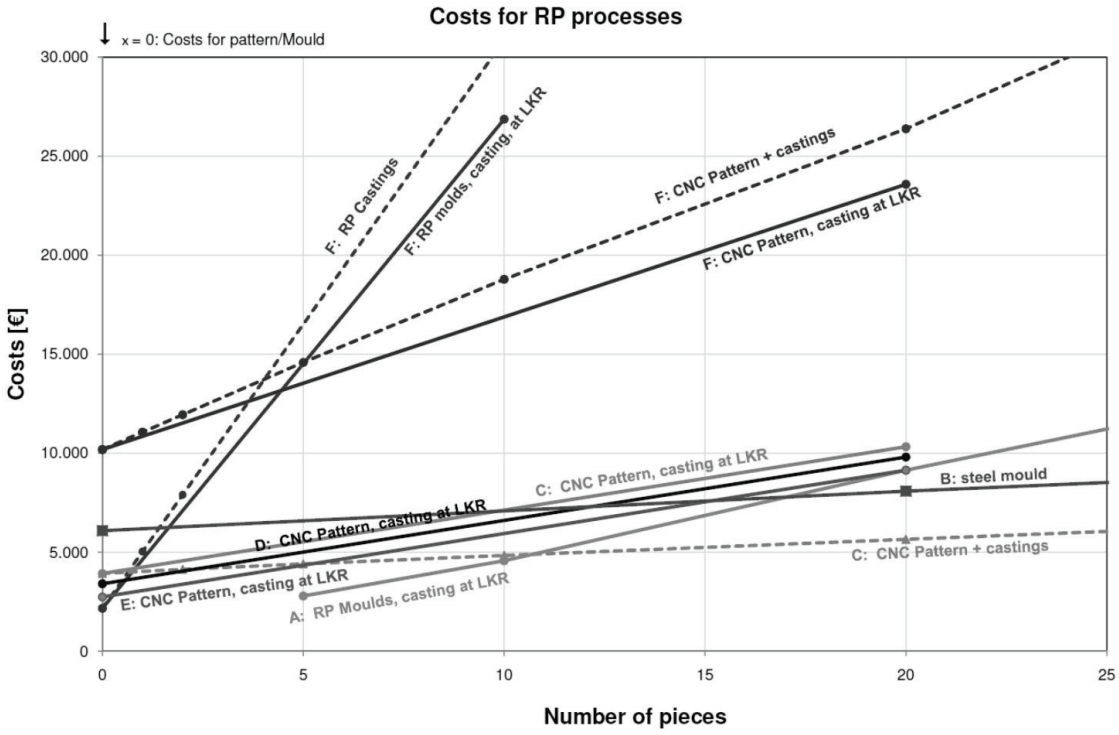

Fig. 8: *Comparison of prototyping costs*

In order to determine the feasibility of different prototyping methods, three different procedures for casting the frame nodes were selected for the three space frame nodes, two parts were cast in the aluminium alloy A356 (AlSi7Mg) and one part was cast in Magnesium AZ91 (Mg-Al9%Zn1%) according to Table 1.

Table 1: *Applied cast processes*

Node Position	Mould	Cast process	Alloy
A-column bottom	mild steel mould + sand core	LPDC perm. Mould	AlSi7Mg
B-column bottom	Prometal RCT™ printer + core	LPDC sand mould	AlSi7Mg
A-column top	Wood pattern sand mold +cores	Gravity sand cast	Mg-AZ91

All three prototyping methods led to sound castings. The functional castings could be cast from Aluminium A356 in a mild steel mould and in “printed” sand moulds by low pressure die casting (LPDC) on a Kurtz AK92 machine and in Magnesium AZ91 in gravity sand casting (conventional made sand mould) as well.

The moulds and the casted nodes are shown in Fig. 9 - 11.

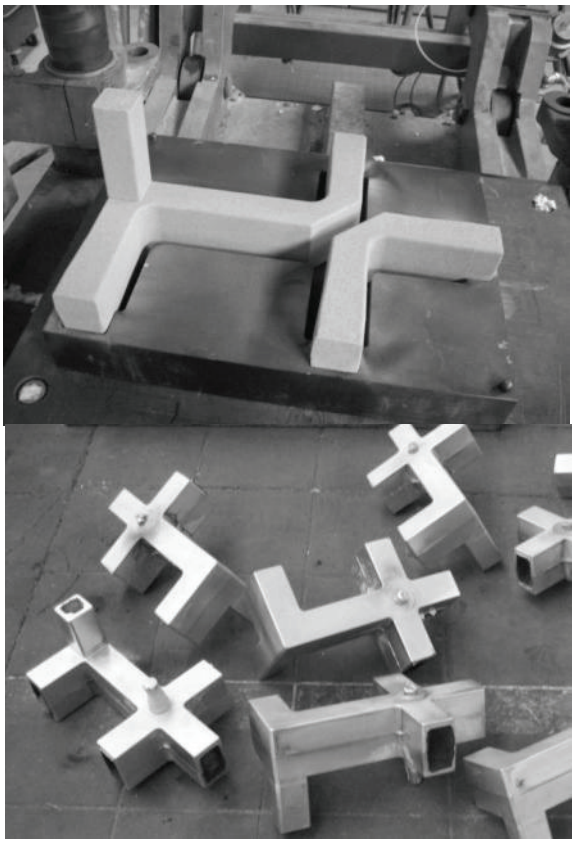

Fig. 9: *Node A-column bottom, steel mold with sand core + castings*

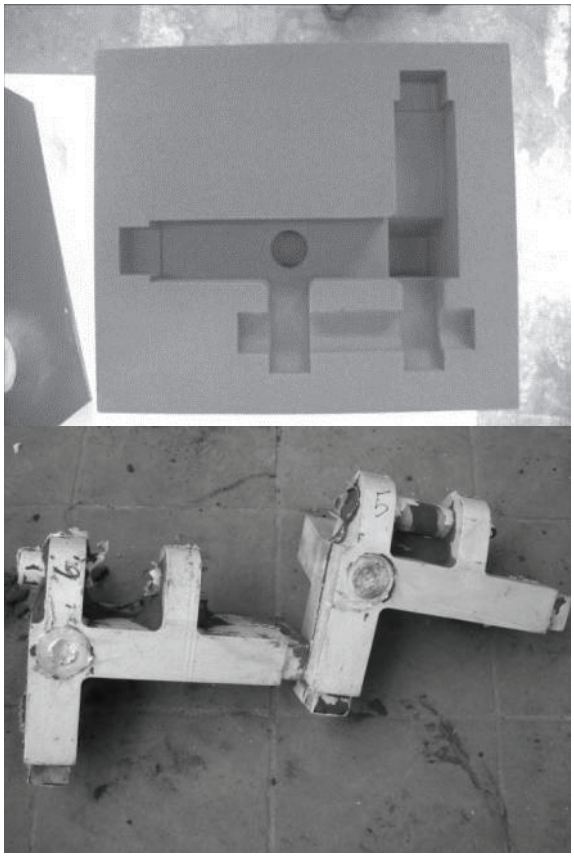

Fig. 10: *Node B-column bottom, printed” sand mould + castings*

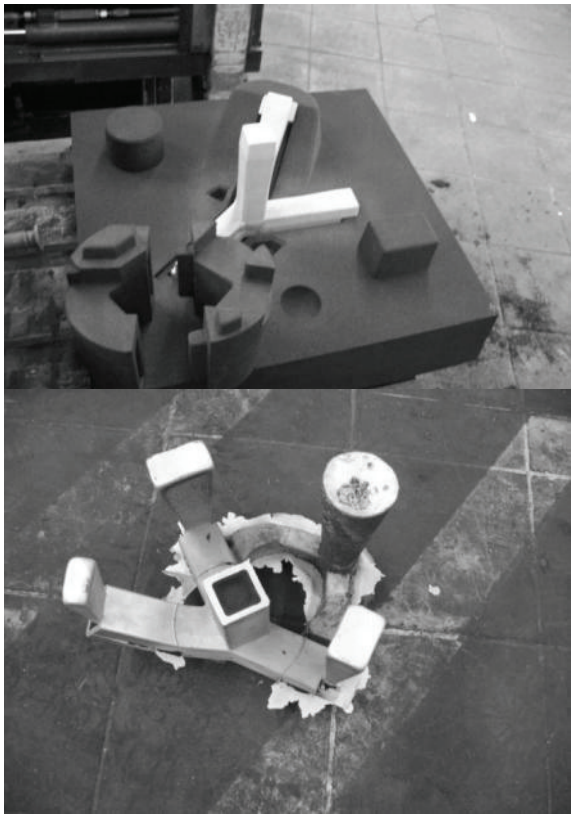

Fig. 11: *Node A-column top, sand mold + Mg castings*

5. Summary and outlook

Multifunctional castings will be major parts of vehicle structures in future. Compared with formed sheets the castings allow a wider scope of geometry. Complex functional elements like mountings for suspension, brakes, hinges etc. can be integrated in castings. On formed sheets the functional elements have to be joined in separate process steps. That leads to a larger number of parts, additional process steps for joining and machining and additional effort in compensating tolerances.

Possible functions, which could be integrated into the castings, are for e.g. mounts for hydraulic or/and electrical devices, lines but also sensors for faults or damage of parts. Considerations about damage sensors in frame components as an alarm information in case of accidents led to an EC project proposal by an international consortium in 2007 [7].

A couple of rapid prototyping methods are can be applied for casting sound structural cast parts. Besides the Conventional cast processes new prototyping methods provide dimensionally accurate sand moulds which are available in very short delivery times. Theoretical, working with sound CAD data from a component, the prototype can be completed within a few days. The methods are suitable for aluminium alloys as well as for magnesium.

6. Acknowledgement

The authors would like to thank The Austrian Institute of Technology (AIT) for the financial support in this project.

Literature

[1] http://de.wikipedia.org/wiki/Karosserie

[2] http://www.w198.de/de/technik-2

[3] http://www.mueller-wengarten.de, 2001

[4] Kretz, R.: Prototypfahrzeug „Clever“ Buchbeitrag: Leichtbau: Prinzipien, Werkstoffauswahl und Fertigungsvarianten, Hrsg. H.P. Degischer, S. Lüftl, Wiley-VCH Verlag GmbH&Co KGaA, ISBN 978-3-527-32372-2, 2009, pp. 327-339

[5] P. Simon: Methoden zur Entwicklung einer Kleinserien-Leichtfahrzeugstruktur in Space Frame Technologie, Grazer Safety Update 2009

[6] http://www.prometal-rct.com/en/products/s-max.html

[7] Lesemann, M.: Project Proposal, Intelligent Rescue Support , Proposal iRESCUE, Collaborative Project, FP7-SST-2007-RTD-1, RWTH Aachen 2007

Energy harvesting by means of integrated piezoelectrics

Juuti, J.; Sobocinski, M.; Palosaari, J.; Leinonen, M.; Jantunen, H.

University of Oulu, Microelectronics and Materials Physics Lab, Oulu, Finland

Abstract

In this paper two different piezoelectric energy harvester components are presented. First harvester is based on 10 µm thick AlN films on silicon cantilevers where two different structures were tested while in the other approach bulk PZT integrated with LTCC package was realized. In the both cases power generation of harvesters was characterized as a function of resistive load at their first bending resonance frequency. The maximum RMS power density per 1 g acceleration with the optimal load for the active material was 2.2-19.7 $\mu Wg^{-1}cm^{-2}$ and 2.2-19.7 $mWg^{-1}cm^{-3}$ for the AlN harvester. Corresponding values of 20.0 $\mu Wg^{-1}cm^{-2}$ and 0.5 $mWg^{-1}cm^{-3}$ were obtained for LTCC-PZT harvester. Generated powers are already sufficient to supply continuous temperature and 3-axis acceleration measurements while the power output can be increased by further optimization. The results pave a way for the autonomous sensors by means of compact piezoelectric energy harvesters that could be utilized even as integrated structural elements in future.

1. Introduction

In recent years, energy harvesting has gained significant attention in research and development in order to decrease the need of batteries or extend their lifetime. This is especially crucial in wireless sensor systems that can be located into structural elements or other places that are not accessible or very difficult or expensive to access. At the same time sensors and wireless data transfer is becoming less energy consuming thus enabling truly wireless autonomous sensor systems to be implemented for e.g. condition monitoring of machines and vehicles or even environment. Piezoelectric harvesters are good candidate for compact low power harvesters especially for places where vibrations are present. [1-2] However, efficient utilization requires careful optimization of the materials, structures and electronics while specifications vary greatly depending on the environment (harsh substances, high temperature, very high accelerations, etc.) where they are applied.

In this paper, characteristics of two different piezoelectric energy harvesters are presented based on piezoelectric AlN and PZT materials. Their generated power and operation was analyzed and properties in terms of energy density are discussed.

2. Experimental

AlN cantilever harvesters were provided by TU Dresden. Structures with and without 500 nm thick SiO_2 buffer layer were realised on 500 µm thick silicon substrates. The substrates were covered by 150 nm thick Al bottom electrode for easy electrical access. A (001)-textured AlN layer of a thickness of 10 µm was reactively sputtered on top of the bottom electrode. A contact mask was applied for the Al top electrode in order to have smaller dimensions than AlN layer (Fig. 1) and to ensure the electrical isolation. As-deposited structures were investigated without any additional annealing.

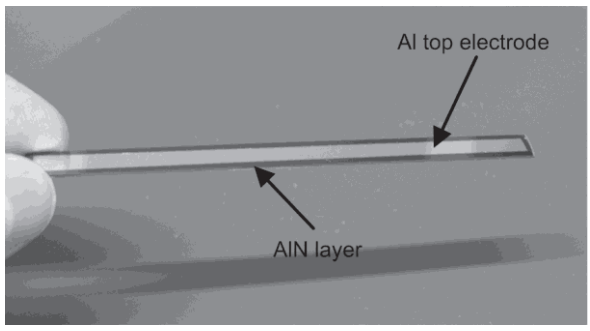

Fig. 1: *Manufactured AlN-silicon cantilever harvester 98x10.1 mm^2*

Commercial piezoelectric bulk ceramic PZ29 (Ferroperm A/S, Denmark) disc was used for LTCC-PZT harvester. The disc (∅ 25 mm) with thickness of 375 µm was laser cut (Siemens Microbeam 3200, Siemens AG, Germany) into designed shape having 3 individual beams each tuned for slightly different resonance frequency for extended operation bandwidth. After laser cutting LTCC tape Heraeus Heralock 2000 (W.C. Heraeus GmbH, Germany) with the same shape with PZT was laminated onto the bottom of the

bulk ceramic in order to create monomorph structure. Subsequently, LTCC base and lid was laminated into pre-laminated LTCC-PZT structure. Both laminations were carried out at 75 °C temperature under 100 bar pressure for 10 min. After laminations the harvester structure was fired in a Nabertherm box furnace (Nabertherm GmbH, Germany) the fired LTCC-PZT sample is shown in Fig. 2. Finally poling of samples was carried out under 2.5 V/µm electric field at 60 °C for 30 min. Details of the process can be found elsewhere [3].

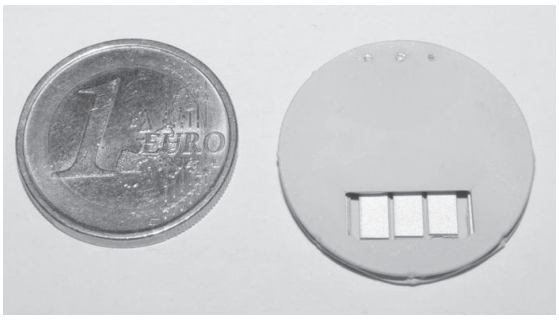

Fig. 2: *Picture of fired LTCC-PZT wideband energy harvester*

Both harvesters were characterized by using fiber-optic laser vibrometer OFV-5000 (Polytec GmbH, Germany) for displacement measurement and its adjustment while electromagnetic mini shaker (Bruel & Kjær, Denmark) was used to generate 5.0 µm and 1 µm peak-to-peak displacement as a function of frequency for AlN and PZT harvesters, respectively. The first bending resonance frequency of the harvesters was measured after which the power generation was measured as a function of resistive load.

3. Results and discussions

Displacement of the tip of the AlN-Si cantilever as a function of frequency with 5 µm base excitation is shown in Fig. 3. The sample exhibited sharp resonance peak typical for piezoelectric cantilevers. Level of 3 dB decrease in energy is shown in Fig. 3 corresponding to mechanical Q factor of 26.3 and ±1.5 % frequency bandwidth from the centre frequency. Efficient piezoelectric energy harvesting is inevitably related to the resonance of the components and therefore limited by the narrow bandwidth of the cantilever type harvesters or otherwise the source of the vibration has to be very stable in the practical conditions.

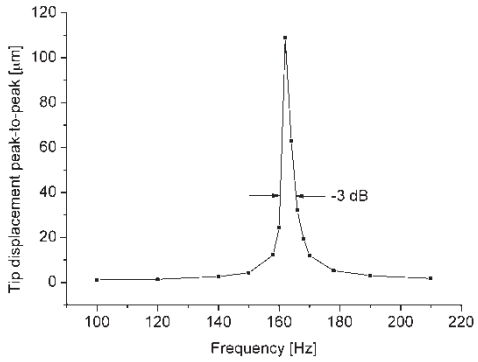

Fig. 3: *Tip displacement of the AlN-Si cantilever as a function of frequency under 5 µm peak-to-peak excitation of the base.*

Alternatively, one can realise multiple beams like in the case of LTCC-PZT harvester where bandwidth for the -3 dB power level was ±2.7 %. For this case the maximum bandwidth of ±3.75 % could be obtained by more consistent fusion of the resonance peaks of the 3 cantilevers whereas all individual peaks are still clearly visible in Fig. 4.

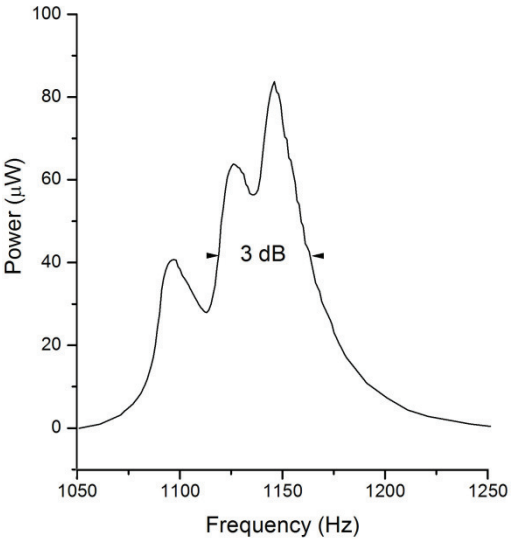

Fig. 4: *Generated peak power for 39.9 kΩ resistive load by the LTCC-PZT harvester as a function of frequency.*

RMS power of the AlN-Si cantilever harvesters is depicted in Fig. 5. Samples 2-1 and 2-2 having a SiO_2 layer underneath the AlN and Al electrode required clearly higher output impedance compared to samples without the layer. Low performance of sample 2-3 without apparent peak in the power suggests the internal defect in the sample. The influence of the optimal electrical load is even more pronounced in the case of LTCC-PZT harvester shown in Fig. 6. Optimum resistive load produced about 15 times greater power thus electrical conditions are as crucial as mechanical ones in order to get the best performance.

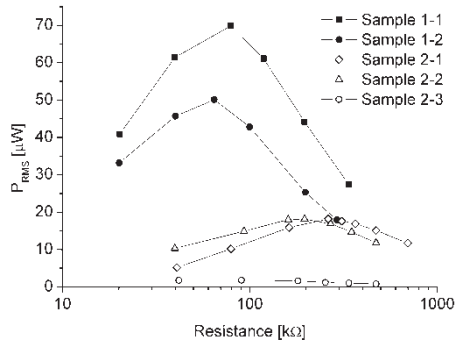

Fig. 5: *Generated RMS power at resonance frequency by AlN-Si cantilever as a function of resistive load.*

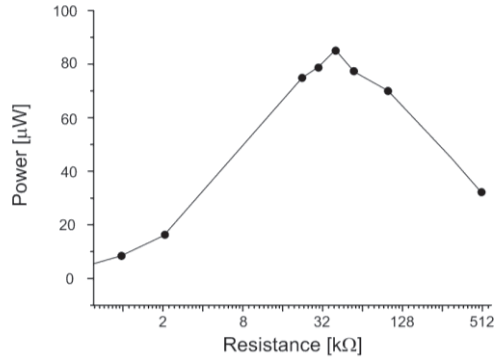

Fig. 6: *Generated RMS power by LTCC-PZT harvester at resonance frequency as a function of resistive load.*

Generated powers and power densities for area and volume of active materials of the harvesters are shown in Table 1.

Table 1: *RMS power and power density of the active material in AlN-Si and LTCC-PZT harvesters at resonance with optimal resistive load*

Sample	***P_{RMS} [µW]***	***RMS power density of active material for area and volume normalized for 1 g acceleration [$\mu Wg^{-1}cm^{-2}$] [$mWg^{-1}cm^{-3}$]***
1-1	*69.9*	*3.8 / 3.8*
1-2	*50.1*	*2.3 / 2.3*
2-1 with SiO_2	*18.2*	*19.7 / 19.7*
2-2 with SiO_2	*18.1*	*10.6 / 10.6*
2-3 with SiO_2	*1.8*	*2.2 / 2.2*
LTCC-PZT	*85.0*	*20.0 / 0.5*

As can be seen LTCC-PZT harvester produced the greatest power up to 85 µW while samples with and without SiO_2 layer produced 78.6-97.9 % and 17.8-41.1 % less power, respectively. However, when taking into account the area, volume and acceleration, i.e. applied force, it is observed that AlN-Si samples with SiO_2 outperform samples without it. At the same time they exhibit power density for area very close to that of LTCC-PZT harvester although it should be noted that operation of this harvesters is extended for the wider frequency range. Interestingly, all AlN-Si samples exhibit higher power densities than LTCC-PZT harvester when volume of the active material is considered. This suggests that AlN may partly compensate its significantly lower volume and piezoelectric coefficients [4] by higher efficiency via greater stresses in the AlN.

Nevertheless, the harvesters already exhibit power levels feasible for various sensor applications, for example LM19 temperature sensor (National Semiconductors, USA) and LIS3DH 3-axes accelerometer (STMicro-electronics, Switzerland) requires only 24 µW and 27.5 µW (50 samples/s, typical settings) of power, respectively [5-6]. Moreover, the generated power is a function of acceleration as well as size of the harvester which can be much greater in real environment than presented here.

Recently, AlN based energy harvester was developed by Elfrink *et al.* where AlN cantilever with size of 5.0x5.0 mm^2 and thickness of 0.8 µm was used together with seismic mass. Cantilever part where active material was locating was thinned to 45 µm by etching. Maximum power output of the harvester was 60 µW at 2 g acceleration while it was decreased to 22 µW and 2.1 µW with open and closed packaged, respectively. [4] This gives power density of 4.2-120 $\mu Wg^{-1}cm^{-2}$ and 10.5-150 $mWg^{-1}cm^{-3}$ for area and volume, respectively. It is clear that design of the structure can influence figures of merits greatly, for example by adopting seismic mass and thinned parts in the area of the active material can increase stress levels significantly. In spite of this the presented values already exhibit competitive results while larger power output can be expected in the future by further designing based on thicker AlN elements i.e. larger volume of the active material.

4. Summary

Efficiency of the piezoelectric energy harvesters depend greatly from the mechanical resonance of the structure which can be expanded by multiple beam topology. The power output of the harvesters depend also strongly from the electrical conditions i.e. impedance matching between the piezoelectric source and the output. AlN and PZT based harvesters exhibited already feasible power levels for sensor applications with small power consumption while applications specific designing can produce more efficient

solutions. Although LTCC-PZT harvester based on bulk PZT exhibited the highest power levels the AlN films obtained higher or similar power densities with normalised acceleration levels. This paves a way for more efficient utilisation of such materials especially when relatively thick and large areas can be easily produced.

5. Acknowledgement

The authors gratefully acknowledge funding of the Scientific Advisory Board for Defence – MATINE (projects EKKO 15/Mdd745/08 and Pi-Ener 15/Mdd760/09). Authors MS and JJ acknowledge funding of the Infotech Oulu Graduate School and Finnish Foundation for Technology Promotion and Academy of Finland (project 124011), respectively. The authors thank G. Suchaneck (TU Dresden) for providing the AlN harvesters.

References

[1] Anton, S.R.; Sodano, H.A.: A review of power harvesting using piezoelectric materials (2003–2006). In: Smart Mater. Struct., 16 (2007) 3, pp. R1-R22

[2] Beeby, S.P.; Tudor, M.J.; White, N.M.: Energy harvesting vibration sources for microsystems applications. In: Meas. Sci. Technol., 17 (2006) 12, pp. R175-R195

[3] Sobocinski, M.; Leinonen, M.; Juuti, J.; Jantunen, H.: Monomorph piezoelectric wideband energy harvester integrated into LTCC. In: J. Europ. Ceram. Soc., 31 (2011) 5, pp. 789-794

[4] Elfrink, R; Kamel,T.M.; Goedbloed, M.; Matova, S.; Hohlfeld, D.; Andel, Y.; van Schaijk, R,: Vibration energy harvesting with aluminum nitride-based piezoelectric devices. In: J. Micromech. Microeng., 19 (2009) 9, p. 094005

[5] National Semiconductors, LM19 datasheet January 26, 2010, cited 22.11.2010

[6] LIS3DH datasheet, Doc ID 17530 Rev 1, 1-42, May 2010, STMicroelectronics

Integration of piezoceramic sensors and actuators into structural components via high pressure die casting

Klassen, A.[1]; Rübner, M.[1]; Ilg, J.[2]; Rupitsch, S. J.[2]; Lerch, R.[2]; Körner, C.[1]; Singer, R. F.[1]

[1]*Friedrich-Alexander Universität Erlangen-Nürnberg, Chair of Metals Science and Technology, Erlangen, Germany*
[2]*Friedrich-Alexander Universität Erlangen-Nürnberg, Chair of Sensor Technology, Erlangen, Germany*

Abstract

The effect of the fabrication procedure on the functionality of piezoceramic patch transducers that are integrated into a light-weight component by high pressure die casting is investigated. It is demonstrated experimentally that a successful integration can be realized by the use of a suitable supporting structure. This structure also enables the off-centre position of the transducer inside the casting. We accomplished to numerically simulate the integration, including mould fill and infiltration of the supporting structure. The numerical results show that under certain process conditions an inhomogeneous infiltration occurs, which may cause mechanical damage of the transducer. Impedance measurements are performed to study the transducer's functionality after the integration.

1. Introduction

Light-weight construction is currently a focus of research and development in the automotive and aerospace industry to save weight and reduce fuel consumption. Health monitoring as well as the control of vibrations are desired features to enhance the functionality of such light-weight components without causing any significant changes in the weight or the structural stiffness. These structures, referred to as smart structures, can be realized through use of additional active elements, often in the form of thin lead zirconate-titanate (PZT) wafers operating as actuator and sensor. To investigate the feasibility of structural vibration control, it is state-of-the-art to bond such PZT components onto the light-weight structure's surface. The performance of these composites is frequently verified and published [1-3]. The integration of active components into light-weight structures is another promising approach to produce smart composites. Compared to the bonding procedure, the PZT element is embedded and thus protected against external influences like moisture and foreign object damage. Consequently, the composite structure can be exposed to various external loads and harsh environmental conditions without any loss of performance. The challenge in integrating the functional component is both the damage-free integration and the exact positioning of the ceramic inside the light-weight component. Especially the positioning off the neutral axis is important in order to enable bending actuation for controlling vibrations.

The integration into metallic light-weight structures by casting is a novel field of interest. A number of casting methods are established for processing light metals like aluminium or magnesium alloys. High pressure die casting (HPDC) is economically the most significant casting process for the fabrication of thin-walled components. It comprises the injection of liquid metal into a permanent mould at high pressure and velocity.

For the successful fabrication of aluminium die castings with integrated piezoceramic sensors and actuators a supporting structure is necessary to prevent damaging during the highly dynamic mould filling and to place the modules accurately inside the cavity. Therefore, the supporting structure must satisfy certain requirements. In particular, the mechanical permeability has to be sufficient for a complete infiltration with liquid metal to achieve a total integration of the active element. Second, the mechanical stability has to be high enough to withstand the melt injection pressures without deformation. Third, the positioning of the piezoceramic module off the neutral axis has to be realized without additional effort. Expanded metal fulfils all these requirements. It is available in a multiplicity of geometries and dimensions. Hence, it is well suited for this particular application [4,5].

This contribution focuses on the verification of the effect of the fabrication procedure including mechanical loads during the cavity fill on the condition and the functionality of the piezoceramic element. Furthermore, the module position is varied to identify the feasibility of the positioning close to the structure's surface.

2. Experimental procedures

2.1 Fabrication

The cold chamber die casting machine FRECH DAK450/54 was employed for the fabrication of the castings with integrated piezoceramic sensors and actuators. The locking force of the machine is 450 tons. Additionally, a FONDAREX vacuum system was connected to the mould in order to evacuate the cavity during the injection of molten metal. This system enabled the fabrication of castings with minor gas porosity. The mould was designed to cast plate-shaped components with dimensions of 178 mm x 178 mm and a wall thickness of 4 mm. All experiments were performed using the standard aluminium casting alloy 226D (AlSi9Cu3(Fe)). The mould temperature was 150 °C, the maximum plunger velocity during mould filling was 2 m/s.

The PZT elements used for the integration are piezoceramic patch transducers (brand name: DuraAct, distributor: PI Ceramic GmbH, Lederhose, Germany) consisting of a thin PZT-layer, contacting and polymeric embedding.

The expanded metal inserted as supporting structure for the piezoceramic modules consists of Al99.5. Three layers of this structure were required to mount the patch transducers securely inside the cavity. The transducer was arranged between two cover layers of the expanded structure to define the position in the through-thickness direction. The third intermediate layer was designed as a frame and served to laterally hold the patch in place. The thickness of the complete insert was adapted to the wall thickness of the casting by machining both cover layers prior to assembling the insert.

The insert with transducer and supporting structure was placed onto ejector pins inside the cavity before mould closure, Fig. 1. When the mould was closed, the pins were retracted, leaving the insert in the desired position solely by clamping between the cover and the ejector die half. The insert is constructed in a manner that allows the clamping forces to act on the frame layer but not on the piezoceramic component, so that mechanical damage of the patch is avoided during this step of the fabrication procedure.

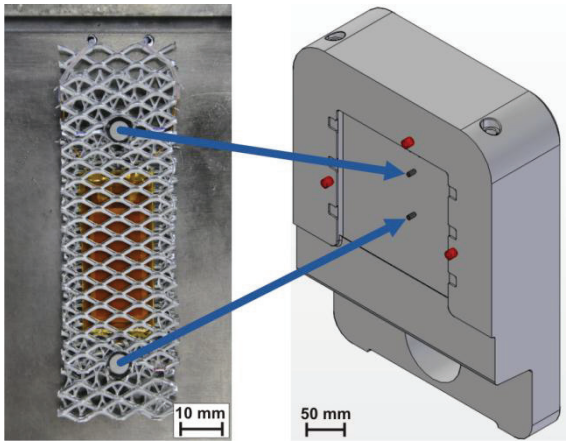

Fig. 1: *The insert, consisting of the piezoceramic module and three layers of expanded metal, is positioned onto two ejector pins inside the mould.*

The realization of the positioning of the piezoceramic components off the neutral axis could be achieved by the use of cover layers with different thicknesses [6]. For the experimental work discussed in this paper, the patch transducer was displaced in three steps off the neutral axis towards the surface of the casting. Fig. 2 schematically shows this displacement with corresponding dimensions.

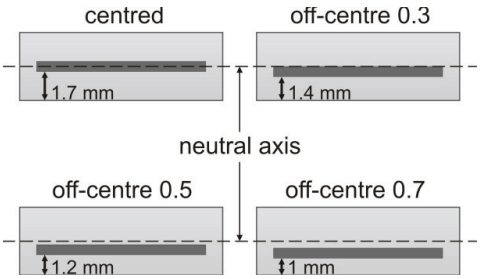

Fig. 2: *Experimentally realized positions of the patch transducer (dark grey) in the through-thickness direction of the casting (light grey) with a wall thickness of 4 mm.*

It should be noted that the thickness of the thinner cover layer cannot be reduced to below 1 mm. A very thin expanded metal layer fails to withstand the relatively high melt injection pressures during the cavity fill because of its lowered stiffness, and hence deforms. As a result, a supporting effect is no longer obtained.

2.2 Characterization

All castings with integrated module were radiographed employing a ct-Alpha big system to verify the condition of the piezomodule inside the casting. Therefore, the piezoceramic foil of the module was divided into six sections, Fig. 3.

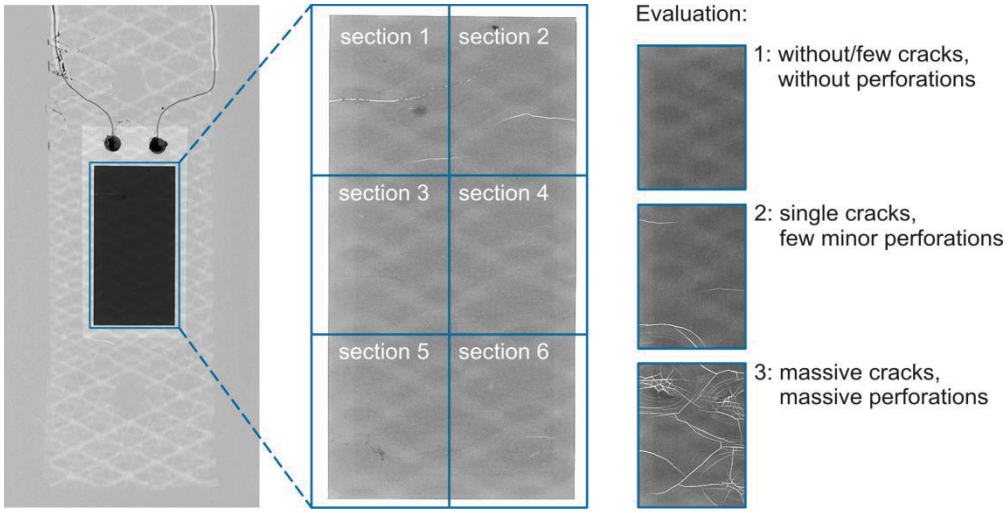

Fig. 3: *Radiograph of an integrated piezoceramic module. The PZT-foil of the module is divided into six sections to evaluate the condition of the ceramic after the fabrication process.*

Every section was evaluated depending on the degree of mechanical damage of the PZT. Rating 1 is a section without damage, rating 3 is a section with many cracks and massive perforations.

The degree of damage to the piezoceramic transducer can be assessed by means of its electrical impedance. This low-level signal cannot be used to characterize the complete smart component, but it is sufficient to demonstrate the functionality of the PZT-element. The measurements were carried out with an impedance analyzer (HEWLETT PACKARD HP4194) within the 10 – 200 kHz frequency range. The progression of the impedance versus frequency depends on the material parameters as well as on the geometrical dimensions of the transducer. In order to investigate the influence of the fabrication procedure on the patch transducer, the aluminium matrix first has to be removed from the PZT module. Otherwise the resonances are almost undetectable when the patch transducer is integrated in the casting [7]. The suppression of the resonances in the integrated state is actually based on the clamping of the transducer inside the casting and should not be misinterpreted as damage in the PZT foil.

The electrical impedance is measured for the four experimentally realized positions of the transducer (Fig. 2).

2.3 Simulation of the infiltration process

Numerical investigations of the form filling and the infiltration of the expanded metal were carried out using the commercial computational fluid dynamics software Flow-3D (Flow Science Inc., Santa Fe, NM, USA). The interaction of the molten metal with the mould during the mould-filling operation is expected to greatly affect the flow pattern of the melt at the time it hits the module insert. From this arises the need to simulate the hydrodynamic and thermal history of the melt as part of the analysis. To address this issue properly, the three-dimensional reproduction of the die casting mould was developed in a way that it includes the following elements:

- the PZT module and the supporting structure, whereby the intermediate layer has been omitted
- the cavity holding the insert
- the runner and gating system
- the shot chamber
- the plunger that forces the melt into the die

The initial state ($t = 0$) of the simulation is the time at which the plunger begins to move. Thereby, the melt is assumed to be fully at rest after it has been poured into the shot chamber. The temperature of the mould and the insert was set to 150 °C, that of the melt to 650 °C. The latter has been determined by taking temperature measurements using a thermocouple. Additionally, isothermal simulations where the heat transfer between the melt and the solid surfaces has been disabled were carried out.

3. Results and discussion

Die cast parts with integrated patch transducers were fabricated employing conventional die casting techniques. The castings show a good surface quality and complete infiltration of the supporting structure [6].

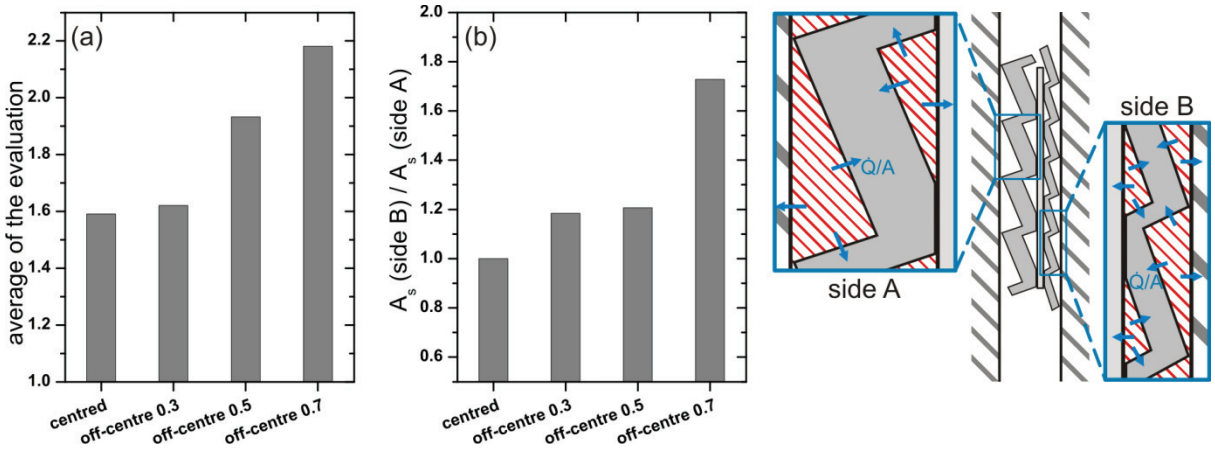

Fig. 4: *Average of the evaluation of the ceramic state according to Fig. 3 and the ratio of the specific contact surfaces of both cover layers for the different realized positions. The scheme on the right side clarifies the heat flow from the liquid metal into the mould, the module and the different cover layers.*

The condition of the integrated modules for different positions is analysed by averaging the ratings of the sections. Fig. 4 (a) shows the average values of the evaluation for the four patch transducer positions. A variance from the rating 1.0 is already detectable for the centred modules. This means, there are some cracks in the PZT-foil caused by the mechanical loads during mould filling. However, the manufacturer of the modules states, that cracks don't influence the performance of the module as long as all single parts are contacted and not shifted against each other [8].

The displacement of the modules off the neutral axis raises the extent of damage. Especially for the positions *off-centre 0.5* and *off-centre 0.7*, the damage is directly related to the centre offset, more and more perforations can be observed.

The damage patterns can largely be attributed to an inhomogeneous infiltration of the insert during the mould fill. This inhomogeneity is believed to originate from differences in the structure of the expanded metals. An appropriate indicating value for this difference is the ratio of the void volume of the expanded metal V_f that has to be occupied by melt (red shaded areas in Fig. 4) and the area of contact A that determines the extraction of heat from the incoming jet of molten metal (blue arrows in Fig. 4). This ratio is called specific contact surface A_s and can be expressed as

$$A_s = \frac{A}{V_f} \quad (1)$$

The ratio of the specific contact surfaces of both cover layers is crucial for the course of infiltration. Fig. 4 (b) shows this ratio for the realized positions. A_s differs from the value 1 with increasing distance from the neutral axis. The higher the imbalance between both specific contact surfaces, the higher the degree of inhomogeneous infiltration. In general, the specific contact surface is directly related to the time the melt takes to cool and finally to solidify. The onset of solidification and further decrease in melt temperature will initiate an increase in viscosity which, in turn, will lead to a significant local deceleration of the melt flow.

In the case of a uniform infiltration of the insert, a condition of equilibrium between the two forces acting in opposite directions upon the module would be maintained until mould filling is complete. However, since the flow velocity inside the thin expanded metal layer is expected to be considerably lower than that of the thick layer, an imbalance in the forces will establish in the course of the infiltration, giving rise to a net force greater than zero. This net force exerted on the module can locally exceed the bending strength of the PZT ceramic and will cause damage in the form of fractures or, less frequently, perforations.

Our theoretical prediction of the damage mechanism is compared to results obtained in fluid flow simulations. If the module is positioned in the neutral axis of the casting, both layers of expanded metal are nearly symmetrically infiltrated, Fig. 5. A similar infiltration behaviour can be observed if an insert with the module being located off-centre is placed inside the die cavity and if any heat exchange between the melt and the die as well as the insert is neglected. The isothermal numerical calculations show that the infiltration is independent of the type of expanded metal utilized; both the thick and the thin layer are infiltrated over the same time interval. In contrast, when considering the loss of heat due to heat transfer to the die and

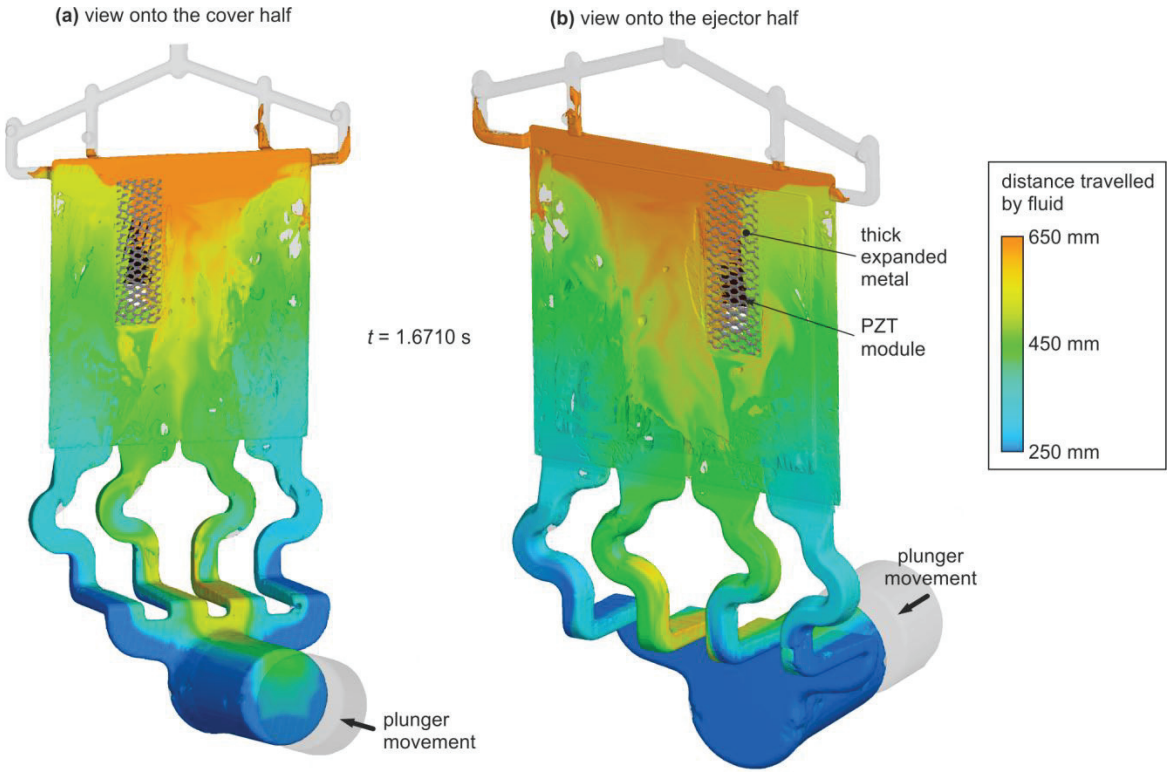

Fig. 5: *Numerical simulation of the mould fill for a patch transducer being located in the neutral axis of the casting. Time t = 0 marks the initial state of the simulation at which the plunger begins to move forward.*

the insert the influence of the fraction solid on infiltration kinetics becomes apparent. At the beginning of the infiltration process, when the molten metal starts to penetrate the region around the module, the melt in both layers of the expanded structure shows a similar flow pattern, Fig. 6 (a). As cycle time progresses, differences in infiltration length become increasingly pronounced. Thus, while for the thick expanded metal layer complete infiltration is obtained, the thin layer still exhibits a non-infiltrated region in the lower section, Fig. 6 (b) and (c). The time period within which a net force greater than zero may develop and, as a consequence of this, may

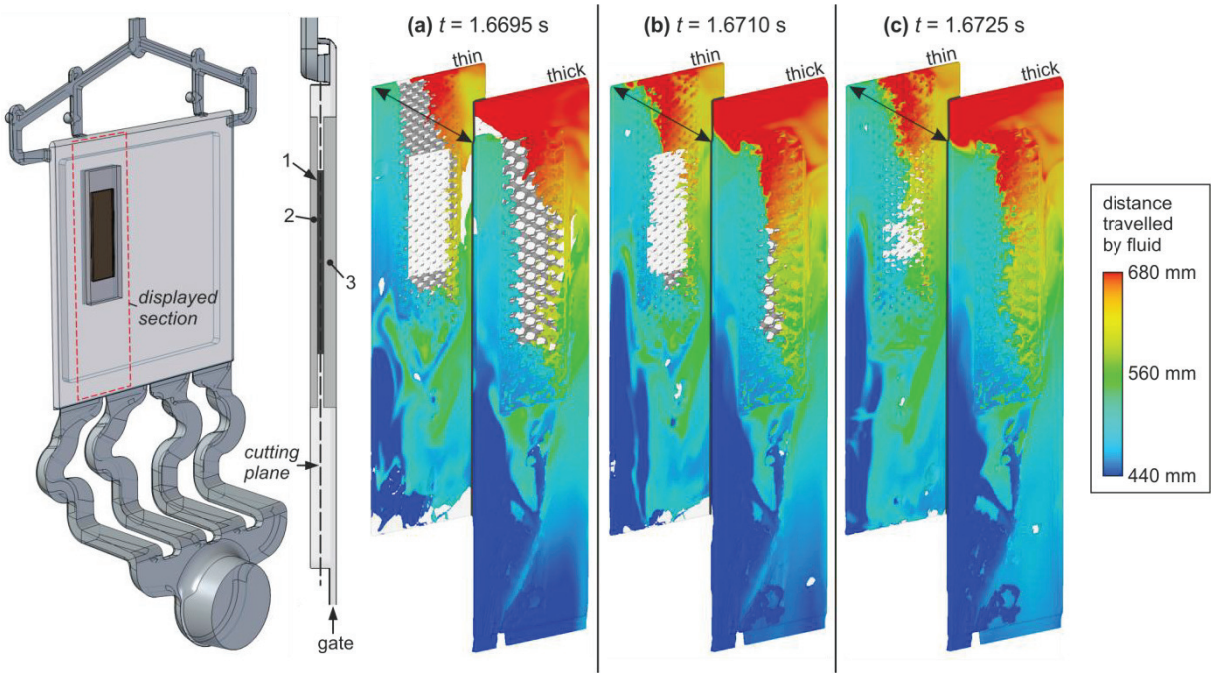

Fig. 6: *Numerical simulation of the mould fill for a patch transducer being located at the position off-centre 0.7. Numbers in brackets denote (1) the patch transducer, (2) the thin and (3) the thick expanded metal layer. Time t = 0 marks the initial state of the simulation at which the plunger begins to move forward.*

damage the ceramic was numerically determined to be between 3 and 4 ms. This delay in infiltration may seem negligible at first, but compared to the mould-filling time of around 20 to 25 ms, it is of considerable significance.

Impedance measurements are performed to identify the influence of the extent of mechanical damage of the PZT foil onto the functionality, see Fig. 7. Two resonances are expected in the considered frequency range. The first one is the resonance in longitudinal direction, the second one the resonance in lateral direction.

For the centred position, the resonance couple in lateral direction resembles that of the as-received state [7]. This demonstrates that no substantial depolarization of the PZT ceramic occurs during the fabrication procedure and hence proves that the transducer is still operational. The effect of the position in the through-thickness direction by means of impedance measurements on transducers that have been separated from the metal matrix is shown in Fig. 7.

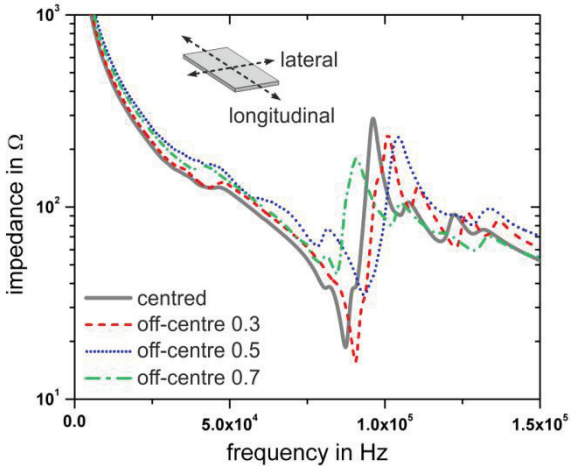

Fig. 7: *Impedance against frequency of the active PZT element for the different positions shown in Fig. 2 after cutting off the matrix.*

The impedance curves indicate that an increase in the displacement of the transducer off the neutral axis towards the surface of the casting involves a decrease in the local resonance amplitude compared to the centred position and therewith a degradation of the transducer's performance. This observation is in agreement with the extent of damage depicted in Fig. 4.

4. Conclusions

Smart composite structures with integrated patch transducers were successfully fabricated by high pressure die casting. The secure placement of the piezoceramic modules inside the die cavity was accomplished by sheets of expanded metal. The realization of an off-centre position required the concurrent use of different types of expanded metal. However, this led to an inhomogeneous infiltration of the module insert, which is the reason for the mechanical damage of the PZT foil. Measurements of the electrical impedance demonstrated that, despite the higher degree of damage, the smart composite structure is still operational.

5. Acknowledgement

The underlying research is gratefully supported by the German Research Foundation (DFG) as part of the special research field SFB/TR 39.

References

[1] *Edery-Azulay L, Abramovich H.: The integrity of piezo-composite beams under high cyclic electro-mechanical loads – experimental results, Smart Mater Struct, 2007, 16, pp. 1226-1238*

[2] *Thielecke B, Gesang T, Wierach P.: Reliability of piezoceramic patch sensors under cyclic mechanical loading, Smart Mater Struct, 2003, 12, pp. 993-996*

[3] *Gall M, Thielecke B, Schmidt, I.: Integrity of piezoceramic patch transducers under cyclic loading at different temperatures. Smart Mater Sruct, 2009, 18, 104009*

[4] *Bräutigam V, Körner C, Singer RF.: Patent specification DE 10 2005 016 402 B4 (2010)*

[5] *Rübner M, Günzl M, Körner C, Singer RF.: Aluminium-aluminium compound fabrication by high pressure die casting. Mat Sci Eng A-Struct, 2011, 528, pp. 7024-7029*

[6] *Rübner M, Körner C, Singer RF.: Integration of Piezoceramic Modules into Die Castings – Procedure and Functionalities, Adv Sci Technol, 2008, 56, pp. 170-175*

[7] *Rübner, M, Klassen, A, Körner, C, Singer, RF, Ilg, J, Rupitsch, SJ, Lerch, R: Dünnwandige Aluminiumdruckgussteile mit integrierten piezokeramischen Sensoren und Aktoren – Fertigung und Charakterisierung, Tagungsband Symposium „Verbundwerkstoffe und Werkstoffverbunde", Chemnitz, Germany, 2011*

[8] *Wierach, P, Schönecker, A: Bauweisen und Anwendungen von Piezokompositen in der Adaptronik, Proceedings of Adaptronic Congress, Goettingen, Germany, 2005*

Piezo-metal-composites in structural parts: Technological design, process simulation and material modelling

Neugebauer, R.[1]; Ihlemann, J.[2]; Lachmann, L.[1]; Drossel, W.-G.[1]; Hensel, S.[1]; Nestler, M.[1]; Landgraf, R.[2]; Rudolph, M.[2]

[1]*Fraunhofer Institute for Machine Tools and Forming Technology IWU, Chemnitz, Germany*
[2]*Chemnitz University of Technology, Chair of Solid Mechanics, Chemnitz, Germany*

Abstract

Subject is the development of a process chain for the production of semi-finished parts with an integrated sensor and actuator functionality and the forming of those to structural parts. Aiming on a non-damaging forming of the integrated piezo module, a swimming-bed inside the piezo-metal-composite is used. The hardening of adhesive surrounding the piezo module between the sheet-metal and the cover-layer takes place after the forming operation. The choice of an applicable adhesive and an application-oriented design of the compound influences the production process as well as the functionality of the compound. By employing a material model for the adhesive and a global forming simulation, including the loads taking effect on the piezo module, a comparison between the numerical simulation and experimental studies is possible. Furthermore, the results of simulation give information about the characteristics of the composite. A subsequent test of functionality will allow the definition of best suitable process parameters and the evaluation of the composites performance dependent on its design.

1. Introduction

As an important current research aspect piezoceramic patches and a new method of their application are investigated. Employed as sensors those patches help to understand the behaviour of structures under dynamic loads, can signal risk of breakage (structural health monitoring) and can even support or optimise technical applications in their usage when employed as actuators [1]. Here, the Piezoceramic-Fibre-Composites (PFC) were shown to be the most promising technology within this sector. More precisely, the Macro-Fibre-Composite (MFC) is the most sophisticated device yet invented [2]. Despite excellent properties of those piezo patches the state of art is their application only after manufacturing to the fabricated parts, which denotes a time and cost intense procedure [3]. In the mass production sector, it is essential to use efficient application methods to maintain short production cycles and provide cost efficiency.

To overcome the existing insufficiencies of the piezo application, a recently developed technology has been presented [3]. On that basis, the aim of this paper is to investigate this new method, which allows the application of the piezo actuators or sensors within an epoxy adhesive as one layer among thin metal sheets with the subsequent forming of these compounds. It has already been shown that bending operations as well as the fabrication of rectangular cups with deep-drawing are feasible deformation processes [3]. Further experimental and simulative investigation should proof this claims and give guidelines for the process optimisation when employing this manufacturing method.

2. Experimental Research

2.1 Forming of Piezo-Metal-Composites

For the forming of piezo-metal-composites a swimming bed, i.e. the piezo module is completely encapsulated within the adhesive, has to be ensured. It allows movement among the metal layers and the piezo module during the forming operation, with the curing of adhesive taking place after the forming process. In addition to the classical complete cover-layer design where the dimensions of the top and bottom layer are identical, the swimming bed design can also be implemented using a cover-layer of a different size, thus providing local covering only. This cover-layer can also be a plastic film. The design of the composites influences its functioning i.e. sensor and actuator behaviour. In order to obtain a final product of the required

quality it might be necessary to modify the tooling when converting between the classical complete cover-layer design and the localised cover-layer design. Possible modification considerations could be altered drawing clearances or tool surfaces. These considerations are however not that important in the feasibility study, but could play a big role in ensuring high quality components during mass production.

The first tests with local cover-layers were performed in a bending operation. Fig. 1 shows the tool with a bending radius of 50 mm and a formed specimen with a local aluminium cover-layer surrounding the Macro-Fibre-Composite. A good bond between the composite layers was achieved.

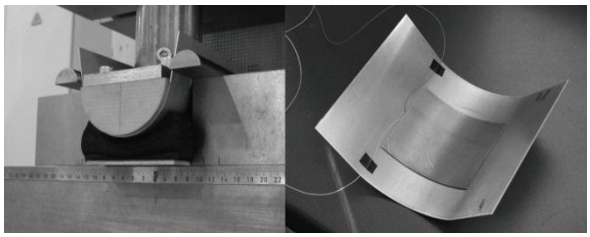

Fig. 1: *Bending tool and finished composite*

In contrast to the punch sided application of the local aluminium cover-layer, a cover-layer made of a plastic film, e.g. polyethylene-naphthalate foil (PEN) is to be applied on the die side.

Based on the results of these bending tests, deep drawing tests of composites with a local cover-layer were performed. In fig. 2 the results of the local application method is compared to that of the classical application method using an aluminium cover-layer with the same dimensions than the basic sheet.

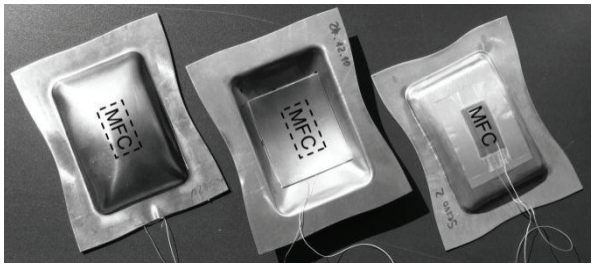

Fig. 2: *Rectangular cups manufactured with deep drawing, left: complete aluminium cover-layer, middle: localised aluminium cover-layer, right: localised plastic cover-layer*

The advantages of localised applications are weight reduction and increased sensor and actuator performance due to reduced component stiffness. The best protection against physical and chemical influences is realised with a complete aluminium cover-layer. Regarding this protection a locally applied aluminium layer is the second best option followed by the locally applied plastic foil. To achieve the desired composite properties the cover-layer, the piezo module and the basic sheet type can be varied.

Miniature cables, soldered to the MFC, are usually used for powering it. In some cases the soldering joints cause marks on the cover layer. In an effort to eliminate these marks a conducting path was used instead of the cables. It consists out of an 18 µm copper layer with NiAu coated soldering pads and polyimide insulation layers, resulting in a total thickness of about 0.13 mm. The soldering process is performed in close cooperation with the BLZ (Bayerisches Laserzentrum GmbH). Fig. 3 shows a connected MFC type M2814P1 on the left and the relevant conducting paths on the right. Forming tests with conducting paths were successfully performed. For the determination of achievable forming limits further studies are needed.

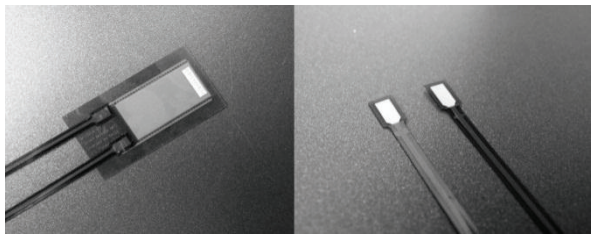

Fig. 3: *Left: conducting paths soldered onto a MFC, right: contact pads of the conducting paths*

2.2 Selection of Adhesive

At the beginning of the Transregional Collaborative Research Center PT-Piesa a low viscosity epoxy adhesive was used, but forming tests have shown that a higher viscosity epoxy leads to better forming results. For this reason the epoxy 3M Scotch-Weld™ DP410, having a higher viscosity than that previously used, was chosen and resulted in a reduction in curing time, because it does not require pre-curing to improve its viscosity [4]. In the mass production environment a high viscosity epoxy will ensure acceptably short process times. One of the main advantages of 3M Scotch-Weld™ DP410 is that it bonds well to both the piezo module and the sheet metal while having an elastic modulus of about 2.3 GPa, which ensures good force transfer from the sheet to the piezo module. Furthermore, the viscosity of the adhesive has to be small enough to avoid a breakdown due to tension load caused by friction forces.

3. Numerical Investigation

3.1 Forming Simulations

The uncured adhesive acts as lubricant during the forming process. Thus the frictional loads transferred from the sheet metal to the MFC due to relative motion are reduced. In a former study [4], the contact pressures during forming for the above designs of local sheet application were investigated numerically (fig. 4 and 5).

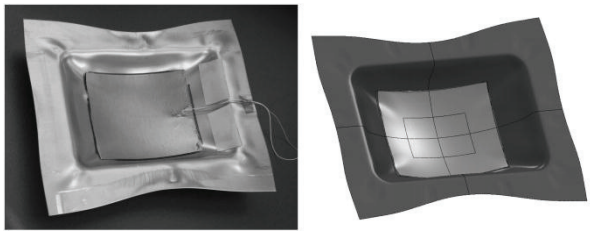

Fig. 4: *Local aluminium-sheet cover (left: experiment, right: simulation)*

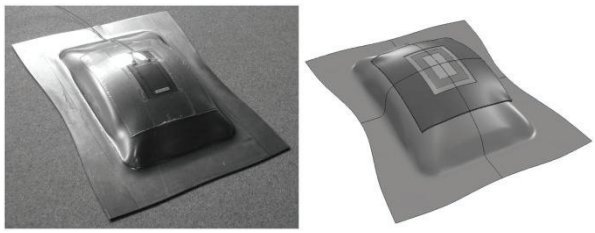

Fig. 5: *Local PEN-sheet cover (left: experiment, right: simulation)*

It was found, that the maximum pressure values differ by one magnitude in the range from 0.5 MPa for local plastic PEN-foil design up to 5.5 MPa for the aluminium-sheet (fig. 6). Hence a consideration of frictional forces caused by the pressure in the forming simulation is necessary to evaluate the total load level for different local cover designs.

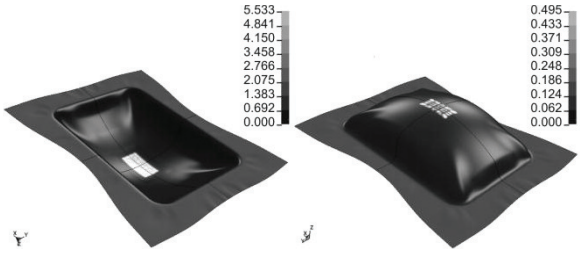

Fig. 6: *Numerically determined contact pressure distribution for two investigated designs (left: aluminium sheet cover, right: PEN-foil cover)*

Macro-Fibre-Composites contain embedded piezo fibres contacted with transverse finger-electrodes. Thus the MFC has different surface profiles for the orthogonal directions along fibres and transverse. To describe the friction behaviour in a global manner, it is necessary to include an analytical orthotropic friction model in the forming simulation.

Experimental friction tests were carried out for three different velocities, four contact pressure levels and for relative motion in fibre direction and transverse direction [4]. The determined friction forces for static (relative velocity $v = 0$) and dynamic ($|v| > 0$) friction behaviour were then evaluated to obtain a global friction model for use in the forming simulation. It was found, that the friction forces are pressure and velocity dependent [4]. The commercial FE-code LS-Dyna, utilized in this study, provides only an isotropic velocity and contact-pressure dependent friction law for elastic bodies. Hence the LS-Dyna Fortran-user-interface had to be employed to implement an orthotropic friction law. LS-Dyna uses for the basic nodes-to-surface contact type a velocity-dependent Coulomb friction coefficient $\mu(v)$ (F_n: normal force, F_f: tangential friction force).

$$\mu(v) = F_f(v) / F_n \tag{1}$$

In the conventional LS-Dyna approach [5] the friction coefficient is expressed as

$$\mu(v) = C_2 + (C_1 - C_2) \cdot \exp(-C_3 |v|) \tag{2}$$

C_1 and C_2 are static and dynamic coefficient of friction, C_3 is a decay constant, which defines the transition period. For the general implementation in the present study this approach was also used, because it provides a simple smooth transition between static and dynamic friction. For each pressure level and the sliding directions, coefficients $C_i^*(p,v)$ were identified from the experimental data with least squares method for model function eq. (2). Hence, a set of analytical functions for velocity dependency is given. To include also pressure dependency in an analytical form, the general functions C_1 and C_2 are defined dependent on contact pressure p under usage of 5th-order polynomials.

$$C_i(p) = \sum_{j=0}^{5} K_j p^j \quad , \quad i = 1,2 \tag{3}$$

Moreover, the decay coefficient C_3 contains a user variable K_c to compensate velocity effects in a scaled simulation, in which computation time is a fraction of the real test time.

$$C_3(p) = 1/K_c \sum_{j=0}^{5} K_j p^j \tag{4}$$

The polynomial constants K_j are found by fitting the experimental data again with the least squares method for model functions eq. (3) and (4). Fig. 7 and 8 show the friction coefficient surfaces $\mu_x(v,p)$ and $\mu_y(v,p)$

dependent on relative velocity v and contact pressure p for motion in fibre direction x and transverse direction y.

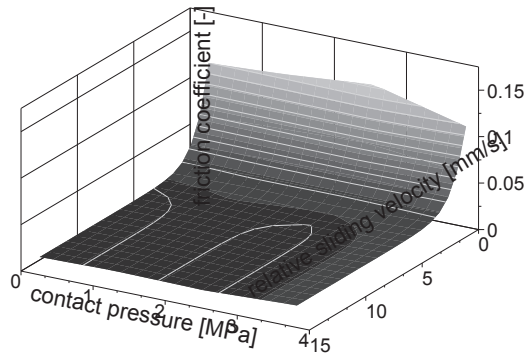

Fig. 7: *Model of friction coefficient for relative motion in fibre direction x*

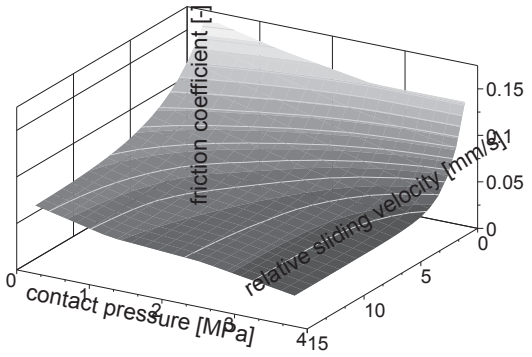

Fig. 8: *Model of friction coefficient for relative motion in transverse fibre direction y*

For an analytical description of orthotropic friction behaviour the results for both directions have to be combined into an effective friction coefficient μ_{eff} dependent on an actual local angle φ, which describes the rotation of relative motion related to fibre direction. The chosen approach

$$\mu_{eff}(p,v,\varphi)=\sqrt{(\mu_x\cos\varphi)^2+(\mu_y\sin\varphi)^2} \qquad (5)$$

fulfills the condition for isotropic friction $\mu_x=\mu_y=\mu_{eff}$. The angle φ is computed each timestep based on the rotations of an initially inputted set of local element coordinate systems and the actual node displacement vector projected onto the sliding surface. The global orthotropic friction model was validated for several parameter combinations by simulations of the experimental friction tests. Fig. 9 shows an exemplary result for $F_n=1000\,N, v=10\,mm/s$ and motion in transverse fibre direction. For the prescribed velocity in the simulation a value of $v_{Sim}=2000\,mm/s$ was chosen to reduce computation time; hence the compensation factor K_c in eq. (4) was set to 200.

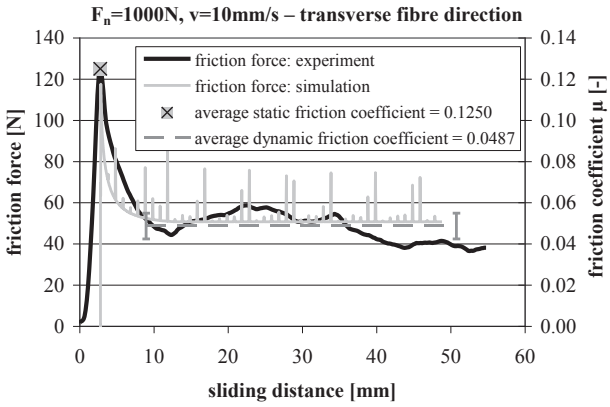

Fig. 9: *Exemplary comparison between results of an experimental and numerically simulated friction test with a normal contact force of F_n = 1000 N (equals 2.55 MPa contact pressure) and a relative velocity of v = 10 mm/s transverse to fibre direction*

In a next step the friction model has to be implemented in the global forming simulations. Within further research it is planned to investigate different MFC-application designs especially according to the frictional behaviour.

3.2 Phenomenological material model for the adhesive including curing

As a part of the previously presented model from subsection 3.1 the epoxy adhesive is of particular importance to the simulation of the forming process of the complete compounds. Therefore, a further focus lies on the experimental investigation and material modelling of the epoxy adhesive to enable more detailed FE-analyses for the future. This can be achieved due to the fact that the manufacturing process, which includes the important curing of the adhesive with all its changes of the material properties, can be considered. In particular, effects like chemical shrinkage, heat expansion (e.g. caused by the exothermal reaction) and their significant impacts on the mechanical properties can be taken into account. Thus, an appropriate material model would give access to a wide range of important simulation possibilities. First, it allows the optimisation of the forming process for the composite parts with respect to parameters like the degree of cure, the adhesive thickness or the process temperature. This is of particular interest for the arising residual stresses within the compound, which might cause damage to the piezo module. Secondly, the main properties of the fully cured adhesive can be taken into consideration, which allow statements due to the mode of action of the piezo module within a structural part undergoing a variety of different operating conditions.

In order to choose an appropriate material model for the simulation of the adhesive, a detailed experimental investigation of the material behaviour under consideration of the curing process needs to be done. Toward this end, typical experimental setups like uniaxial tension tests, thermal analysis techniques or rheological experiments have been chosen.

Within the material modelling approach, several physical fields have to be taken into account, i.e. the chemical process, the mechanics and the thermodynamics. The chemical process during the curing of the adhesive can be described by a scalar variable $q(t)$ called degree of cure [6]. This variable has a value range of $0 \le q(t) \le 1$ and specifies the percentage of the progress of the curing process. The experimental characterisation of the degree of cure can be achieved by thermal analysis techniques e.g. by using Differential Scanning Calorimetry (DSC) [7]. An investigation on the chosen adhesive approved the strong temperature dependencies of the curing rate and the maximum attainable degree of cure. Fig. 10 illustrates the degree of cure of the chosen adhesive for DSC-measurements at different constant temperatures.

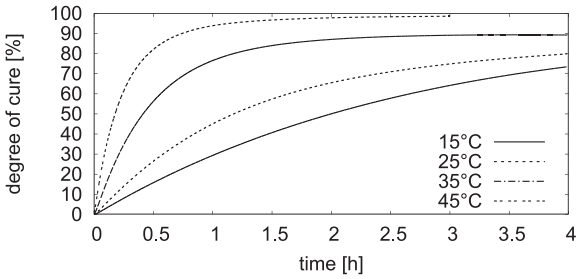

Fig. 10: *Degree of cure for the chosen adhesive at different constant temperatures (DSC-measurements)*

To embed the description of the chemical process into the phenomenological material model, an analytical function for the degree of cure has to be defined. This is done by formulating a differential equation of the form

$$\dot{q} = \frac{dq}{dt} = f(q, \theta, t, \ldots) \ . \qquad (6)$$

A further part of the experimental characterisations concerns the mechanical properties of the adhesive. Since it is crucial to capture the basic material behaviour at the fully cured stage of the adhesive, uniaxial tension tests at room temperature and different deformation procedures have been carried out. As an example, fig. 11 shows the results of relaxation tests at different deformation rates for the loading interval.

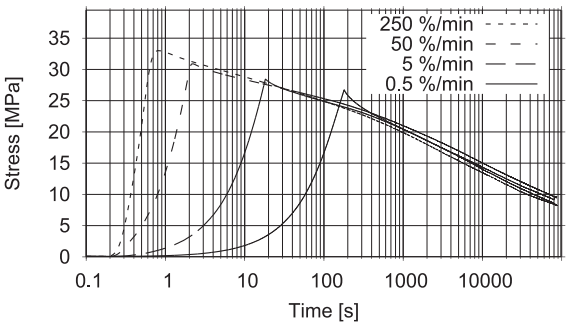

Fig. 11: *Uniaxial relaxation tests at different loading rates for the loading interval ($\varepsilon_{\max} = 1.5\%$)*

Since there is a significant stress-relaxation, the material has to be treated as time-depending with certain viscoelastic properties. Consequently, the material model needs to account for the inelastic behaviour at the cured stage. Since the material model should be applied for large deformation processes, it is based on a continuum-mechanical formulation in which the deformation is described by the deformation gradient $\underline{\underline{F}}$. In order to capture volume changes due to varying temperatures or the progressing degree of cure, a multiplicative decomposition of the deformation gradient is applied as follows.

$$\underline{\underline{F}} = \underline{\underline{F}}_M \cdot \underline{\underline{F}}_{\theta C} \qquad \underline{\underline{F}}_{\theta C} = \sqrt[3]{\varphi_{\theta C}(\theta, q)}\ \underline{\underline{I}} \qquad (7)$$

The second part $\underline{\underline{F}}_{\theta C}$ describes the isotropic heat expansion and chemical shrinkage. This is formulated by a scalar material function $\varphi_{\theta C}(\theta, q)$ which represents the volume change due to changes in temperature θ and the degree of cure q. The second part of eq. (7) is the remaining pure-mechanical deformation gradient $\underline{\underline{F}}_M$. According to the experimental observations, this part might either consist of a formulation of viscoelasticity [8] or viscoplasticity [9]. Furthermore, to simulate thermodynamically consistent material behaviour, the laws of thermodynamics need to be taken into account. Therefore, a free energy function is formulated and evaluated within the laws of thermodynamics.

With this described modelling approach, a thermodynamically consistent material model including the main chemical, mechanical and thermal effects is achieved. As an example, fig. 12 shows the calculated stress-strain-curve of such a material model based on finite viscoplasticity at a uniaxial, sinusoidal loading with constant strain amplitude. The model consists of a constant elasticity parameter μ, a constant viscosity η as well as a curing dependent yield stress $K_F(q) = K_{F0} \cdot q$.

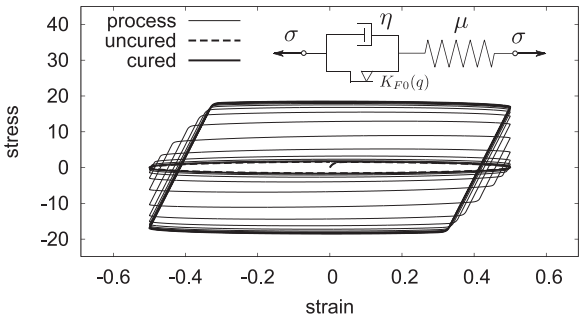

Fig. 12: *Simulated stress-strain-behaviour of finite viscoplasticity with curing dependent yield stress*

Within this approach, the rising yield stress results in a stiffening of the material and therefore leads to increasing stresses.

4. Summary and Outlook

In this study a method is presented, which overcomes the present restrictions for application of Macro-Fibre-Composites on flat part geometries. By integrating the application step into the part forming process chain, a significant improvement in cost effectiveness and part cycle reduction for mass production structures can be achieved. As one approach several design concepts for such an integrated application were experimentally investigated. Therefore, the contacting strategy for MFC was adapted to meet the requirements of deep drawing processes including the integrated application step. Moreover, several design concepts with focus on the loading of the piezo-structure were numerically investigated. Special point of interest in this study is the frictional behaviour of the MFC. Toward this end, an orthotropic friction model was developed and implemented in the commercial FE-code LS-Dyna. As another research aspect, the experimental characterisation as well as the development of a continuum-mechanical material model including the curing behaviour of the adhesive has been presented.

The upcoming research objectives are the experimental investigation and numerical description of the whole process chain. This includes the optimisation of the contacting process as well as further examinations with a demonstrator structure. Moreover, function degradation of the MFC due to forming loads will be an aspect. By integrating the continuum-mechanical material model into FE-simulations, the prediction of the MFC's loadings due to the adhesive's residual stresses and the mechanical behaviour of the finished parts can be achieved.

5. Acknowledgement

This Paper is based on the work within the Transregional Collaborative Research Centre 39 PT-PIESA "Production Technologies for light metal and fibre reinforced composite based components with integrated PIEzoceramic Sensors and Actuators", which is funded by the German Research Foundation (Deutsche Forschungsgemeinschaft) DFG. The authors gratefully acknowledge the support of the DFG.

References

[1] Wierach, P.; Schönecker, A.: Bauweisen und Anwendungen von Piezokompositen in der Adaptronik. Adaptronic Congress 2005. Conference proceedings: June, Göttingen

[2] Lloyd, J. M.: Electrical Properties of Macro-Fiber Composite Actuators and Sensors, PhD Thesis, Virginia Polytechnic Institute and State University, USA, 2004

[3] Neugebauer, R.; Lachmann, L.; Drossel, W.-G.; Nestler, M.; Hensel, S.: Multi-layer compounds with integrated actor-sensor-functionality, Production Engineering - Research and Development (WGP), 2010

[4] Neugebauer, R; Lachmann, L.; Drossel, W.-G.; Nestler, M.; Hensel, S.: Smart Semi-Finished Parts for the Application in Sheet-Metal Structures, Proceedings of Production Engineering, Article in press, 2011

[5] Livermore Software Technology Corporation: LS-Dyna Keyword User's Manual Vol.1, Vers.971 / Rev.5, May 2010

[6] Lion, A.; Höfer, P.: On the phenomenological representation of curing phenomena in continuum mechanics, Arch. Mech., 59, 1, pp. 59-89

[7] Lion, A.; Yagimli, B.: Differential Scanning calorimetry – continuum mechanical considerations with focus to the polymerisation of adhesives, ZAMM 88 (5), 2008, pp. 388-402

[8] Landgraf, R.; Ihlemann, J., Vergleich zweier Ansätze zur Beschreibung nichtlinearer Viskoelastizität auf Basis des Maxwell-Elements, PAMM - Proc. Appl. Math. Mech.10, 2010, pp.303-304

[9] Shutov, A.V.; Kreißig, R., Finite strain viscoplasticity with nonlinear kinematic hardening: Phenomenological modeling and time integration, Comput. Methods Appl. Mech. Eng. 197, 2008, pp. 2015-2029

Fiber reinforced polymers in automotive applications –
History - state-of-the-art - future trends

Deinzer, G. H.; Haverkamp, C.

Audi AG Neckarsulm, Neckarsulm, Germany

Abstract

The actual and future requirements for the automotive industries show the urgent need of further reducing the weight of the vehicles. At present, modern light weight car bodies are built as a material mix solution. High strength steel as well as aluminum castings, extrusions and sheet and magnesium castings are used in a space frame design. The next generation of innovative body design foresees the use of carbon fiber reinforced polymers (CFRP) as the next generation of light weight material. Nevertheless, there are still technical and commercial issues to be solved before CFRP will be used in high volume car body design.

1. Introduction

With regard to the global competition and the requirements given by regulation, market and society the automotive industry faces a number of new challenges. More and more topic like sound use of natural resources and sustainability are getting focused on. Light weight design has been a major driver for innovative solutions both in Design and Engineering as well in manufacturing of modern cars. High strength steel grades help to meet the rising safety requirements. Innovative aluminum concept are more and more used in automotive high volume production. Magnesium die castings are used in engine and drive train applications. New developments are aiming to introduce carbon fiber reinforced material in hang on parts as well as in structural components of the car body. Based on close cooperation of competent supplies and research institutes, the automotive industry will continue to improve light weight designs and optimize materials and processes.

2. History and state-of-the-art in the sue of CFRP

While aluminum is on the way to high volume application the focus of material and process engineers is actual on the implementation of CFRP in car body design and manufacturing.

Fig. 1: *CFRP - History at Audi*

Audi has a broad history in the use of CFRP in racing car. Sports cars and small volume applications. Examples are the Rallye Quattro in 1981, the sport Quattro in 1983 and the drive shaft for the USA version of the Audi 90.

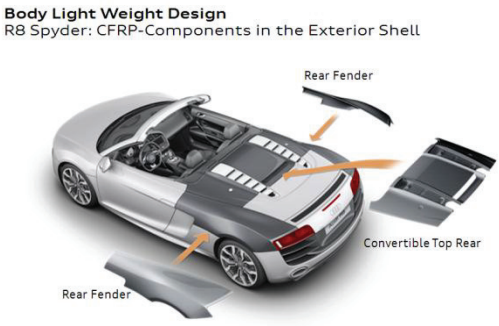

Fig. 2: *CFRP-parts in the shell of the AUDI R8 Spyder*

Actually, Audi products show CFRP as visible light weight design in the outer shell of the body. The R8 Spyder shows the fender rear and the convertible top cover that is integrated in the body structure with a perfect class A surface finish.

3. Light Weight Potential of CFRP

Fiber reinforced materials in general whether they may reinforced with glass, aramide or carbon fiber are specific compared to metals as they show a significant anisotropy with regard to their mechanical properties. This means an advantage especially when components are loaded in a distinct direction, or gives a new degree of freedom to the designer to optimize the layout of a component to draw maximum benefit of this specific properties. Fig. 3 shows the potentials

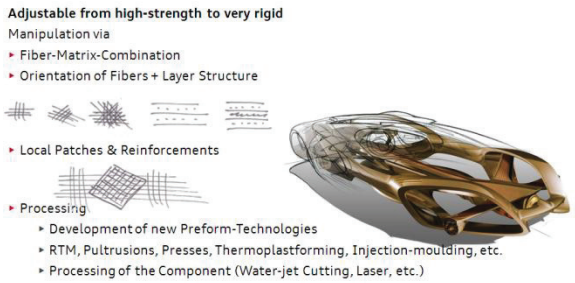

Fig. 3: *CFRP: A material with high degrees of freedom for the designer*

Compared to aluminum solutions, carbon fiber offers a weight reduction of 20% up to 33 %. The key factor to achieve such figures is the fiber volume content that should above 50%. In this case the right manufacturing technology is key to meet those targets.

4. Commercial Issues

The results of actual developments show that there is a urgent need of significant cost reduction along the process and value chain. Material cost must be cut by 50%. Manufacturing at present is only poorly automated with a huge amount of manual work. Therefore cost potentials must be optimized and brought down to 10%. In case of class A surface often half of the costs is due to the extensive work to achieve top surface quality in the paint shop.

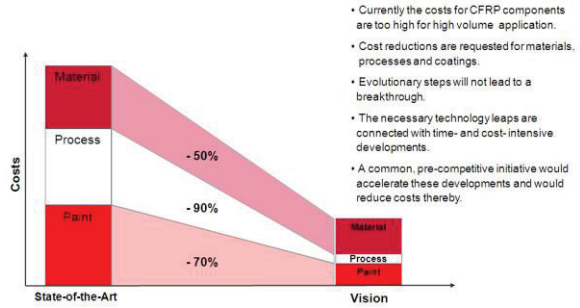

Fig. 4: *Cost reduction requirements along the value chain*

5. Conclusion

There is an enormous potential to reduce weight in future automotive products by the help of fiber reinforced especially carbon fiber reinforced concepts and design. In order to roll out this applications to high volume production all faculties as there are design, numerical calculation, materials engineering and automation and process technology have to contribute significantly by increasing the light weight ratio while reducing the costs.

The automotive industry will step forward in close cooperation with the most competent partners at the supplier base as well as in the scientific community.

Literature

[1] G. Deinzer, K. Durst. Industrialising CFRP – challenges for the automotive industry. JEC-Forum, Paris, 2010

[2] K. Durst. Beitrag zur systematischen Bewertung der Eignung anisotroper Faserverbundwerkstoffe im Fahrzeugbau. Cuvillier Verlag, Göttingen, 2008

[3] M. Dick. Leichtbau mit CFK – Herausforderungen für die Mobilität der Zukunft. CCeV-Automotive-Forum, Neckarsulm, 2010

[4] H. Timm. Wo liegt der Bedarf für CFK im Automobilbau. CCeV-Automotive-Forum, Neckarsulm, 2010

[5] H.-G. Haldenwanger. Hochleistungsfaserverbundwerkstoffe im Automobilbau. VDI-Verlag, Düsseldorf, 1993

Process development for high volume manufacture of thermoplastic composites with integrated piezoceramic modules

Gude, M.[1]; Hufenbach, W.[1]; Modler, N.[1]; Schmidt, M.[2,3]; Geiger, M.[2]; Heber, T.[1]; Winkler, A.[1]; Pfeiffer, C.[2]; Albert, F.[2]; Roth, S.[2]

[1]*Technische Universität Dresden, Institute of Lightweight Engineering and Polymer Technology (ILK), Dresden, Germany*
[2]*Bayerisches Laserzentrum GmbH, Erlangen, Germany*
[3]*Friedrich-Alexander-Universität Erlangen-Nürnberg, Chair of Photonic Technologies, Erlangen, Germany*

Abstract

This publication gives a contribution for the development of novel thermoplastic-compatible piezoceramic modules, their efficient manufacture and contacting, and their robust integration in composite structures. Therefore the development of a continuous process chain from the single components to the active composite structure is introduced. The process chain development is demonstrated by exemplary experimental studies concerning the major process steps module manufacturing, contacting, and integration. Hence, the investigations show the unique possibility for high volume manufacture of thermoplastic composites with integrated piezoceramic modules considering a persistent material homogeneity.

1. Introduction

High demands with respect to environmental and convenience issues lead to innovative solutions for future high performance applications in machine, vehicle and device manufacture as well as in medical technology. Here, fibre-reinforced thermoplastic composites with novel thermoplastic-compatible piezoceramic modules (TPM) offer specific advantages due to the possibility to actively control their static, dynamic and vibro-acoustic behaviour [1-5]. The use of these innovative materials enables the development of a new generation of active lightweight structures with material-integrated structural health monitoring, energy-harvesting, or active vibration damping functionalities [6-10]. At present, the lack of robust manufacturing technologies is a major obstacle for the intensive use of these new active composites especially in automotive applications.

The integration of piezoceramic modules into anisotropic fibre-reinforced structures requires the development of manufacture processes adapted to the interfaces between matrix, reinforcement and the piezoceramic material. Conventional piezoceramic actuators are predominantly manufactured and applied to the structure by adhesive technologies. This requires a high manual application effort and can cause compatibility problems at the interface between composite structure and piezoceramic module [11-14]. By use of the here developed continuous process chain, the high volume manufacture of thermoplastic composites with integrated piezoceramic modules without compatibility problems becomes possible for the first time [15-18].

2. Process chain

The process chain starts with the TPM-manufacturing, which consists of the electrode application, TPM-assembly and -converting, and TPM-consolidation. Therefore, a process based on the roll-to-roll-technology was designed (fig. 1).

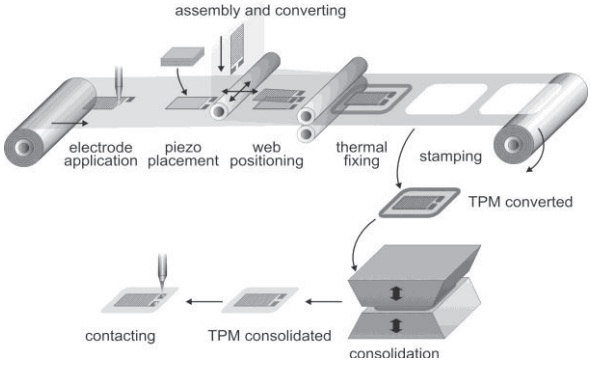

Fig. 1: *Schematic TPM-manufacture process*

The electrode application takes place by adapted additive or subtractive technologies like screen printing or laminating and etching, respectively. Before the placement of piezoceramic functional layers on a lower thermoplastic film web, the functional layers were produced as monolithic piezoceramic films or composites of piezoceramic fibres and thermoplastic matrix material, depending on the TPM functional principle. After that, the functional layer is covered by an upper thermoplastic film web with applied electrode structures, whereby both film webs are exactly positioned against each other in order to reach a congruent alignment of upper and lower electrode structure. The aligned components are fixed by a welding step, stamped as converted TPM, and consolidated during an adapted hot-pressing step.

After contacting with the help of an especially developed contacting process based on laser technology, the consolidated and contacted TPM are embedded in a composite structure by means of a subsequent film-stacking process. Before consolidation, the film-stacking lay-up has to be prepared starting with the production of thermoplastic films with contacted TPM. This includes the application of conducting paths on thermoplastic films, the exact positioning of the TPM to these paths, and the contacting and fixation of the TPM by a thermal or ultrasonic welding step (fig. 2). Accordingly, the thermoplastic film with conductors and contacted TPM has to be cut into defined sections, called e-preforms.

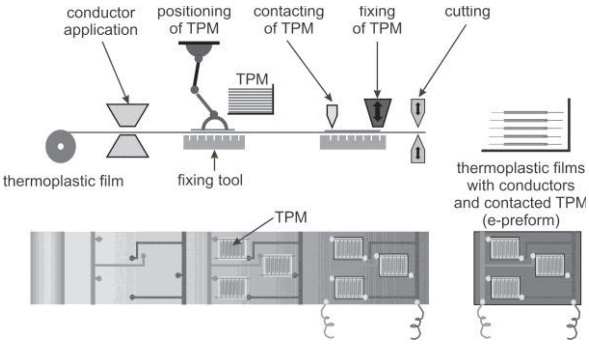

Fig. 2: *Scheme of the e-preforming process*

The thermoplastic films with contacted TPM are passed to a transfer station, where a robot takes these layers and stacks an individual lay-up together with fibre-reinforced thermoplastic preforms and single thermoplastic composite layers with the help of adapted handling devices (fig. 3). The preform assembly is followed by the pre-heating and hot-pressing of the assembled composite. Here, the pressing parameters e.g. the process temperature, time, and pressure have to be well adjusted to ensure a proper consolidation of the composite and no damage of the TPM. During the consolidation process of the film-stacking compound, a novel efficient online-polarization of the embedded TPM realizes the change-over from a passive to an active composite under purposeful use of the processing parameters.

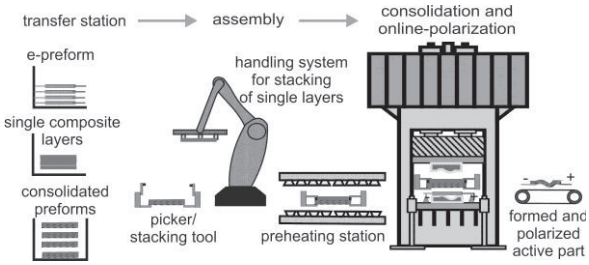

Fig. 3: *Scheme of processing to active composite part*

3. Manufacture of thermoplastic-compatible piezoceramic modules

In order to realize a reproducible high volume production of thermoplastic-compatible piezoceramic modules, an automated assembly and converting unit was designed and installed (fig. 4), which substantially consists of the functional layer placement, an optical web control, a thermal film joining station, and a die cutter with collecting tray.

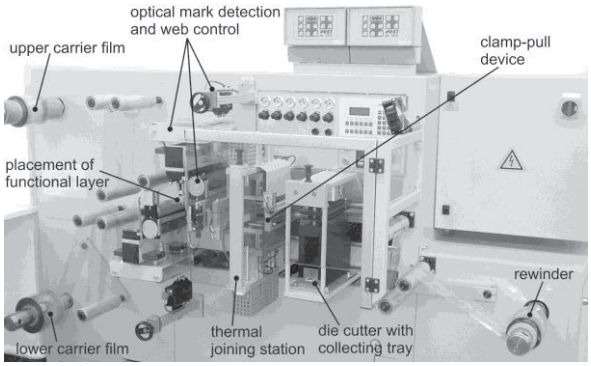

Fig. 4: *TPM-assembly and -converting unit*

The major challenge while designing this device is the adherence to tolerance guidelines during the positioning of upper and lower electrode structure resulting from theoretical and experimental TPM-design studies. For the optical detection and web control parallel and perpendicular to the web direction, appropriate marks where applied on the thermoplastic films simultaneous to the previous electrode application process.

Fig. 5 shows the measurement of the electrode misalignment over 20 module sections with a repeating pattern of 70 mm. For both directions, the misalignment is within the tolerance guidelines.

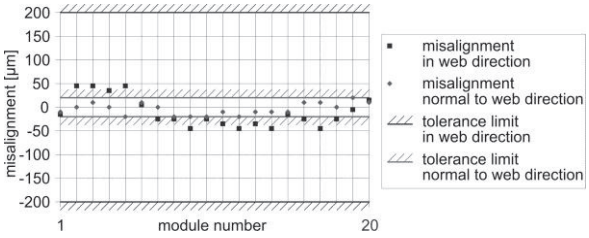

Fig. 5: *Electrode misalignment within the tolerance*

After the TPM-assembling and -converting follows the subsequent processing to consolidated TPM using an adapted hot-pressing technology. In order to determine material- and module-specific process parameters, the entire manufacture process is investigated by means of process chain analysis. Therefore the process is split in objects, constitutional changes, properties, and influencing variables; exemplarily shown for the consolidation step in fig. 6.

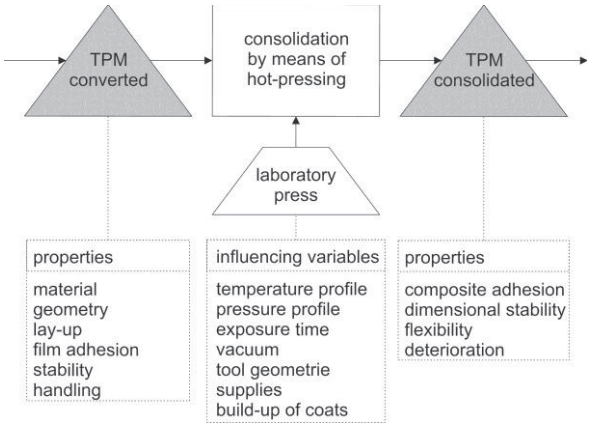

Fig. 6: *Vertical Structure of the process step "TPM-consolidation"*

Under systematic adjustment of the interactions between technical and technological parameters accompanying with various destructive and non-destructive analysis, the TPM design was specifically adapted and the process parameters were localized. Finally, the reproducible consolidation of prototypic TPM with polyamide (PA) or polyetheretherketone (PEEK) thermoplastic carrier films could be realized by means of hot-pressing technology without damaging the sensitive piezoceramic and electrode components. Fig. 7 shows a prototypic PEEK-TPM after consolidation under a pressure of 3 bar and a maximum consolidation temperature of 380 °C.

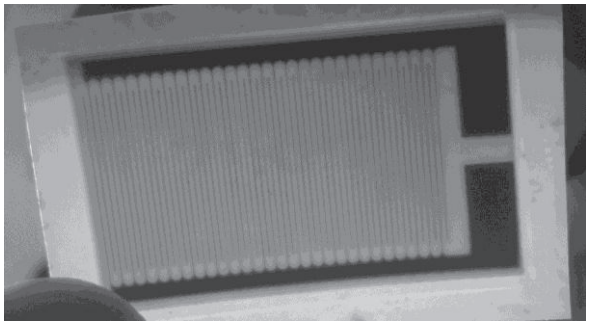

Fig. 7: *Prototypic PEEK-TPM*

4. Laser contacting of the piezoceramic modules

After TPM consolidation, the electrode structures are covered with the thermoplastic carrier films. In order to establish an electrical contact by laser soldering on the piezoceramic foil, the metal plating on the piezoceramic needs to be exposed locally. Thus, a module adapted technology was developed, consisting of an ablation and a successive contacting step.

The polyamide film was locally removed by a picosecond laser treatment. A frequency tripled Nd:YVO_4 laser with a wavelength of λ = 355 nm was used and the following process parameters were applied: pulse duration t_p = 10 ps, pulse frequency f = 10 kHz, laser spot size d_f = 10 µm, line pitch 10 µm. An important demand is that the ablation process must remove the polyamide film without residue but must not damage the electrode on the piezoceramic. The laser process for the ablation of the isolation meets this requirement. A wide process window was established, see fig. 8.

The contacting step was performed with a solder ball bumper (SB²-Jet from Pac Tech, Nauen, Germany) and Sn95,5Ag4Cu0,5 solder preforms of 600 µm diameter. The conductor, a copper wire, was positioned on the previously exposed section of the piezoceramic film and a single molten solder drop was placed on the desired contact location. Nitrogen was used as a protective gas.

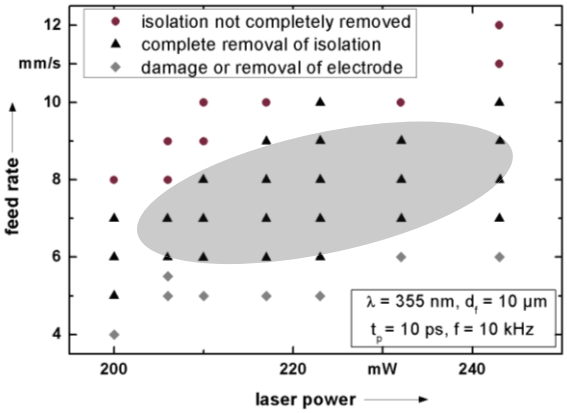

Fig. 8: *Process window for the ablation of the isolation by a picosecond laser treatment*

The energy which is necessary to melt the solder droplet is the sum of the energy to heat the solder ball to melting temperature and the melting energy of the ball. In the case of a Sn95,5Ag4Cu0,5 solder preform of 600 µm diameter, this is about 90 mJ. With an assumed absorption coefficient of 3% and disregarding other energy losses, the laser energy necessary for the process is 3000 mJ, which correlates to the experiments very well. After impacting the surface of the joint location, the solder drop wets the wire as well as the piezoceramic film and a solder joint is created. The wetting process is reproducible and satisfactory, wetting angles slightly lower than 90° are achieved. A cross section of a solder spot is shown in fig. 9.

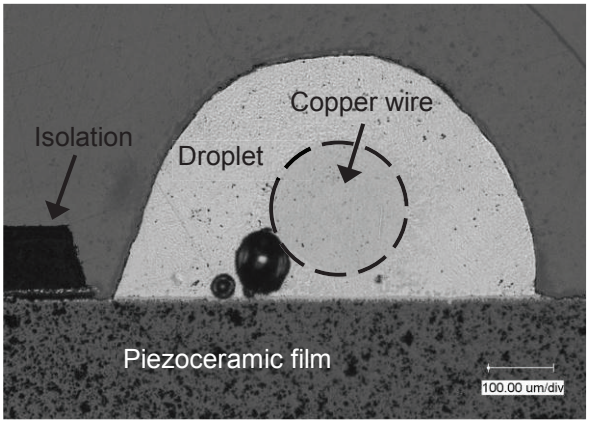

Fig. 9: *Cross section of a solder joint of a copper wire on a TPM with SnAgCu solder.*

The copper wire can be seen as slightly darker circular area in the middle of the solder spot. On the left side of the picture, the remaining isolation (black) is visible. The piezoceramic film on the bottom of the picture is without visible damage and the electrode on the piezoceramic is also preserved. Pores in the solder joint are frequent, their impact on the strength of the joint will have to be determined.

In order to investigate the durability and long-term stability of the solder joints, in further investigations mechanical tests with and without a prior ageing of the joints are planned.

5. Composite manufacture and integration process

After the contacting step the TPM will be assembled on a thermoplastic film for the integration into the composite structure. Therefore, a special positioning device was developed (fig. 10).

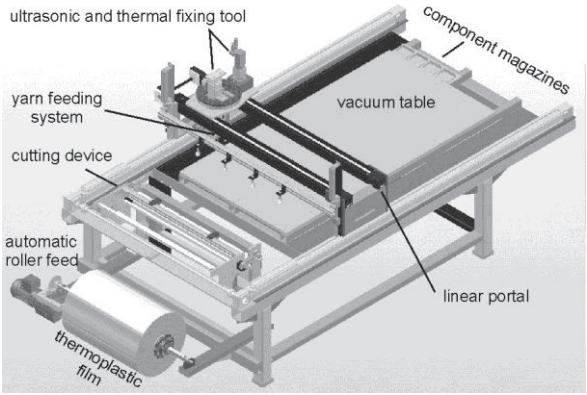

Fig. 10: *Positioning table for assembling of thermoplastic films*

In front of the device a thermoplastic film roll is positioned, which will be transferred automatically to a vacuum table by two grippers. After that, the foil will be fixed on the table by vacuum and cut by a cutting device. Then the TPM, which are positioned in special magazines, will be taken by a vacuum gripper and transferred by a linear portal to its position on the thermoplastic film. There, it will be fixed by a thermal stapling or ultrasonic device. Afterwards the conductive paths (copper wire or conductive threads) will also be applied to the thermoplastic film by a special yarn feeding system, which allows rotation angles up to 360°. Therefore, nearly all geometries for the conductive paths can be realized. The fixations of TPM and conductive paths will be realized by ultrasonic welding and by thermal stapling. Initial studies exhibit the best connection quality of fixed TPM by ultrasonic and of fixed conductors by temperature.

The assembled thermoplastic films with TPM and conductive paths will be transferred to a magazine for the next process step, the hot pressing process. In this part of the manufacture, a consolidated preform is used as the structural layer of the part. It is positioned and clamped in a picker/stacking tool (fig.11). A robot transfers the

tool into an infrared heating field where the composite will be heated up to 30 °C over melting temperature. During this time the assembled thermoplastic film with TPM and conductive paths is positioned in the pre-heated pressing tool (140 °C).

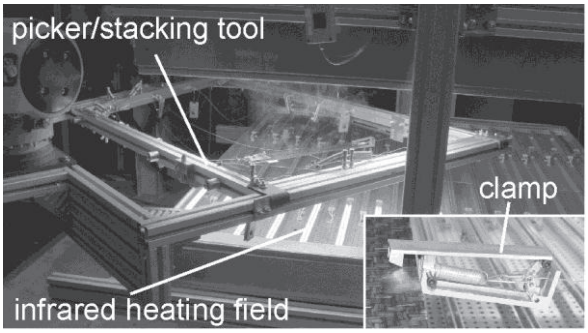

Fig. 11: *Picker/stacking tool*

Then the molten preform will be transferred quickly into the press (3 s) and the pressing tool will be closed very fast as well. Therefore, basic tests with a laboratory pressing tool were accomplished to determine the heating and cooling parameters of the preform and the pressed part (fig. 12).

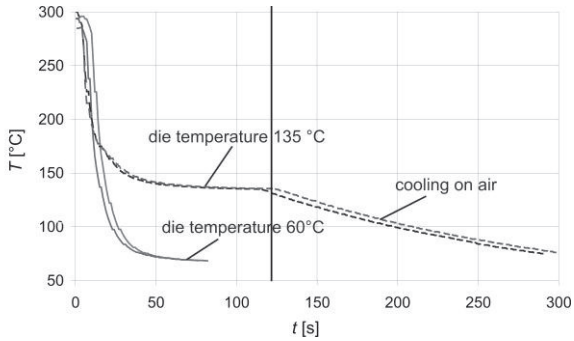

Fig. 12: *Cooling behaviour of the composite in the compression moulding die*

During the pressing and cooling an Online-Polarization step is integrated into the process to utilize the relatively high temperatures and the pressure for a quick and proper polarization of the integrated TPM. The investigations show that an increased temperature has a positive influence on the polarization of the modules (fig. 13).

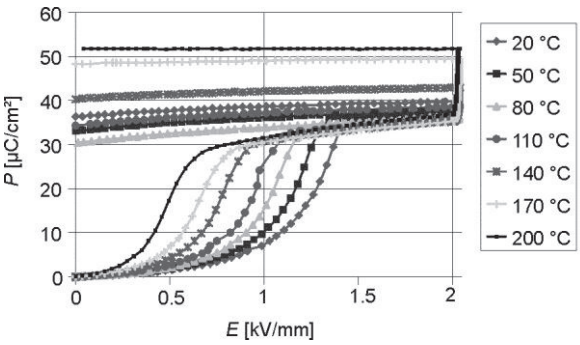

Fig. 13: *Polarization according to temperature of prototypic TPM (maximum electrical field 2 kV/mm)*

With higher temperatures, the polarization rises at lower electrical fields compared to lower temperatures. The remanent polarization is also higher for samples polarised with higher temperatures. Investigations concerning the dependency of pressure and polarization show no significant influence in the feasible range.

At the end of the manufacture process a fibre-reinforced thermoplastic part with integrated and fully functional TPM will be picked out of the press (see fig. 14).

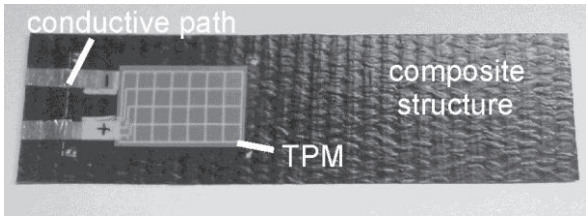

Fig. 14: *Active part with embedded TPM*

6. Conclusions

New fibre-reinforced thermoplastic composites with embedded novel thermoplastic-compatible piezoceramic modules offer specific advantages for new active structures. Investigations for a new efficient manufacture process on the basis of a material- and actuator-adapted hot-pressing technology were carried out. The studies show the possibility for a robust serial manufacture of active thermoplastic composite parts by high-volume manufacture, contacting, and integration of thermoplastic-compatible piezoceramic.

7. Acknowledgement

The authors like to thank the DFG (Deutsche Forschungsgemeinschaft) for the financial support of the investigations in the frame of the Collaborative Research Center/Transregional Research Center (SFB/TR) 39.

Literature

[1] *Crawley, E. F.; Luis, J. de: Use of Piezo-ceramic Actuators as Elements of Intelli-gent Structures. In: AIAA Journal 25, 10 (1987), pp. 1373-1385*

[2] *Gibson, R. F.: A review of recent research on mechanics of multifunctional composite materials and structures. In: Composite Struc-tures 92 (2010), pp. 2793-2810*

[3] *Gude, M.: Modellierung von faserver-stärkten Verbundwerkstoffen und funktions-integrierenden Leichtbaustrukturen für komplexe Beanspruchungen, Technische Universität Dresden, Habilitation, 2008*

[4] *Modler, N.: Nachgiebigkeitsmechanismen aus Textilverbunden mit integrierten aktorischen Elementen, Technische Universität Dresden, Dissertation, 2008*

[5] *Nuffer, J.; Pfeiffer, T.; Flaschenträger, N.; Melz, T.; Brückner, B.; Freytag, C.; Schnetter, J.; Schönecker, A.: Piezoelectric composites: application and reliability in adaptronics. In: Proceedings International Symposium on Piezocomposite Appli-cations, 2009*

[6] *Adhikari, S.; Friswell, M. I. ; Inman, D. J.: Piezoelectric energy harvesting from broad-band random vibrations. In: Smart Materials and Structures 18 (2009), p. 115005 (7pp)*

[7] *Daue, T.; Kunzmann, J.: 20 years of Advanced Low Profile Actuators, where are all the applications? In: Proceedings Inter-national Symposium on Piezocomposite Applications, 2009*

[8] *Edery-Azulay, L.; Abramovich, H.: Active damping of piezo-composite beams. In: Composite Structures 74 (2006), pp. 458-466*

[9] *Hufenbach, W.; Gude, M.; Czulak, A.: Actor-initiated snap-through of unsymmetric com-posites with multiple deformation states. In: Journal of Materials Processing Technology 175, 1-3 (2006), pp. 225-230*

[10] *Qing, X. P.; Beard, S. J.; Kumar, A.; Ooi, T. K.; Chang, F.-K.: Builtin Sensor Network for Structural Health Monitoring of Composite Structure. In: Journal of Intelligent Material Systems and Structures 18 (2007), pp. 39-49*

[11] *Bianchini, E.: Piezoelectric device and meth-od to manufacture a piezoelectric device. U.S. Patent No. 7,105,988 B2, 2006*

[12] *Jin, C. ; Wang, X.: The Effect of Adhesive Layers on the Dynamic Behavior of Surface-bonded Piezoelectric Sensors with Debond-ing. In: Journal of Intelligent Material Systems and Structures doi: 10.1177/ 1045389X11404956 (2011)*

[13] *Wierach, P. ; Schönecker, A.: Bauweisen und Anwendungen von Piezokompositen in der Adaptronik. In: Proceedings Adaptronic Con-gress, 2005*

[14] *Yin, J. ; Foster, F. S. ; Ha-Rasiewicz, K. A.: Piezoceramic composites and methods for manufacturing same. WO 2004/102795 A3, 2004*

[15] *Hufenbach, W.; Gude, M.; Heber, T.: Devel-opment of novel piezoceramic modules for adaptive thermoplastic composite structures capable for series production. In: Sensors and Actuators A 156 (2009), pp. 22-27*

[16] *Hufenbach, W.; Gude, M.; Heber, T.: Em-bedding versus adhesive bonding of adapted piezoceramic modules for function-integrative thermoplastic composite structures. In: Composites Science and Technology 71 (2011), pp. 1132-1137*

[17] *Hufenbach, W.; Gude, M. ; Heber, T.; Geiger, M.; Schmidt, M.; Neugebauer, S.: Auslegung und Fertigung von thermo-plastverbundkompatiblen Piezokeramik-Modulen für adaptive Leichtbaustrukturen. In: Tagungsband 17. Symposium Verbund-werkstoffe und Werkstoffverbunde, 2009*

[18] *Hufenbach, W.; Gude, M.; Modler, N.; Heber, T.; Winkler, A.; Friedrich, J.: Processing studies for the development of a robust manufacture process for active composite structures with matrix adapted piezoceramic modules. In: Kompozyty Composites 9, 2 (2009), pp. 133-137*

Integration of piezoceramic and electronic functional elements in glass fibre-reinforced polyurethane composite structures

Hufenbach, W.[1]; Fischer, W.-J.[2]; Michaelis, A.[3,4]; Gebhardt, S.[4]; Geller, S.[1]; Tyczynski, T.[1]; Heinig, A.[2]; Weder, A.[2]; Hohlfeld, K.[3]

[1]*Technische Universität Dresden, Institute of Lightweight Engineering and Polymer Technology (ILK), Dresden, Germany*
[2]*Technische Universität Dresden, Institute of Semiconductors and Microsystems (IHM), Dresden, Germany*
[3]*Technische Universität Dresden, Institute of Material Science, Dresden, Germany*
[4]*Fraunhofer Institute for Ceramic Technologies and Systems IKTS, Dresden, Germany*

Abstract

For serial applications of intelligent composite structures, large-scale production technologies are required. Glass fibre polyurethane composites (GPC) are particularly suitable for the fabrication of intelligent lightweight parts with integrated sensor elements. Within the Collaborative Research Center / Transregio 39 “PT-PIESA” a novel Multi-Fibre-Injection (MFI) process based on the highly productive Long-Fibre-Injection (LFI) technology is developed. Piezoceramic and electronic functional elements are embedded in the composite structure to realise a piezoelectric functional element with sensory properties. Thus the previously separate production steps module manufacture and part fabrication are merged into one efficient production process. Theoretical and experimental studies pertaining to the elaboration of scientific and technological basics for the production of GPC with integrated sensor elements are presented. Manufacture of different piezoceramic components like fibres or pearls and the development of adapted electronic functional elements is introduced. In first processing studies the effects of process related loads on integrated piezoceramic and electronic functional elements are analysed. Therefore several modes of integration as well as different alignments of PZT-fibres and their interaction with the expanding und curing fibre matrix mixture are investigated

1. Introduction

Glass fibre polyurethane composites are predestined for the manufacture of large lightweight parts [1]. For the series production of intelligent composite structures with integrated sensor elements, the automated Long-Fibre-Injection (LFI) technology is particularly suitable. In the LFI process, glass fibre-reinforced composite structures are manufactured in a single-stage process. Rovings are fed into a special cutting unit, chopped to defined lengths and discharged simultaneously with the polyurethane matrix into an open mould. After the spraying operation and the closing of the mould, the fibre polyurethane mixture cures in the closed cavity where it expands depending on the used polyurethane system. Due to the discharge into an open mould, this spraying technology offers several possibilities for the integration of electronic and piezoceramic elements. These can either be applied on the mould surface and then be back-foamed or integrated as desired into the cross section of the component. However, the good adhesive properties of the polyurethane matrix permit a secure bonding and integration of the elements which can be demonstrated on foam-backed piezoceramic modules (Fig. 1).

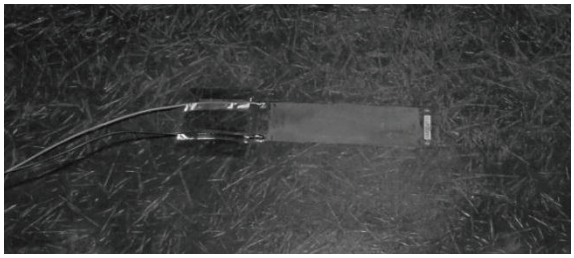

Fig. 1: *Foam-backed piezoceramic module*

In first applications using manual integration of piezoceramic elements and adapted electrode structures, the function of a prototype sensor element could be demonstrated. This is motivation for the development of a novel Multi-

Fibre-Injection (MFI) method based on the LFI spraying technology which allows the process-immanent fabrication of intelligent composite structures with sensory properties by integration of piezoceramic and electronic functional elements in GPC. Therefore the design of suitable piezoceramic components and the development of adapted electronic systems to create intelligent sensor networks are necessary.

2. Process development of the Multi-Fibre-Injection technology

The technological basis of the novel MFI process is the LFI processing unit which includes the mixing head and a special cutting unit, where fibre rovings are cut to defined lengths. The chopped fibres are charged through the mixing head supported by blowing air to its exit where they are impregnated with the effluent polyurethane matrix [2, 3].

With the current state of technology, the processing of fibre lengths from 12.5 mm to 200 mm is theoretically possible, but often fibre lengths up to max. 100 mm are used. With the new method to be developed, piezoceramic elements (such as PZT-fibres) are added through a separate supply system. The embedding of additional components such as suitable electrode structures is realized by adapted automated handling systems. In current studies, appropriate forms of piezoceramic elements and corresponding metering techniques are investigated. The analysis of the manufacturing process effects on embedded piezoceramic and electronic components is focussed in extensive processing studies. Concurrently, the design and technological implementation of an MFI mixing head are realized [4]. In addition, the development of adapted methods for contacting and polarization as well as the design and construction of highly sensitive sensor electronics with integrated wireless systems for data and energy transmission are focus of research activities. The investigations are supplemented by non-destructive tests of intelligent GPC using X-ray and computer tomography as well as characterization of the sensor functions.

3. Development and fabrication of piezoceramic components

The polysulfone process which is known from membrane fabrication was modified at Institute of Material Science TU Dresden/Fraunhofer IKTS to produce dense piezoceramic components with different geometries. Therefore the piezoceramic powder is dispersed in a binder solution forming a homogeneous mass. By adding different additives, the properties of the slurry can be adapted to specific production processes. Generally the slurry is forged through a spinning unit and placed into a precipitation bath (water). Therein the binder coagulates by an exchange reaction between solvent and water. The green body built in that way is dried and sintered to gain a compact ceramic element.

By altering technology guidance and slurry viscosity, the dimension of the piezoceramic components can be adjusted to application needs (Fig. 2).

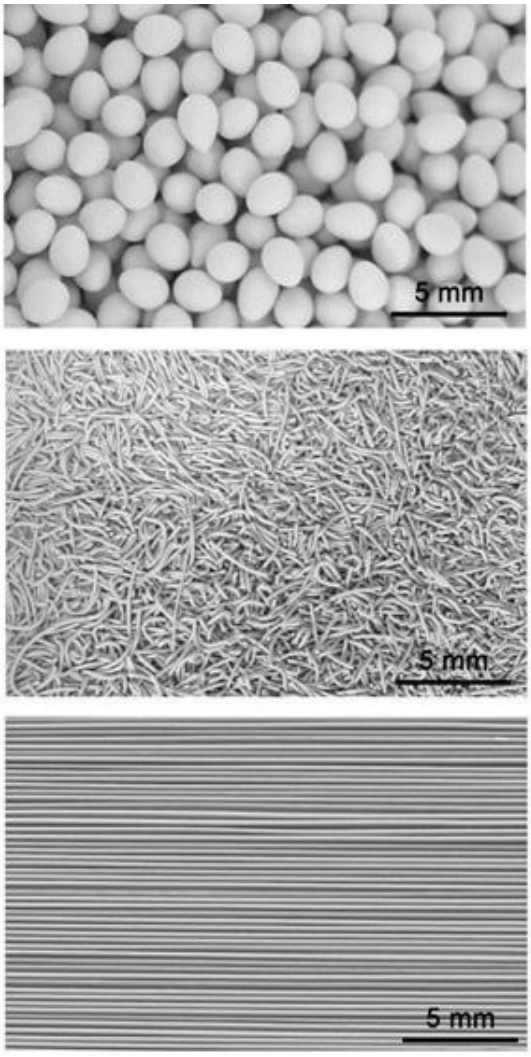

Fig. 2: *Types of piezoceramic components (downwards: pearls, fibre fragments, regular fibres)*

To prepare samples with almost spherical appearance (“pearls”) slurry viscosity has to be low and the spinning process has to be pulsed. For the manufacturing of long piezoceramic fibres a fibre spinning process is used where the slurry is continuously extruded through a nozzle. In cooperation with Hoyer Montagetechnik GmbH, Schwarzhausen, a fibre spinning machine FhG-0053 was developed and constructed which allows a semi-serial production of ceramic fibres. The machine enables spinning with two nozzles and across an overall range of about 300 meters at once. The traversing area is divided into two sub-areas, which can be used separately. The fibres are placed onto PTFE-plates lying in the precipitation bath. By this constellation, the fibre-loaded plates of one sub-area can be exchanged while the unit is still working at the second one. The fabrication of sintered piezoceramic fibres with diameters of 200-1000 µm is achieved by the use of changeable spinning nozzles.

Apart from straight fibres by the continuous fibre spinning process, short fibres can be produced either by a non-continuous spinning process or by use of fibre fragments which are generated during long fibre production. For the integration as sensor elements in the subsequent MFI process, also leftovers of fibre production with irregular size can be used.

4. Processing studies on embedded piezoceramic and electronic functional elements

Integrated piezoceramic and electronic functional elements are subject to several process-related loads like pressure and temperature. Thus, the expansion and cross linking reaction of the polyurethane components run strongly exothermic, which may generate temperatures up to 200 °C depending on the material system and component cross-section. Since this temperature is regarded as not critical for integrated piezoceramic components, the corresponding investigations are focussed on the electronic components to be integrated. In first studies, special sensor nodes developed at Institute of Semiconductors and Microsystems/ Fraunhofer IPMS have been integrated in representative prototype structures to evaluate typical temperatures during the production process. The sensor is placed on the fibre reinforcement which covers the mould surface and than connected to an adapted measuring system which allows permanent evaluation of the temperature during fabrication. Temperature measurement is started simultaneously with mixing the components. Subsequent to filling in the polyurethane mixture, the cavity is closed. After a start time of one minute, the material begins to expand, characterised by an increase of the temperature, which rises up to a value of 120 °C. After a short peak, cooling starts with a small gradient due to the low thermal conductivity of the polyurethane foam. Integrated elements have to endure a temperature of more than 100 °C for at least 2 minutes (Fig. 3).

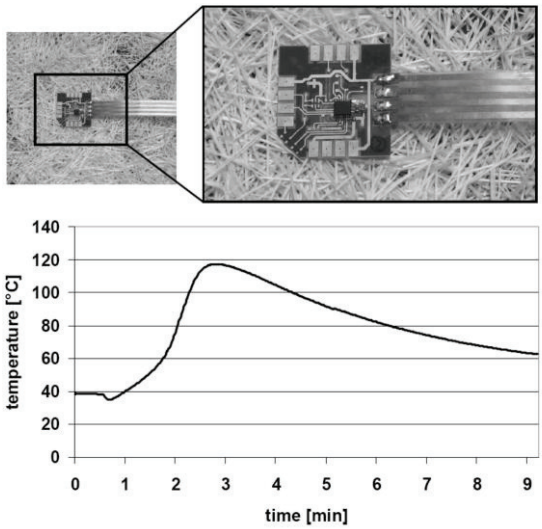

Fig. 3: *Integration of adapted sensor nodes and measuring process temperatures during expansion*

In additional investigations, the effect of these process temperatures on other electronic components is examined. RFID-tags like transponders enable wireless communication, which can be used for part identification or data transmission. Special transponders with integrated temperature sensor have been placed on the mould surface followed by back-foaming. A functional demonstration on the manufactured part with integrated transponder shows that information transfer is possible (Fig. 4).

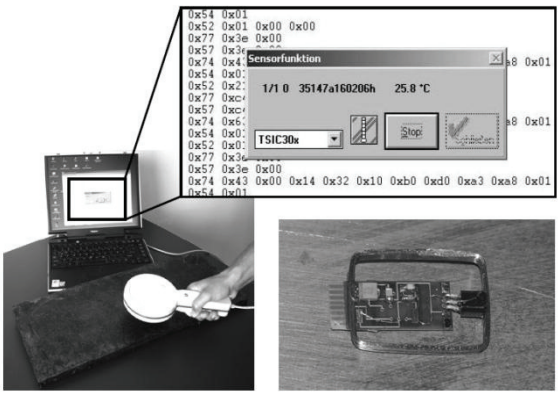

Fig. 4: *Functional demonstration on integrated transponders*

Further processing studies focus on interference on the performance of batteries for power supply. Therefore, different types of batteries like nickel metal hydride cells have been integrated in glass fibre-reinforced polyurethane composite structures. The coin cells have been discharged systematically before and after integrating. By comparison of the discharging charts, no significant decrease of the cell voltage is detectable (Fig. 5).

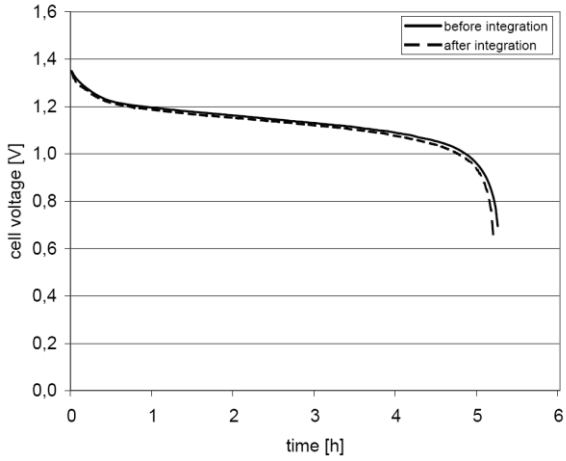

Fig. 5: *Comparison of discharging charts before and after integration of batteries*

But not only thermal resistance of integrated functional elements is required. Analogously to the LFI spraying process, an all-over discharge of the fibre polyurethane mixture is thought with the novel MFI technology. Nevertheless, slight flowage of the material can result depending on the arrangement of the robotic path, which as well as the expansion process of the polyurethane matrix can lead to deformation of the integrated structures and displacements between the piezoceramic and electronic components. This is especially considered in the design of suitable methods for electrode positioning and contacting.

Studies on piezoceramic modules which have been integrated in structures with textile reinforcement have shown that damage of the ceramic can occur due to bending stresses induced by the continuous fibres [5, 6]. Analogously, the expanding glass fibre polyurethane mixture in the LFI process generates pressure and bending loads which induce a critical stress on integrated piezoceramic components.

In corresponding studies, the influence of the process-related stress on embedded piezoceramic modules and PZT fibres is analysed. The fibres have diameters of about 280, 520 and 800 µm and lengths between 150 and 200 mm. The modules with dimensions of about 22 x 35 mm and a total thickness of about 200 µm consist of a PZT film which is provided with electrode layers. In a first analysis, modules are placed on the mould surface and back-foamed subsequently. Here, both glass content and the amount of polyurethane matrix are varied to investigate different pressure conditions. Subsequent X-ray analyses show no damage to the embedded modules independent of the fibre mass content and amount of matrix.

In additional studies, manually applied PZT fibres are integrated in GPC. The positioning of the fibres is similar to the PZT film on the mould surface whereat parallel, latticed and random forms of alignment are investigated. Additional modes of integration are explored by application of fibres on the discharged fibre matrix mixture directly before closing the mould or by embedding the fibres between several sprayed layers. The deformation and damage behaviour depends only on the type of PZT fibres but not on the way of their integration. Above all, the fibres with a diameter of 280 µm show deformation after back-foaming. With fibre diameters of 520 µm and 800 µm, however, no or only slight deformations are recognizable.

With parallel fibre alignment, these deformations do not lead to fracture of the PZT fibres. In contrast, latticed and random arrangements cause isolated fractures at the crossovers. The fracture behaviour at these intersections is examined in detail using defined latticed alignments. Once again, the fibres with the smallest diameter of 280 µm show bigger deformations and additionally are more prone to fracture than fibres with diameters of 520 µm and 800 µm. Due to their structural rigidity, these fibres show only minimal deformation and no damage (Fig. 6).

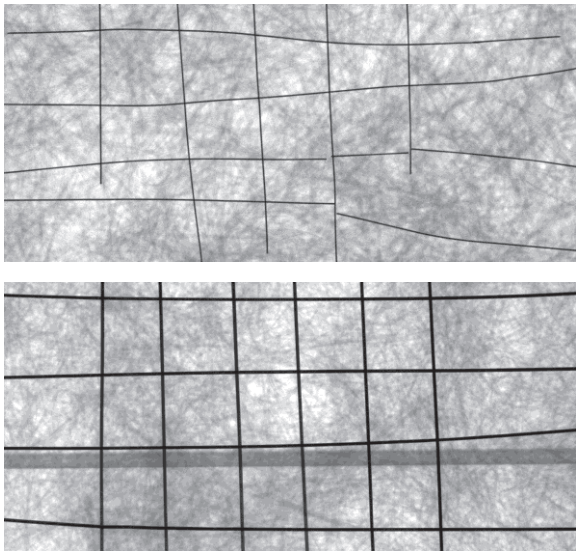

Fig. 6: *Deformation and fracture behaviour depending on fibre diameter (downwards: 280 µm and 800 µm)*

Therefore, in further research fibres with higher fibre diameters are preferred.

5. Conclusions

The suitability of glass fibre polyurethane composites to produce intelligent lightweight structures with integrated sensor elements could be demonstrated. With the innovative Multi-Fibre-Injection method based on the LFI technology, a manufacturing process is developed, that permits the process-immanent integration of piezoceramic sensor elements in GPC structures. In processing studies, the influence of process-related loads on embedded piezoceramic and electronic functional elements has been analysed. Due to gentle embedding by spraying discharge and low pressure compared to other production technologies, the integrated components are not affected heavily. Electronic components endure the temperature during processing as well as piezoceramic elements. Sensors and transponders are able to deliver information after embedding; batteries supply the same amount of electric energy like before. PZT elements show different deformation and low damage behaviour depending on their geometry. In following research activities, polarization studies on different piezoceramic elements in connection with suitable electrode structures and the detection of the resulting sensor function is focussed.

6. Acknowledgements

The authors would like to express their gratitude towards the German Research Foundation (DFG), who funds the Collaborative Research Centre/Transregio 39 “PT-Piesa” (subprojects A1, B6) at Technische Universität Dresden.

References

[1] Partusch, G.: Polyurethanschaum, der Werkstoff für fast alle Problemlösungen. Fachtagung Polymerschäume, 2003, S. D.1-11

[2] Frehsdorf, W.; Söchtig, W.: Hohe Ansprüche, niedrige Investitionskosten. LFI-PUR-Verfahren: ausgereifte Technik mit hoher Flexibilität. Kunststoffe, Band 91 (2001), Heft 3, pp. 67-70

[3] Starke, J.: LFI-PUR-Prozess; Praxiserfahrungen bei der Umsetzung in die Serie. Polyurethan Formteile Neue Trümpfe im Wettbewerb. Frankfurt am Main: Fachverband Schaumkunststoffe e.V. (FSK), 1999, pp. 207-227

[4] Hufenbach, W.; Gude, M.; Modler, N.; Zichner, M.; Heber, T.; Geller, S.: Seriengerechte Integration piezokeramischer Sensorelemente in Glasfaser-Polyurethan-Verbundstrukturen. Schriftenreihe Werkstoffe und werkstofftechnische Anwendungen. Band 41: Verbundwerkstoffe und Werkstoffverbunde. Chemnitz: Eigenverlag, 2011, pp. 283-288

[5] Hufenbach, W.; Gude, M.; Modler, N.; Heber, T.; Winkler, A.; Friedrich, J.: Processing studies for the development of a robust manufacture process for active composite structures with matrix adapted piezoceramic modules. Composites 9: 2 (2009) 133-137

[6] Hufenbach, W.; Gude, M.; Modler, N.; Heber, Th.; Winkler, A.: Untersuchungen zur Entwicklung robuster Fertigungsprozesse für die Herstellung aktiver Thermoplastverbundbauteile mit integrierten neuartigen thermoplastkompatiblen Piezo-Keramik-Modulen (TPM). Tagungsband 17. Symposium "Verbundwerkstoffe und Werkstoffverbunde", Bayreuth, 01.-03. April 2009, pp. 601-607

Methods for reliable modeling of piezoceramic materials

Rupitsch, S. J.[1]; Nicolai, M.[2]; Wolf, F.[1]; Ilg, J.[1]; Schönecker, A.[2]; Lerch, R.[1]

[1]Friedrich-Alexander Universität Erlangen-Nürnberg, Chair of Sensor Technology, Erlangen, Germany
[2]Fraunhofer Institute for Ceramic Technologies and Systems IKTS, Dresden, Germany

Abstract

This contribution deals with methods enabling reliable computer based modeling of piezoceramic materials. Thereby, the small as well as the large signal behavior are discussed. For the small signal behavior, a mathematical Inverse Method is introduced yielding realistic material parameters. The large signal behavior is modeled with two different approaches, namely a phenomenological and a viscoplastic. While the phenomenological approach offers an outstanding computation performance, the viscoplastic approach can be used to obtain detailed information of physical processes taking place inside the piezoceramic. As the comparisons of various simulations and measurements clearly show, the presented methods allow for a reliable prediction of the piezoceramic material behavior.

1. Introduction

Due to their outstanding properties, piezoceramic materials are oftentimes utilized in sensor and actuator devices [1,2]. These materials offer large actuating forces in short response times for electrical and mechanical excitations. However, the mechanical strains provided, and, thus the operating displacements are rather small for which reason a stacking of several piezoceramic layers is often employed. Recently, there is great demand for light-weight constructions with integrated active elements enabling structural health monitoring as well as controlled suppression of mechanical vibrations [3-5]. Such light-weight constructions are commonly referred to as smart structures. Appropriate active elements are piezoceramic elements which are directly integrated into the structural elements during the fabrication process. In order to predict and optimize the behavior of piezoceramic sensors and actuators as well as of light-weight structures containing piezoceramics, numerical simulations are carried out [6]. It is obvious that the reliability of the simulation results strongly depends on the model of the material behavior which is assumed within the simulations. In this contribution, we focus on approaches enabling the reliable description of the material behavior. Generally, we distinguish between small signal models and large signal models. While piezoceramic sensors can be modeled by means of the small signal behavior, a plenty of actuator devices require the consideration of the large signal behavior.

Figure 1 illustrates the typical electrical as well as mechanical behavior of piezoceramics. Furthermore, the orientations of electrical polarization of the so-called domains inside the material are shown schematically [6]. Both the electrical polarization and the mechanical strain exhibit a certain hysteretic characteristic with respect to the applied electrical field. The virgin curve refers to the initial polarization process of the piezoceramic which can be understood as the activation of the electro-mechanical-coupling. Only if this electro-mechanical-coupling is activated, the piezoceramic material can be utilized efficiently for sensor and actuator applications [1]. With a view to modeling the major loop and minor loops (Fig. 1), it is of utmost importance to take into account the large signal behavior of the piezoceramic. However, for small electrical and mechanical excitations, the minor loops can be described with the aid of an appropriate linearization, the so-called small signal model.

The paper is organized as follows. In Sec. 2, the governing equations for the small signal behavior are discussed. Moreover, a mathematical Inverse Method is briefly introduced which is utilized to identify realistic material parameters of piezoceramics. Section 3 deals with two different approaches (phenomenological and viscoplastic approach) we employ to model the large signal behavior of piezoceramic materials. The paper concludes in Sec. 4.

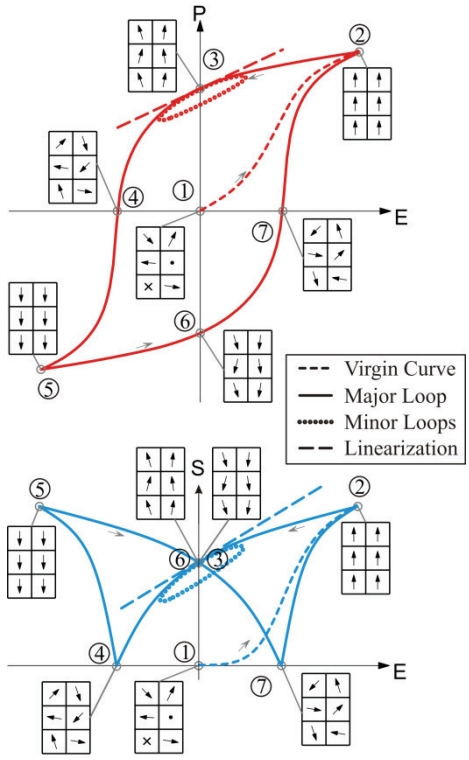

Fig. 1: *Electrical polarization* $\boldsymbol{P}$ *and mechanical strain* $\boldsymbol{S}$ *plotted against the electrical field intensity* $\boldsymbol{E}$*. Equal numbers (1-7) in the graphs refer to the same instant of time. The arrows in the squares schematically illustrate the orientations of the electrical polarization of the domains inside the piezoceramic material.*

2. Small Signal Behavior

For the majority of sensor and several actuator applications, the small signal model yields an appropriate description for the behavior of the involved piezoceramic materials. Basically, the small signal behavior of piezoceramics is modeled with [6-8]

$$\begin{aligned} \vec{T} &= [c^E]\vec{S} - [e]^{\mathrm{t}}\vec{E}, \\ \vec{D} &= [e]\vec{S} + [\varepsilon^S]\vec{E}\,. \end{aligned} \tag{1}$$

$\vec{E}$ and $\vec{D}$ denote the vectors for the electrical field intensity and the electrical flux density, respectively. $\vec{T}$ and $\vec{S}$ stand for the mechanical stress and the mechanical strain (vectors; Voigt notation), respectively. The tensors of elastic modulus $[c^E]$, of dielectric constants $[\varepsilon^S]$ and of piezoelectric moduli $[e]$ primarily determine the linearized behavior of the piezoceramic material. For the material class 6mm (transversal isotropic properties), which is frequently utilized for sensor and actuator devices, the three tensors contain overall 10 independent components [8]. Since these components are decisive for the material behavior and its modeling, they are commonly indicated as material parameters.

Common approaches to determine the independent components of the three material tensors are based on the IEEE/ANSI standard [7]. Within the framework of this standard, test specimens of the piezoceramic material are investigated exhibiting both, distinct geometric dimensions and directions of polarization. For these test samples, mono-modal mechanical vibrations are assumed whereas the tensor entries can be identified separately. As a matter of fact, the assumption of mono-modal vibrations is not valid in reality. That is the reason why the identified material parameters lead to insufficient simulation results of piezoceramic materials.

Since the IEEE/ANSI standard does not provide material parameters yielding reliable numerical simulations, we developed a so-called Inverse Method (see, e.g., [8]). Briefly, the idea of the mathematical Inverse Method is the iterative matching of simulations to measurements. In the course of the matching procedure, the material parameters are altered in a convenient way yielding the sought-after quantities of the investigated piezoceramics. Thereby, both measurements and simulations for the frequency resolved electrical impedance as well as spatially resolved normal surface velocity of the investigated piezoceramic test sample serve as input quantity of the Inverse Method. In contrast to the impedance, the velocity leads to spatially resolved information. Thus, the velocity provides more information than the impedance [8]. The numerical simulations required within the Inverse Method are conducted in the non-commercial finite element simulation tool CFS++ (Coupled Field Simulation) which is optimized for the calculation of coupled fields (e.g., electrostatic and mechanical field).

Figure 2 shows a comparison of measurements and simulations for the surface normal velocity of a piezoceramic disc (diameter 25.2 mm; height 2.0 mm) made of Pz27 which is excited with 1.0 V_{pp} at the excitation frequency 1.0 MHz. At this point it has to be mentioned, that this velocity curve did not serve as input quantity of the Inverse Method. As can be noticed, the manufacturer's parameters which are determined according to the IEEE/ANSI standard, lead to unrealistic simulations. By contrast, the material parameters identified by means of the Inverse Method yield reliable simulation results for the spatially resolved surface normal velocity. Note that the material parameters resulting from the Inverse Method exhibit to some extent deviations of more than 30 % with respect to parameters

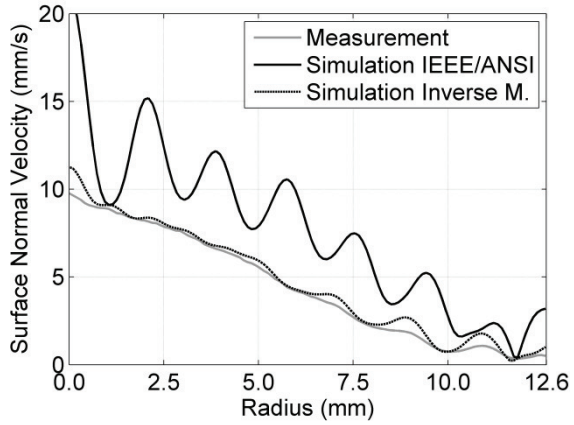

Fig. 2: *Comparison of simulations and measurements for the surface normal velocity of a piezoceramic disc (diameter 25.2 mm; height 2.0 mm; material Pz27; distributor Ferroperm) for the electrical excitation 1.0 V_{pp} at 1.0 MHz.*

provided from the IEEE/ANSI standard. This example clearly points out that appropriate material parameters are of utmost importance for reliable simulation results of piezoceramic materials.

3. Large Signal Behavior

With a view to achieving large mechanical strains, piezoceramic actuators have to be excited with large electrical excitation signals. In doing so, the piezoceramic materials show non-linear behavior, strictly speaking a hysteretic behavior (Fig. 1). When the piezoceramic actuator is utilized, for instance, as positioning element, this hysteresis has to be considered. To model the hysteretic behavior, we apply two different methods, namely a phenomenological approach and a viscoplastic approach. While the viscoplastic approach can be used to obtain a deeper understanding of the mechanisms inside the piezoceramic material, the phenomenological approach offers an outstanding computation performance. Therefore, the phenomenological approach is applicable even for large dimensions of the investigated piezoceramic material. In the following, both methods are discussed in detail.

3.1 Phenomenological approach

Our phenomenological approach is based on the so-called Preisach hysteresis operator which comprises weighted fundamental switching operators $\gamma_{\alpha\beta}$ [9,10]. Each fundamental switching operator features two distinct output values, namely -1 and 1 (Fig. 3). The switching between these two values takes place at the switching points α and β. The fundamental switching operators are weighted individually with the weighting factors $\mu(\alpha,\beta)$ which can be displayed in the so-called Preisach-plane. Note that these weighting factors exclusively determine the shape of the hysteresis curve. Instead of discretizing the Preisach-plane, we utilize appropriate analytic functions to describe the weighting factors $\mu(\alpha,\beta)$. As a result of several experiments, we figured out that (see, e.g., [9])

$$\mu(\alpha,\beta) = \frac{B}{1+[(\alpha+\beta)^2\sigma_1^2+(\alpha-\beta-h)^2\sigma_2^2]^\eta}. \qquad (2)$$

is such an appropriate analytic function. This function depends only on five parameters (B, h, σ_1, σ_2, and η) giving the additional benefit of being unique when they are identified.

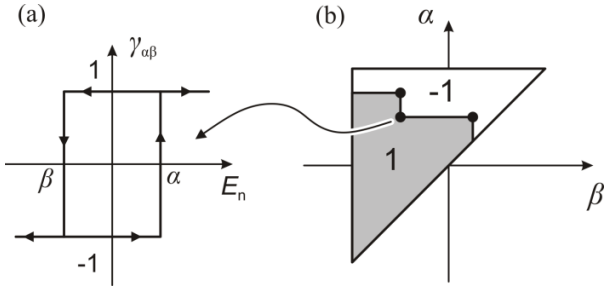

Fig. 3: *(a) Fundamental switching operator $\gamma_{\alpha\beta}$ for the switching points α and β. (b) Preisach plane containing the actual output values of the fundamental switching operators.*

Applied to the electrical field intensity E_n (normalized), the electrical polarization P_n (normalized) of a piezoceramic material can be calculated by means of the presented phenomenological approach as (time *t*)

$$P_n(t) = \iint_{\alpha\geq\beta} \mu(\alpha,\beta)\gamma_{\alpha\beta}\,[E_n](t)\,\mathrm{d}\alpha\mathrm{d}\beta. \qquad (3)$$

The five parameters required for the analytic function of the weightings (Eq. (2)) can be obtained from a a comparison of the model output of the phenomenological approach and measurements. In order to obtain appropriate model outputs for the mechanical strain S_n (normalized) of the piezoceramic material, the progression of electrical polarization can be squared. For strain outputs being more realistic, an additional coefficient relating to polarization to the power of four is required.

We utilized the Preisach hysteresis operator to model the electrical polarization and mechanical strain of piezoceramic materials for both, different electrical and mechanical loads [10,11]. For instance, we investigated the electrical polarization of a piezoceramic disc in case of

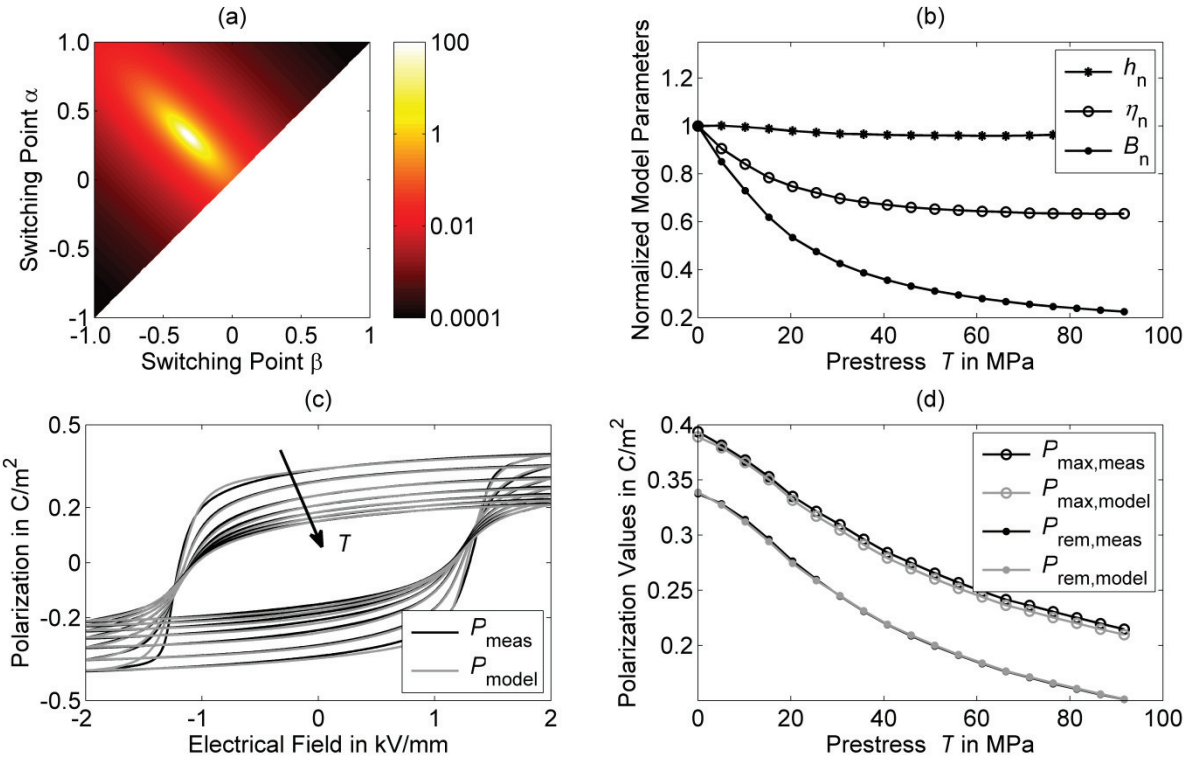

Fig. 4: *(a) Preisach plane containing the weighting factor $\boldsymbol{\mu(\alpha,\beta)}$ for the mechanically unloaded case (i.e., 0 N) of the piezoceramic disc. (b) Normalized parameters of the analytic weighting function $\boldsymbol{\mu(\alpha,\beta)}$ plotted against the applied uniaxial mechanical loading causing a prestress of the piezoceramic. (c) Measurements and model outputs for the electrical polarization. (d) Measurements and model outputs for the maximum and remanent polarization. Investigated piezoceramics disc: diameter 25.2 mm; height 2.0 mm; material Pz27; distributor Ferroperm.*

varying static and isotropic mechanical loadings which were applied with a material testing machine. Note that these mechanical loadings cause a certain prestress of the piezoceramics altering the behavior of the material. Figure 4a illustrates the Preisach plane containing the weighting factors $\mu(\alpha,\beta)$ for the unloaded case (i.e., no mechanical loading) of the investigated piezoceramic disc made of Pz27. Figure 4b depicts the progress of the parameters B, η, and h (Eq. (2)) with respect to the applied mechanical loading. These parameters result from the comparison of measurements and simulations. In the particular case, the remaining parameters (σ_1 and σ_2) were not altered with respect to the applied mechanical load since they do not affect the hysteresis curve in that way which was observed in the measurements. As one can see in Fig. 4c, the model output coincides quite well with the measurements. This is confirmed, if measurements and simulations are compared for characteristic quantities of the hysteresis curve (e.g., remanent polarization P_{rem}), see Fig. 4d. Hence, the presented phenomenological approach is applicable to model the behavior of piezoceramic materials even in case of varying mechanical loadings.

3.2 Viscoplastic approach

In addition to the phenomenological approach for the large signal behavior of piezoceramic materials, we developed a viscoplastic model which allows the consideration of direct coupling of mechanics and electrostatics. Thereby, we utilize a three-dimensional as well as homogeneous model to describe the behavior of common piezoceramic materials composed of rhombohedral and tetragonal domains. Within this model, the electrical polarization of a finite element representing several domains is aligned in space. In reality, the amount of possible orientations of polarization is infinite. However, we figured out that the restriction to 14 possible orientations yields reliable simulations. Compared to microscopic approaches [12-15], the application of this homogeneous scheme requires only a rough spatial discretization of the investigated material which leads to a feasible computation effort. Note that the presented model is applicable for a fine spatial discretization of piezoceramic materials, too. Therewith, one can obtain a deeper understanding of the processes taking place inside the material.

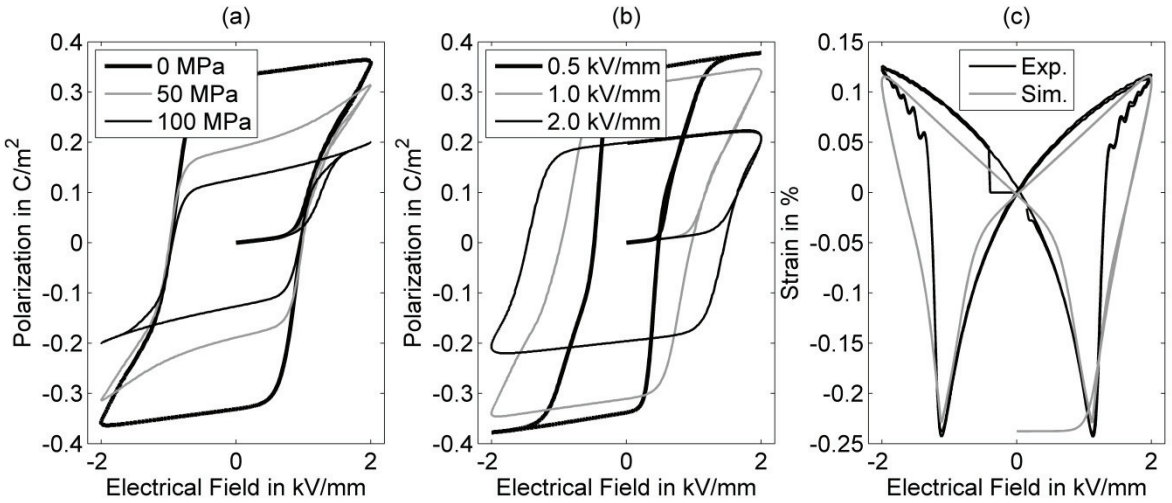

Fig. 5: *(a) Electrical polarization plotted against the electrical field intensity for different uniaxial mechanical loadings. (b) Electrical polarization plotted against the electrical field intensity for different electrical coercive field strengths. (c) Measurements and simulations for the mechanical strain plotted against the electrical field intensity. Investigated piezoceramic disc: diameter 10.0 mm; height 1.0 mm; material SP505; distributor CeramTec.*

Starting point of our viscoplastic approach are the material tensors (e.g., $[c^E]$, $[\varepsilon^S]$, and $[e]$, see Eq. (1)) for a completely polarized piezoceramic material. Each orientation i $(i = 1, \dots, 14)$ of the 14 which are possible is assigned with spatially transformed material tensors and the probability ξ_i. The mechanical and electrical quantities for a single finite element result from the vectorial sum of the transformed material tensors scaled by the probability. Note that a variation of the local electrical or mechanical loadings leads to a change in the probabilities causing altered electrical and mechanical quantities of the finite element.

To calculate the actual electrical and mechanical state of the finite element, the interaction between the different orientations of electrical polarization is required. The interaction between the directions j to i is defined as transformation system and characterized by the transformation rate ϖ^{ij}. According to the viscoplastic approach, this transformation rate can be calculated as

$$\omega^{ij} = \omega_0 \left\{ exp\left[1 - \frac{f^{ij}}{f_{\text{krit}}}\right]\right\}^m (\xi_i)^v. \qquad (4)$$

The parameters ω_0, v, and m denote appropriate model parameters. f^{ij} stands for the energy which is related to electrical and/or mechanical loadings projected on the polarization orientation i. f_{krit} represents the switching value of this energy. For the electrostatic field, this switching value is given by $f_{\text{krit}} = E_c P_0$ where E_c stands for the electrical coercive field strength and P_0 denotes the maximum value of the remanent polarization.

In a further step, the determined transformation rates ϖ^{ij} are applied to update the probability of polarization orientation. The change $\dot{\xi}_i$ of probability for orientation i is given by

$$\dot{\xi}_i = \sum_{i=1, j\neq i}^{14} (-\omega^{ij} + \omega^{ji}). \qquad (5)$$

By means of this change, the probabilities ξ_i for the polarization orientation can be determined for the subsequent time step. With this updated probabilities, the actual state of the electrical as well as mechanical quantities can be calculated for the finite element. Note that both, the spatial discretization of the piezoceramic material and the time discretization primarily affect the accuracy of the viscoplastic approach.

We utilized the viscoplastic approach to study the behavior of piezoceramic materials in case of different loadings as well as combinations of mechanical and electrical loadings. For the presented results, only one finite element was used within the simulation. Figure 5a depicts the hysteresis curves for the electrical polarization with respect to mechanical loadings applied to the piezoceramic. As expected, the extent of the hysteresis is reduced for increasing mechanical loadings. Mainly, this can be ascribed to the reduction of the domain wall mobility. In Fig. 5b, one can see the hysteresis of the electrical polarization for varying electrical coercive field strengths. Since the polarization energy density within the piezoceramics is limited from the physical point of view, an increasing coercive field strength reduces the electrical polarization due to the reduction of the domain wall mobility. It can be noticed in Fig. 5b, that the viscoplastic

approach captures this behavior of piezoceramic materials. Finally, we employed the viscoplastic approach to simulate the mechanical strain of a piezoceramic disc (diameter 10.0 mm; height 1.0 mm) made of SP505 in case of electrical excitations, see Fig. 5c. Although only one single finite element was used within the calculation, the comparison of the simulations and measurements reveals that the model yields reliable results. Hence, the presented viscoplastic approach is applicable to predict the large signal behavior of piezoceramics for both, electrical polarization and mechanical strain.

4. Conclusion

In this contribution, we presented appropriate simulation models to describe both, the small signal and the large signal behavior of piezoceramic materials. As the results for the small signal modeling clearly points out, the choice of material parameters is decisive for reliable simulations results. Therefore, we developed a mathematical Inverse Method yielding such appropriate material parameters. For the modeling of the large signal behavior of piezoceramics, we utilized two different approaches. The phenomenological approach is based on the Preisach hysteresis operator. Within the viscoplastic approach, 14 orientations of polarizations are assumed leading to the possibility of considering mechanical loadings applied in different directions. As the comparisons of measurements and simulations shows, both approaches can be utilized for reliable simulations of the large signal behavior of piezoceramic materials even in case of varying mechanical loadings.

5. Acknowledgement

The underlying research is gratefully supported by the German Research Foundation (DFG) as part of the special research field SFB/TR 39.

References

[1] *Heywang, W.; Lubitz, K.; Wersing, W.: Piezoelectricity: Evolution and future of a technology. Springer, 2008.*

[2] *Lerch, R.; Sessler, G.; Wolf, D.: Technische Akustik. Springer, 2009.*

[3] *Varadan, V.K.; Vinoy, K.J.; Gopalakrishnan, S.: Smart material systems and MEMS. John Wiley and Sons, 2006.*

[4] *Irschik, H.: A review on static and dynamic shape control of structures by piezoelectric actuation. Engineering Structures, vol. 24(1), pp. 5-11, 2002.*

[5] *Hufenbach, W.; Gude, M.; Modler, N.; Heber, T.; Tyczynski, T.: Sensitivity analysis for the process integrated online polarization of piezoceramic modules in thermoplastic composites. Smart Materials and Structures, vol. 19(10), pp. 1-6, 2010.*

[6] *Kaltenbacher, M.: Numerical simulation of mechatronic sensors and actuators. Springer, 2007.*

[7] *IEEE Standard on Piezoelectricity, ANSI-IEEE Std. 176-1987, 1988.*

[8] *Rupitsch, S.J.; Lerch, R.: Inverse Method to estimate material parameters for piezo-electric disc actuators. Applied Physics A, vol. 97, pp. 735-740, 2009.*

[9] *Sutor, A.; Rupitsch, S.J.; Lerch, R.: A Preisach-based hysteresis model for magnetic and ferroelectric hysteresis. Applied Physics A, vol. 100, pp. 425-430, 2010.*

[10] *Wolf, F.; Sutor, A.; Rupitsch, S.J.; Lerch, R.: Modeling and measurement of creep- and rate-dependent hysteresis in ferroelectric actuators. Sensors and Actuators A, Article in press, doi.: 10.1016/j.sna.2011.02.026.*

[11] *Wolf, F.; Sutor, A.; Rupitsch, S.J.; Lerch, R.: Modeling and measurement of influence of mechanical prestress on hysteresis of ferro-electric actuators. Proceedings Eurosensors 2011, Article in press.*

[12] *Belov, A.Yu.; Kreher, W.S.: Viscoplastic models for ferroelectric ceramics. J. European Ceramic Society, vol. 25, pp. 2567-2571, 2005*

[13] *Landis, C.M.: Fully coupled, multi-axial, symmetric constitutive laws for poly-crystalline ferroelectric ceramics. J. Mech. Phys. Solids, vol. 50, pp. 127-152, 2002.*

[14] *Huber, J.E.; Fleck N.A.; Landis C.M.; McMeeking, R.M.: A constitutive model for ferroelectric polycrystals. J. Mech. Phys. Solids, vol. 47, pp. 1663-1697, 1999.*

[15] *McMeeking R.M.; Landis C.M.: A phenomenological multiaxial constitutive law for switching in polycrystalline ferro-electric ceramics. Int. J. Eng. Sci., vol. 40, pp. 1553-1577, 2002.*

Pyroelectric response as a sensitive tool for the characterization of piezoelectrics

Movchikova, A. A.[1]; Malyshkina, O. V.[1]; Suchaneck, G.[2], Gerlach, G.[2]; Steinhausen, R.[3]; Langhammer, H. T.[3]; Beige, H.[3]

[1]Tver State University, Dep. of Ferroelectric and Piezoelectric Physics, Tver, Russia
[2]Technische Universität Dresden, Solid State Electronics Lab, Dresden, Germany
[3]Martin-Luther-Univ. Halle-Wittenberg, Department of Physics, Halle, Germany

Abstract

This work reviews the application of thermal wave methods with regard to piezoelectrics.

1. Introduction

It is well known that the polarization state has sufficient influence on the physical properties of materials and processes occurring under various excitations not only on surfaces, but also in the bulk of a crystal [1]. A key problem of ferroelectrics research is the non-destructive measurement of polarization and space-charge profiles [2]. During the past several decades, a number of techniques based on an external stimuli (optical, thermal, mechanical or electrical) have been developed to generate local changes in the permittivity of the sample resulting in a response carrying information on the spatial polarization distribution. Particularly, a popular concept is the thermal wave method also known as the dynamic method for investigation a pyroelectric effect [3, 4] where the sample is heated by a modulated heat flux. Different ways of thermal wave modulation were reported: Most frequently, sinusoidal [2, 4-14] or rectangular [3, 4, 13-19] waves are employed. The incident thermal wave changes the sample temperature leading to changes of the polarization value. A part of the charges screening the spontaneous polarization is freed when polarization decreases with temperature. The redistribution of these charges in the external electric circuit is the pyroelectric current which is recorded by an external measuring device. The registration of the pyrocurrent is mostly performed in two ways:

1) By the frequency dependence of the pyroelectric current including the phase shift between pyroelectric response and the heat flux in the case of sinusoidal modulation of a light beam (Laser intensity modulation method (LIMM)) [2-7],
2) By the time dependence of the pyroelectric response in the case of low-frequency thermal square-waves (the Thermal Square Wave Method-TSWM) [18-19].

2. Direct and inverse methods

From the mathematical point of view, the data analysis may be performed in two ways: By the direct method and by the inverse method.

In the direct method, a known polarization distribution across the sample thickness is assumed and the pyroelectric response is calculated. Comparing calculated data with experimental ones, one can analyze the polarization distribution in the ferroelectric material. Also, the direct method can be used for determination the thermal diffusivity of ferroelectric and non-ferroelectric materials [20].

In the inverse method, the polarization profile is calculated from the experimental data for the frequency or the time dependence of the pyroelectric response. Mathematically, the direct method is simpler than the inverse method. In this work, we use direct and inverse TSW-methods.

3. Investigation of piezoelectric materials by TSWM

The proposed by us inverse TSW-method [18, 19] was applied so far to $LiTaO_3$ single crystals [19], undoped and doped $(Sr,Ba)Nb_2O_6$ single crystals [21-24], PMN-0.28PT single crystals [25], $Pb(Zr,Ti)O_3$ ceramics and thin films [26, 27]. The TSW-method was used also for the investigation of $BaTi_{1-x}Sn_xO_3$ (BTS) ceramics [28, 29]. This novel type of lead-free material is widely used in piezoelectric actuators and microsensors. Ceramics with continuously varying chemical composition acquires an inhomogeneous distribution of dielectric and

piezoelectric properties after poling. Such functional gradient materials are especially suitable for bending actuators, e.g., in bimorph layered systems. Among the advantages of these materials are low internal stresses, low production costs and the possibility to design lead-free systems fulfilling EU directives.

Functionally graded BTS with tin concentration of $0.075 \leq x \leq 0.15$ varying over the sample thickness were investigated. The samples were fabricated with smooth gradients of concentration by sintering of the bi-, tri- and tetramorph green bodies [29]. The results were compared with the pyroelectric profiles of BTS samples without tin gradient with x = 0.075, 0.10, 0.125 and 0.15. The investigation of the polarization profiles in BTS ceramics by the thermal square wave method demonstrates that homogeneous samples of uniform composition poled at the ferroelectric phase transition temperature have uniform polarization distribution. Nonuniform polarization distribution necessary for a number of applications is realized only by a depoling process resulting in a decrease of pyroelectric coefficient and ferroelectric properties. On the other hand, nonuniform polarization distribution may be obtained at room temperature in BTS ceramics with composition gradients provided the samples contain components existing at this temperature in different phases (ferroelectric and paraelectric) [28].

The direct TSW-method was applied for the determination of thermal diffusivity coefficients of thin dielectric films. Approbation of the technique was carried out as-deposited, unannealed PZT film on a lithium tantalate crystal and on polarized PZT film. A decrease of the thermal diffusivity coefficient (from $1{,}5 \cdot 10^{-7}$ to $0{,}006 \cdot 10^{-7}$ m^2/s) with the decreasing film thickness (from 240 to 0,4 μm, respectively) was observed. The difference between the values of the thermal diffusivity coefficient of PZT films and of PZT bulk ceramics [29, 30] can be attributed to the fact that thin polycrystalline films are more porous than the bulk samples. Also the presence of size effect in the propagation of heat in the sample should be taken into account.

4. Conclusions

We have shown that the use of TSW-method enables:

- to investigate the polarization profile in a bulk materials and thin films,
- to determine influence of nonuniform structure and composition on polarization distribution in ferroelectrics,
- to determine the thermal diffusivity of dielectric thin films.

References

[1] *Prokhorov A. M.; Kuz'minov Yu. S.: Ferroelectric Crystals for Laser Radiation Control. Nauka, Moscow; 1982 (in Russian)*

[2] *Lang S. B.; Das-Gupta D. K.: A technique for determining the polarization distribution in thin polymer electrets using periodic heating. In: Ferroelectrics, 39 (1981)1, pp. 1249-1252*

[3] *Chynoweth A. G.: Dynamic method for measuring the pyroelectric effect with special reference to barium titanate. In: J. Appl. Phys., 27 (1956) 1, pp. 78-84*

[4] *Chynoweth A. G.: Surface space–charge layers in barium titanate. In: Phys. Rev., 102 (1956) 3, pp. 705-714*

[5] *Lang S. B.; Das-Gupta D. K.: Laser intensity modulation method: a technique for determination of spatial distributions of polarization and space charge in polymer electrets. In: J. Appl. Phys., 59 (1986) 6, pp. 2151-2160*

[6] *Ploss B.; Emmerich R.; Bauer S.: Thermal wave probing of pyroelectric distributions in the surface region of ferroelectric materials: A new method for the analysis. In: J. Appl. Phys., 72(1992) 11, pp. 5363-5370*

[7] *Sandner T.; Suchaneck G.; Koehler R.; Suchaneck A.; Gerlach G.: High frequency LIMM-a powerful tool for ferroelectric thin film characterization. In: Integrated Ferroelectrics, 46 (2002) 1, pp. 243-257*

[8] *Bauer S.; Bauer-Gogonea S.: Current practice in space charge and polarization profile measurements using thermal techniques. In: IEEE Trans. Dielectr. Electr. Insul., 10 (2003) 5, pp. 883-902*

[9] *Lang S. B.: Fredholm integral equation of laser intensity modulation method (LIMM): Solution with the polynomial regularization and L-curve methods. In: J. Mat. Sci., 41 (2006) 1, pp. 147-153*

[10] *Bezdetnyj N. M.; Zejnaly A. H.; Hytorskij V. E.: Study the polarization distribution in the ferroelectrics by the dynamic pyroelectric method. In: Izv. AN USSR Ser. Phys, 48 (1984), pp. 200-203*

[11] *Marty-Dessus D.; Berquez L.; Petre A.; Franceschi J. L.: Space-charge cartography by FLIMM: a three-dimensional approach. In: J. Phys. D: Appl. Phys., 35 (2002), pp. 3249-3256*

[12] *Stewart M.; Cain M.: Use of scanning LIMM (Laser Intensity Modulation Method) to characterize polarization variability in dielectric materials. In: J. Phys: Conf. Ser., 183 (2009), p. 012001*

[13] *Kremenchugskij L. S.: Ferroelectric radiation detectors. Kiev, Naukova Dumka Publishers; 1972 (in Russian)*

[14] *Lang S. B.: Sourcebook 321 of pyro-electricity. New York; London; Paris: Gordon and Brech Sci. Publishers; 1974*

[15] *Glass A. M.: Dielectric, thermal, and pyro-electric properties of ferroelectric LiTaO3. In: Phys. Rev., 172 (1968) 2, pp. 564-571*

[16] *Zajosz H. I.; Grylka A.: Thermally-generated electric fields and the linear transient pyroelectric response. In: Infrared Phys., 23 (1983) 5, pp. 271-276*

[17] *Bogomolov A. A.; Malyshkina O. V.: Surface layers in DTGS crystals. In: Izv. AN USSR. Ser. Phys, 57 (1993), pp. 199-203*

[18] *Malyshkina, O.V.; Movchikova, A.A.; Suchaneck, G: A new method for determining the coordinate dependences of the pyroelectric current in ferroelectric materials. In: Physics of the Solid State, 49 (2007) 11, pp. 2144-2147*

[19] *Malyshkina O. V.; Movchikova A. A.; Grechishkin R. M.; Kalugina O. N.: Use of the Thermal SquareWave Method to Analyze Polarization State in Ferroelectric Materials. In: Ferroelectrics, 400 (2010) 1, pp. 63-75*

[20] *Lang S.B.: Technique for the measurement of thermal diffusivity based on the laser intensity modulation method (LIMM). In: Ferroelectrics, 93 (1989) 1, pp. 87-93*

[21] *Movchikova A.A.; Malyshkina O.V.; Pedko B.B.; Lisitsin V.S.; Burtsev A.V.: Influence of thermocycling on the polarization distribution of doped SBN crystals. In: Ferroelectrics, 399 (2010) 1, pp. 14-19*

[22] *Malyshkina O.V.; Movchikova A.A.; Pedko B.B.; Boitsova K.N.; Sorokina I.I.: Polarization distribution and domain structure in SBN crystal doped by Eu or Rh. In: Ferroelectrics, 398 (2010) 1, pp. 64-70*

[23] *Malyshkina O.V.; Movchikova A.; Pedko B.B.; Potemkin V.V.; Ivanov V.V: The Influence of doping on electric properties of strontium-barium niobate crystals. In: Ferroelectrics, 405 (2010) 1, pp. 45-49*

[24] *Movchikova A.; Suchaneck G.; Malyshkina O.V.; Pedko B.B.; Gerlach G.: The influence of doping on the pyroelectric response of SBN single crystals. In: Ferroelectrics, 378 (2009) 1, pp. 186-194*

[25] *Movchikova A.A.; Malyshkina O.V.; Suchaneck G.; Gerlach G.: The role of the secondary pyroelectric effect in a ferroelectric relaxor $0.72Pb(Mg_{1/3}Nb_{2/3})O_3$–$0.28PbTiO_3$. In: Bulletin of the Russian Academy of Sciences: Physics, 74 (2010) 9, pp. 1270-1271*

[26] *Malyshkina O.; Movchikova A.; Kalugina O.; Suchaneck G.; Gerlach G.: Thermal wave analysis of the pyroelectric response of thin PZT films. In: Abstracts book of "19th International Symposium on the Applications of Ferroectrics and 10th European Conference on the Applications of polar Dielectrics" Edinburgh (Scotland), (2010), p. 95*

[27] *Malyshkina O.V.; Movchikova A.A.; Barabanova E.V.; Embil I.A.; Pugachev S.I.; Golovin V.A.; Daineko A.V.; Solovjev M.A.: The polarization profile of PZT-based ceramics. In: Abstracts book of "The XXII International Conference on relaxation phenomena in solids": Voronezh (Russia), (2010), p. 101*

[28] *Malyshkina O.; Movchikova A.; Steinhausen R.; Langhammer H.T.; Beige H.: Study of the pyroelectric profile in BTS piezo-ceramics by the single frequency Thermal Square Wave Method. In: J. Eur. Ceram. Soc., 30 (2010) 2, pp. 211-214*

[29] *Movchikova A.; Malyshkina O.; Suchaneck G.; Gerlach G.; Steinhausen R.; Langhammer H.T.; Pientschke C.; Beige H.: Study of the pyroelectric behavior of $BaTi_{1-x}Sn_xO_3$ piezo-ceramics. In: J. Electroceram, 20 (2008) 1, pp. 43-46*

[30] *Bauer S.; Ploss B.: Design and Properties of a Microcalorimeter. In: IEEE Transactions on Electrical Insulation, 27 (1992) 4, pp. 861-866*

Pulsed magnetron sputtered AlN thin films - a lead-free material for piezoelectric applications

Glöß, D.[1]; Bartzsch, H.[1]; Gittner, M.[1]; Barth, S.[1]; Frach, P.[1]; Herzog, T.[2]; Walter, S.[2]; Heuer, H.[2]

[1]*Fraunhofer Institute for Electron Beam and Plasma Technology (FEP), Dresden, Germany*
[2]*Fraunhofer Institute for Non-Destructive Testing (IZFP, Dresden branch), Dresden, Germany*

Abstract

Reactive pulse magnetron sputtering of Al targets in a gas mixture of Argon and Nitrogen allows the deposition of AlN layers at high deposition rates of up to 200 nm/min. In the reported experiments AlN films were deposited onto unheated substrates with a thickness of typically 10 µm. Deposited films have been characterized for a variety of layer properties using e.g. XRD, SEM, profilometry, weighting and piezoelectric measurements regarding crystalline structure and orientation, surface morphology, density, film stress and piezoelectric coefficient d_{33}. Surprisingly films with high piezoelectric properties could be obtained both by strong and moderate particle bombardment during deposition using adapted parameter sets. The films show a nearly pure (001) orientation of the crystalline structure, an undisturbed surface morphology, a high density and a very high piezoelectric coefficient d_{33} of up to 7.2 pm/V on silicon substrate. The suitability for the intended application in high frequency ultrasonic phased array sensors systems is investigated using pulse echo measurements. Moreover, principle suitability of the films for energy harvesting is presented.

1. Introduction

New 3-dimensional integrated electronic devices, next generations of textured materials like carbon fiber reinforces polymers (CFRP) and complex multilayered devices like solar cells require new approaches for non-destructive evaluation techniques. One area of research and development are high frequency ultrasonic phased array sensors systems that combine the performance of phased array methods with the resolution of a scanning acoustic microscope. The very high frequencies in phased array sensors require a very thin transducer thickness and cannot be realized with traditional piezoelectric materials like PZT ceramics, piezoelectric 1-3 composites or polymers like polyvinylidenfluoride (PVDF). A promising alternative piezoelectric material is aluminum nitride (AlN).

Aluminum nitride is a piezoelectric but not ferroelectric material with a Wurtzite crystal structure. Compared to the widely used ferroelectric materials like PZT, AlN cannot be electrically polarized. Therefore piezoelectric activity can only be observed in single crystals or in a polycrystalline structure with a strong crystal orientation. To achieve a thickness vibration of the sensor, a crystalline orientation in (001) direction is necessary (c-axis of the AlN crystalline structure being oriented perpendicular to the substrate surface).

In this paper, piezoelectric AlN films with a thickness of up to 10 µm were investigated. The reactive pulse magnetron sputtering process was optimized for high rate deposition of AlN thin films with strong piezoelectric properties.

2. Experimental

Coatings were carried out in cluster type sputter equipment using the Double Ring Magnetron DRM 400 developed at Fraunhofer FEP. This type of magnetron combines two concentric discharges allowing uniform coating of substrates with a diameter up to 200 mm [1]. Figure 1 shows the schematic of the deposition set up. Pulse powering at 50 kHz in unipolar or bipolar pulse mode was applied using the pulse unit UBS-C2 of Fraunhofer FEP and standard DC power supplies. Pure metallic aluminum targets were sputtered in a mixture of argon and oxygen as reactive gas. A closed loop control of the reactive gas inlet allowed stabilizing the process in the so-called transition mode, where stoichiometric films are deposited at high deposition rates.

Using the DRM 400, the pulse mode of the pulse magnetron sputtering process can be changed between unipolar and bipolar. In the unipolar pulse mode, a pulsed dc is applied between each of the two targets and the separate hidden anode. In the bipolar pulse mode, a voltage with alternating polarity is applied between the two targets. For the two pulse modes, the plasma properties are completely different (Table 1). Thus, variation of the pulse mode allows new degree of freedom to optimize deposition process. On one hand, the unipolar pulse mode shows low thermal substrate load and it allows e.g. coating of very temperature sensitive substrates. On the other hand, in the bipolar pulse mode a very intense energetic ion bombardment occurs that allows deposition of very dense films.

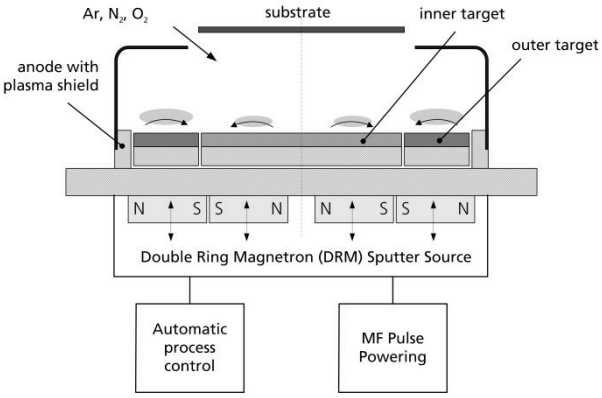

Fig. 1: *Deposition setup for sputter deposition*

Table 1: *Results of Langmuir Probe and temperature measurements, SiO_2 sputtering at 7.5 kW*

Pulse mode		unipolar	bipolar
Plasma density	*[1/cm³]*	*$1.8 \cdot 10^{10}$*	*$11.0 \cdot 10^{10}$*
Electron temperature	*[eV]*	*10*	*6*
Thermal substrate load	*[W/cm²]*	*0.15*	*0.75*

From literature it is known, that the sputter parameters strongly influence the piezoelectric behavior [2]. Thus, for each of the two pulse modes the power and voltage applied to the sputter target as well the pressure was varied to find optimal process parameters for the deposition of AlN layers with highest piezoelectric properties. In Table 2, deposition parameters are summarized.

Table 2: *Range of AlN deposition parameters*

Sample		AlN-UP	AlN-BP
Pulse mode		*unipolar*	*bipolar*
Preheating		*room temperature*	*room temperature*
Power	*[kW]*	*6…13*	*6…13*
Pressure	*[Pa]*	*0.15…2*	*0.15…2*
Deposition rate	*[nm/min]*	*100...200*	*80...160*

For the evaluation of piezoelectric properties, a simple ultrasound transducer test layout was used. An electrode structure with 10 mm diameter was deposited on an isolated silicon wafer. An AlN film in a circle structure with a diameter of 13 mm was deposited, followed by a second aluminum electrode to fabricate the sensor and the interconnection pad on the top side. The structures were realized by using laser cutted aluminum oxide ceramic masks with a high stiffness to prevent bending when being reused. The area of the deposited sensor layer needs to be larger than the electrodes themselves, because there occur edge effects during the deposition process, which influence the piezoelectric behavior of the sensor.

3. Structural, electrical and mechanical properties

The characterized AlN films can be classified into 2 groups. The first group shows a nearly pure (001) orientation of the crystalline structure, an undisturbed surface morphology, a high density and a very high piezoelectric coefficient d_{33} of up to 8 pm/V. The second group exhibits a dominating but not pure 001 orientation, disturbances in the surface morphology, a slightly lower density and a piezoelectric coefficient close to zero. The range of the process parameters pulse mode, pressure, sputtering power and reactive working point to achieve the layers of the first group is very narrow. Surprisingly films belonging to the first group with high piezoelectric constant can be obtained both by moderate and strong particle bombardment during deposition in unipolar and bipolar pulse mode respectively.

Figure 2 shows the XRD diagrams of films with nearly pure (001) orientations (002 and 004 peaks) deposited in unipolar and bipolar mode. Figure 3 shows the results of SEM investigations on these samples. The fracture in the SEM micrograph exhibits in both cases a dense

microstructure. Surface morphology is rather coarse in bipolar compared to unipolar pulse mode.

In Table 3, most important layer properties for the two layers with highest piezoelectric properties are summarized. Films deposited in bipolar mode exhibit slightly higher values of piezoelectric coefficient, density, resistivity and breakdown field strength, but show significantly stronger compressive stress.

Table 3: *Deposition parameters and layer properties for piezoelectric AlN layers*

Sample		AlN-UP	AlN-BP
Pulse mode		*Unipolar*	*Bipolar*
Crystalline orientation (fraction)		*002 (99.9%)*	*002 (99.9%)*
Density	*[g/cm^3]*	*3.16*	*3.20*
Break down field strength	*[MV/cm]*	*2.3*	*3.1*
Resistivity	*[Ωcm]*	*5.3·10^{12}*	*1.2·10^{13}*
piezoelectric charge constant d_{33}	*[pm/V]*	*6.5*	*7.2*
Mechanical stress	*[GPa]*	*-1*	*-2*

4. Characterization of piezoelectric properties

The AlN thin films were used already for SAW filters, microwave filter or resonator and ultrasound transducers [3-5]. One possible new application is as sensor thin films in special phased array ultrasound transducers. For this application, the transformation of electrical energy in acoustical energy and vice versa has to be verified and quantified. Acoustical measurement in pulse echo mode were carried for each sensor to characterize the vibration behavior and the maximum signal voltage. Afterwards the electrical properties and piezoelectric charge constants were measured with a Berlincourt-Meter.

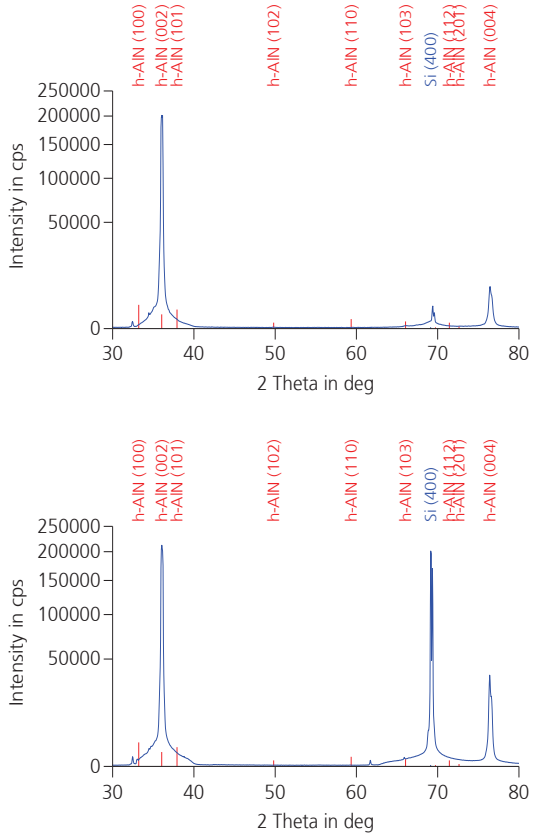

Fig. 2: *XRD diagrams (a: unipolar pulse mode, b: bipolar pulse mode)*

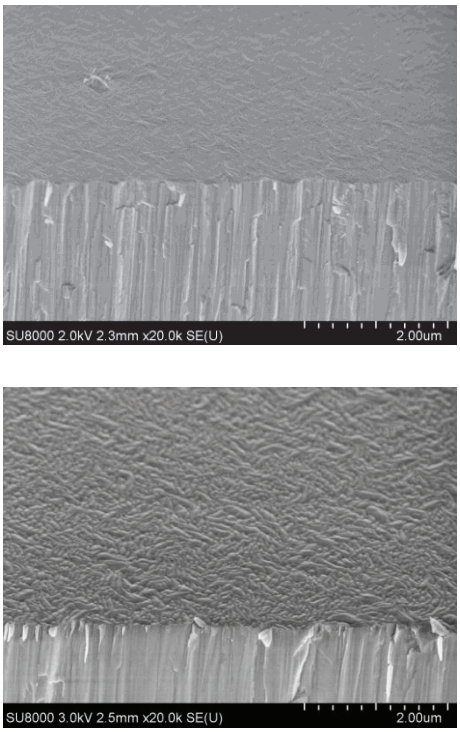

Fig. 3: *SEM-micrographs of AlN films, thickness 10µm (a: unipolar pulse mode, b: bipolar pulse mode)*

4.1 Pulse Echo Mode

In the pulse echo measurements the AlN sensor serves as an acoustic transmitter and receiver. The pulser and receiver DPR 500 (JSR Ultrasonics) was used to excite an acoustic sound wave. The ultrasound wave propagates through the silicon substrate, is reflected at the interface silicon-air and travels back to the AlN layer. The aluminum metal electrode with 150 nm thickness has only a very small influence and can be neglected. The mechanical vibration pulse gets transformed to an electrical signal, which can be measured.

The illustration in Fig. 4 shows the schematic setup of the pulse echo measurements. All AlN sensors were connected to the pulse generator and were excited with a needle pulse at high amplitude (-143 V) and very short pulse time (~1.4 ns). The receiver was set to a gain of 36 dB and a high frequency pass filter between 30 MHz and 500 MHz was used.

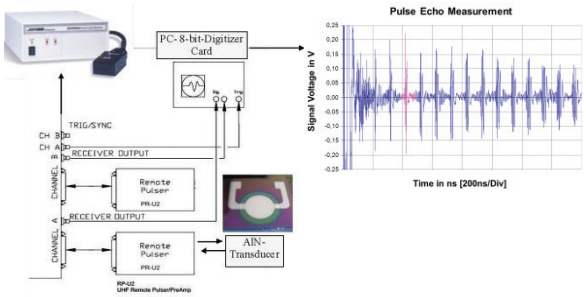

Fig. 4: *Measurement setup with Pulser/Receiver and PC Digitizer Card.*

In the first tests the receiver output was connected to an oscilloscope, but during the evaluation of all AlN sensors the receiver signals where transmitted to a PC Digitizer Card (Aquiris U1071 A, Agilent Technologies). This hardware has an real-time sampling rate up to 2 GS/s and the amplifier response are optimized to ensure that high-frequency measurements can be made with a bandwidth (-3 dB) of maximum 1 GHz. The sending pulse after excitation could be observed, followed by multiple reflections from the silicon back wall. The distance between the multiple echoes equals the time the ultrasound longitudinal wave needs to pass through the silicon and return back. Because of the small damping behavior of silicon, the echo pulse signal is relatively long. The evaluated sensors were deposited on silicon substrates with the same thickness and were excited with the same electrical pulse. Therefore the amplitudes of the received signals could be used to compare the sending-receiving efficiency of the different AlN transmitters indirectly.

In the right handed diagram of Fig. 4, a typical time response with multiple back wall echoes is shown. To avoid an influence of the sending signal, the first back wall echo was not evaluated, but the fourth. In Fig. 5, the fourth back wall echoes are shown for the optimized layers deposited in the unipolar and bipolar pulse mode as well as for a not optimized layer. Strong differences in the transmitting and receiving properties of AlN based sensor could be verified as result from the different sputtering and deposition parameters.

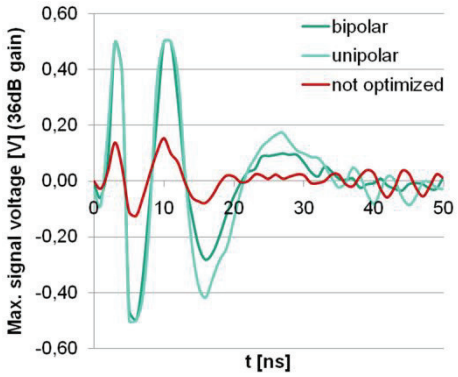

Fig. 5: *Examples of signal amplitudes of one back wall echo depending on the deposition parameter set.*

4.2 Berlincourt-Meter

Additionally the piezoelectric charge constant (d_{33}) was measured with a Berlincourt piezometer PM 300 (PiezoTest). The samples were clamped and loaded with an alternating force. The generated electric charge was compared to the value of a reference sample to obtain the piezoelectric charge constant. The measurements were carried out by applying an alternating force of 0.25 N and a frequency of 110 Hz. Quasi-static measurements of the dissipation factor tan δ and the electric capacity of the AlN sensor layers was performed at a frequency of 1 kHz.

Measured Samples piezoelectric charge constant d_{33} for AlN thin films was between below 1 pC/N and 7.2 pC/N in maximum. The reasons for these differences is the different microstructure and c-axis orientation of the AlN thin films. Fig. **6** shows, that the d_{33} value can be correlated to the maximum signal voltage obtained in the pulse echo measurements. Therefore the Piezometer can be used for a very fast estimation of the thin film quality for AlN sensors with the same substrate material and film thickness.

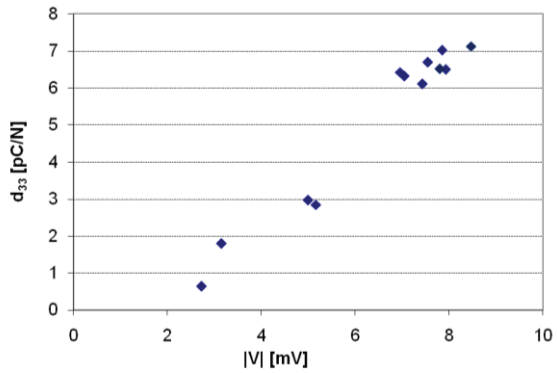

Fig. 6: *Correlation of maximum pulse amplitude and piezoelectric charge constants.*

5. Investigation of suitability for energy harvesting

AlN is a promising piezoelectric material for energy harvesting applications. The investigation of energy harvesting properties were carried out in corporation between Fraunhofer FEP, Dresden University of Technology and University of Oulu. The energy harvester allowed to vibrate the samples (10 µm AlN with electrode structure on Silicone substrate) and measuring generated power as a function of vibration frequency and resistive load.

In Fig. 7, the energy harvesting characteristic of an AlN film is shown. Peak power was 3.1 µW and average power was 1.1 µW for the best sample. The average power density was 0.215 µW/cm^2 and 214.6 µW/cm^3.

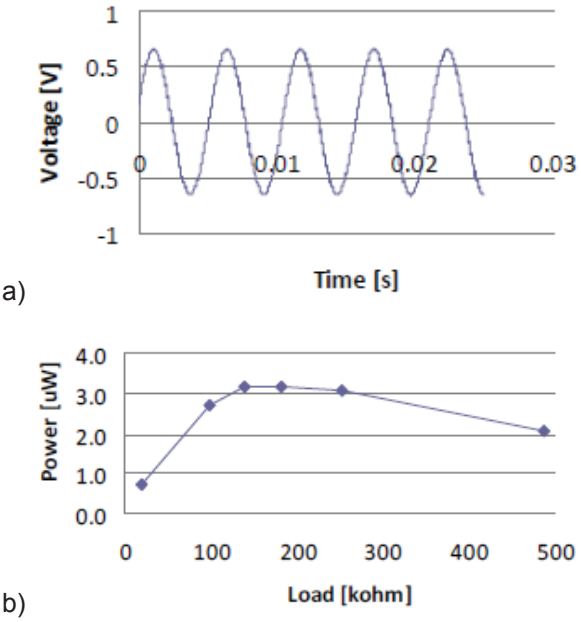

Fig. 7: *Energy harvesting characteristic of an AlN film in resonance (a: voltage curve, b: peak power as function of load).*

6. Conclusions

In this paper, the piezoelectric behavior of ultrasound sensors based on the AlN thin films was investigated. The process parameters like pulse mode during sputtering, power and process pressure strongly influenced the crystalline growth and the orientation of the thin films. As result, sensor samples with excellent c-axis orientation were obtained, that were investigated regarding their structural, electrical and mechanical properties. The electro acoustic measurements and the evaluation of the piezoelectric charge constants have shown good piezoelectric activity. But, the piezoelectric activity is depending strongly on the deposition parameters. For AlN thin films on silicon substrates, d_{33} was about 7.2 pC/N in maximum for films with nearly perfect c-axis orientation and it was below 1.0 pC/N for films with weak c-axis orientation. Also in pulse echo measurements, the AlN sensors with good c-axis orientation showed a much higher echo amplitude.

7. Acknowledgment

This work has been partially supported by a Grant-in-Aid for Technology Funding by the European Regional Development Fund (ERDF) 2007-2013 and the State of Saxony. The authors would like to thank Gunnar Suchaneck (Dresden University of Technology, Germany) and Jari Juuti (University of Oulu, Linnanmaa, Finland) for collaboration and for measurement of energy harvesting properties.

References

[1] P. Frach, Chr. Gottfried, H. Bartzsch, K. Goedicke: Surf. Coat. Technol. 90, 1997, pp. 75-81.

[2] E. Iborra, A. Sanz-Hervás, M. Clement, L. Vergara, J. Olivares, and J. Sangrador: Proc. of the IEEE Ultrasonics Symposium , 2005, p. 1808.

[3] M.-A. Dubois, P. Muralt: Appl. Phys. Lett., Vol. 74, No. 2, 17 May 1999, p.3032.

[4] L. Valbin, L. Sevely: Proc. of SPIE , Vol. 4559, 2001.

[5] P.M. Martin, M.S. Good, J.W. Johnston, G.J. Posakony, L.J. Bond, S.L. Crawford: Thin Solid Films 379, 2000, pp. 253-258.

Evaluation of the polarization state of integrated piezoelectrics using thermal waves

Suchaneck, G.; Hu, W.; Gerlach, G.

Technische Universität Dresden, Solid-State Electronics Lab, Dresden, Germany

Abstract

In this work, we describe the evaluation of the polarization state of PZT plates embedded into LTCC and macrofibers embedded into epoxy resin based on their pyroelectric response after applying a thermal wave. The integrated piezoelectric element was modeled as a piezoelectric plate or a square-rod piezoelectric, respectively, which exhibit thermal losses to the environment characterized by a single relaxation time. Measurements show that the thermal wave method is useful to describe the influence of fabrication effects on the polarization state of integrated piezoelectric elements and modules embedded in mechanical functional structures.

1. Introduction

Many piezoelectric materials exhibit pyroelectric properties which are strongly coupled to the piezoelectric properties. Such cases enable to evaluate their piezoelectric properties by measuring the pyroelectric properties. Integrated piezoelectrics embedded in complex modules represent a complex thermal problem which has to be taken into account for recalculating the piezoelectric polarization profiles. Several approaches were developed to calculate pyroelectric response of multilayer structures based on the solution of the heat-flow equation for appropriate boundary conditions [1-4]. More complex structures such as Macrofiber Composites (MFC) can be modeled only by means of numerical techniques like finite element modeling [5].

In this work, we demonstrate that PZT piezoelectric plates and rods embedded into a LTCC or epoxy resin environment can be described by a simple model of a harmonically heated piezoelectric plate or rod exhibiting heat losses to the environment which can be characterized by a thermal relaxation time.

2. Theory

We consider a thermal wave with a certain modulation frequency caused by laser radiation which hits the surface of a layer stack with the embedded piezoelectric element. By travelling through the top layer of the piezoelectric module packaging, higher harmonics of a square wave disappear and the thermal wave gradually becomes sinusoidal [6]. Therefore, the thermal problem of a harmonically heated piezoelectric plate exhibiting heat losses to the environment is characterized by a thermal relaxation time

$$\tau_{th} = \frac{c\rho \cdot d_f}{2H} \tag{1}$$

where c, ρ and d_f are specific heat, density and thickness of the piezoelectric plate, respectively, and H is the thermal conductance at the interface between plate and piezoelectric element.

The steady-state periodic solution of this problem in form of infinite series is given by [6, 7]:

$$\Theta(z) = \Theta_\infty \left[\frac{\tau_{th}}{1+i\omega\tau_{th}} + 2 \cdot \sum_{n=1}^{\infty} \cos\left(\frac{n\pi \cdot z}{d_f}\right) \frac{\tau_d / n^2}{1+i\omega\tau_d / n^2} \right] \exp(i\omega t) \tag{2}$$

with $\Theta = T\text{-}T_0$, and where T_0 is the temperature of the environment, $\Theta_\infty = \Phi_0/c\rho d_f$ the asymptotic value of $\Theta(t,z)$ at $t \to \infty$, Φ_0 the heat flux absorbed by the plate surface, $\tau_d = d_f^2/\pi^2\alpha$ the heat diffusion time, and α the thermal diffusivity of the plate. The pyroelectric response piezoelectric of the plate yields [7]:

$$I_\sim(\omega) = \frac{\Phi_0 A}{c\rho \cdot d_f} \left(p_0 \frac{i\omega\tau_{th}}{1+i\omega\tau_{th}} + \sum_{n=1}^{\infty} p_n \frac{i\omega\tau / n^2}{1+i\omega\tau / n^2} \right) \exp(i\omega t) \tag{3}$$

where A is the plate area and

$$p_0 = \frac{1}{d} \int_0^{d_f} p(z)dz \quad , \tag{4}$$

$$p_n = \frac{2}{d_f}\int_0^{d_f} p(z)\cos\left(\frac{n\pi z}{d}\right)dz \qquad (5)$$

are the average and spatially dependent parts of the pyroelectric coefficient. Note, that eq. (2) reads in the case of square wave modulation with a period $T = 2\pi/\omega_0$

$$\Theta(z) = \Theta_\infty\left[\frac{\tau_{th}}{1+i\omega\tau_{th}} + 2\cdot\sum_{n=1}^{\infty}\cos\left(\frac{n\pi\cdot z}{d_f}\right)\frac{\tau_d/n^2}{1+i\omega\tau_d/n^2}\right]\times \qquad (6)$$
$$\times\sum_{m=1}^{\infty}\frac{(-1)^{m-1}}{2m-1}\exp(im\omega_0 t)$$

For a harmonically heated piezoelectric plate, the average charge induced due to the pyroelectric effect depends on the mean temperature and is given by:

$$\langle Q\rangle = \langle p\Theta\rangle \approx \frac{p_0}{d_f}\,\mathrm{Re}\int_0^{d_f}\Theta(z)\exp(i\omega t)dz\,. \qquad (7)$$

3. Experimental

For our experiments we used two samples:

- A LTCC/PZT module consisting of a sintered PZT plate (CeramTec Sonox® P53) with a size of 25x10x0.2 mm^3 embedded in the center of a sintered LTCC module (Heraeus HeraLock® Tape-HL2000, size 45 x 20 x 0.7 mm³). Sample fabrication is described in detail in [8]. The sample capacitance was 30 nF, the dielectric loss tangent amounted to about 2% at 10 kHz.
- A commercial Macro-Fiber Composite (MFC) M-8528-P2 piezoelectric actuator (Smart Material Corp., USA) with a sample capacitance of 170 nF.

The samples were periodically heated by an array of six semiconductor lasers (LCU98A041A, LASER COMPONENTS GmbH, Olching, Germany) square-wave-modulated with frequencies of up to 1 kHz each with a power of 14 mW at a wavelength of 980 nm.

Charge-to-voltage conversion was performed by a 5015A charge meter (Kistler Instruments AG, Winterthur, Schweiz). The resulting voltage signal was recorded using a Waverunner® Xi-A oscilloscope (LeCroy Chestnut Ridge, USA) performing 50 sweeps in DC- or AC-mode (periodic part only).

Polarization was determined obtaining thepyroelectric current spectrum. The pyroelectric current was transformed into a voltage by a current-voltage-converter and amplitude and phase were determined by an impedance-phase analyzer (Solartron 1260, Solartron Analytical, Farnborough, UK). The current spectra were corrected by laser power measurements using internal photodiodes of the lasers. In order to reduce noise, up to 100 measurement repetitions were used for averaging.

4. Results and discussion

According to eq. (7), sample heating can be determined by charge monitoring. Figure 1 shows the time dependence of the charge generated due pyroelectric effect at the LTCC/PZT sample´s electrode at a modulation frequency of 30 Hz. The mean sample temperature increases nearly linearly during the heating cycle (laser at high intensity) and decreases in the same manner during cooling (laser at low intensity). This behavior is superimposed with the long-term heating up to the steady state described by the non-periodic solution of the thermal problem.

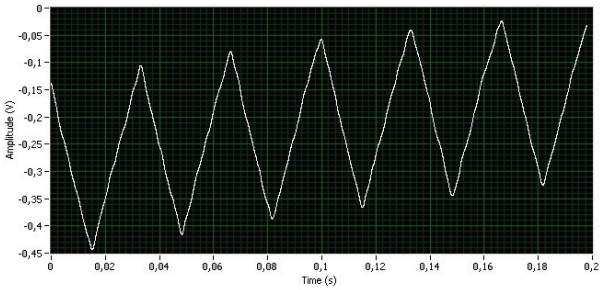

Fig. 1: *Charge meter output voltage at a modulation frequency of 30 Hz (DC-mode, time constant 1s, low-pass filter 1 kHz).*

Nearly constant heating and cooling rates were obtained up to 800 Hz as illustrated by the periodic part of the charge meter output voltage (Figs. 2, 3). A constant heating and cooling rate is the main presupposition of polarization profile determination from the time dependence of the pyroelectric response by using, for instance, the thermal square wave method at single frequency [9].

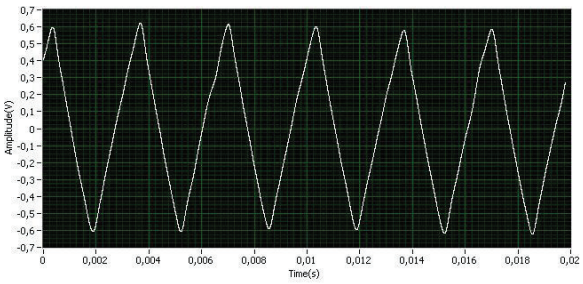

Fig. 2: *Charge meter output voltage at a modulation frequency of 300 Hz (AC-mode, time constant 10 ms, low-pass filter 3 kHz).*

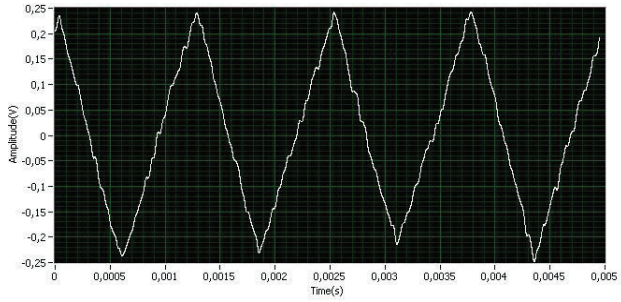

Fig. 3: *Charge meter output at a modulation frequency of 800 Hz (AC-mode, time constant 10 ms, low pass filter 30 kHz).*

Figure 4 illustrates the pyroelectric current amplitude of a piezoelectric LTCC/PZT module in dependence on frequency for 50 measurement repetitions in comparison with a fit to eq. (3). Above 0.6 Hz, the thermal wave is confined within the sample. At frequencies above 10 Hz only the top LTCC layer is heated. The pyroelectric response below 10 Hz is determined by thermal losses induced by heat conduction and radiation to the surroundings. The estimated value of the thermal relaxation time τ_{th} amounts to 0.135 s resulting in a thermal conductance of 3650 W/m^{2}K. Beyond a frequency of 10 Hz, the pyroelectric response is described by a pyroelectric capacitor periodically heated by thermal waves from the LTCC top layer absorbed in the PZT plate top electrode.

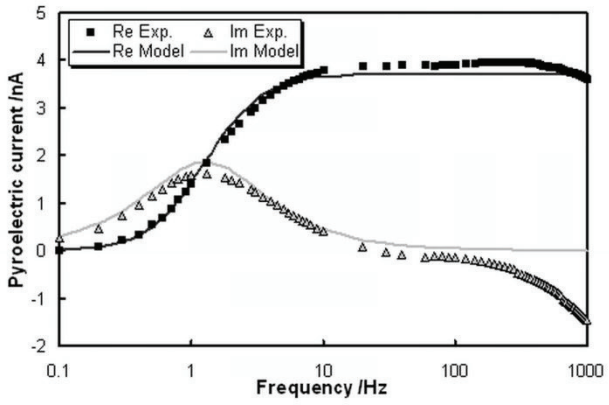

Fig. 4: *Pyroelectric current spectrum of the piezoelectric LTCC/PZT module in comparison with a fit to eq. (3).*

Surprisingly, also the pyroelectric response of the MFC actuator is well described by eq. (3) (Fig. 5). Consequently, expensive finite element models and solutions of this complex thermal problem may be avoided. Here, the thermal relaxation time equals 0.14 s yielding a thermal conductance of 3175 W/m^{2}K.

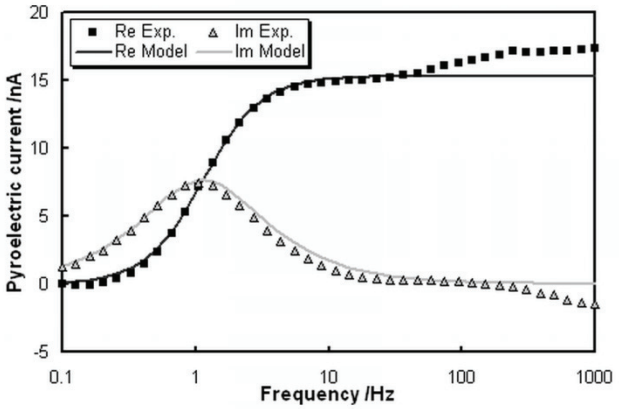

Fig. 5: *Pyroelectric current spectrum of the piezoelectric MFC M-8528-P2 actuator in comparison with a fit to eq. (3).*

5. Conclusions

Thermal waves were demonstrated to be an appropriate tool for the non-destructive evaluation of the polarization state of piezoelectric elements embedded in integrated sensor-actuator modules.

References

[1] *van der Ziel, A.: Pyroelectric response and D* of thin ferroelectric films on substrate. In: J. Appl. Phys., 44 (1973) 2, pp 546-549*

[2] *Peterson, R.L.; Day, G.W.; Gruzensky, P.M.; Phelan, R.J.: Analysis of response of pyroelectric optical detectors. In: J. Appl. Phys., 45 (1974) 8, pp. 3296-3303*

[3] *Mandelis, A.; Zver, M.M.: Theory of photopyroelectric spectroscopy of solids. In: J. Appl. Phys., 57 (1985) 9, pp. 4421-4430*

[4] *Samoilov, V.; Yoon, Y.S.: Frequency response of multilayer pyroelectric sensors. In: IEEE Trans. Ultrason. Ferroelectr. Freq. Contr., 45 (1998) 5, pp 1246-1254*

[5] *Binette,P.; Dano, M.-L.; Gendron,G.: Active shape control of composite structures under thermal loading. In: Smart Mater. Struct. 18 (2009) 2, pp. 025007*

[6] *Carslaw H.S.; Jaeger, H.C.: Conduction of Heat in Solids, 2nd ed. New York, Oxford Univ. Press; 1959.*

[7] *Bauer, S.; Ploss, B.: A method for the measurement of the thermal, dielectric, and pyroelectric properties of thin films and their applications for integrated heat sensors. In: J. Appl. Phys., 68, (1990) 12, pp. 6361-6367*

[8] *Flössel, M.; Gebhardt, S.; Schönecker, A;. Michaelis, A.: Development of a novel sensor-actuator-module with ceramic multilayer technology. In: J. Ceram. Sci. Technol., 1 (2010) 1, pp. 55-58ww*

[9] *Malyshkina, O.V.; Movchikova, A.A.; Suchaneck, G: A new method for determining the coordinate dependences of the pyroelectric current in ferroelectric materials. In: Physics of the Solid State, 49 (2007) 11, pp. 2144-2147*

Novel approaches for the determination of the process specific polarization of piezoceramic modules embedded in thermoplastic composites

Brückner, B. W.[1]; Gerlach, G.[2]; Winkler, A.[3]; Hu, W.[2]; Hufenbach, W. A.[3]; Michaelis, A.[1]; Modler, N.[3]; Schönecker, A. J.[1]; Suchaneck, G.[2]

[1]*Fraunhofer Institute for Ceramic Technologies and Systems IKTS, Dresden, Germany*
[2]*Technische Universität Dresden, Institute of Solid-State Electronics Lab (IFE), Dresden, Germany*
[3]*Technische Universität Dresden, Institute of Lightweight Engineering and Polymer Technologies (ILK), Dresden, Germany*

Abstract

Fiber-reinforced thermoplastic composites with embedded sensors promise the implementation of advanced functionalities. Currently, the technological gap for industrial applications arises from the lack of high-volume manufacturing technologies. The DFG research project CRC/TR 39 is aimed at the development of the required production technologies. One process route focuses on the matrix-homogeneous integration of thermoplastic-compatible piezoceramic modules (TPM) in fiber-reinforced thermoplastic structures. Hence, a crucial question concerns the determination of the piezoceramic polarization during the hot pressing process.

The paper introduces a new approach to determine and monitor the polarization state of piezoceramic elements during thermal load of the production process. The new method is based on the measurement of the free charge that is released from the poled, ferroelectric material due to the temperature increase. This signal is measured with respect to temperature and time.

Alternatively, the polarization state is determined using an advanced thermal wave method. This newly developed method was shown to be well suited to measure packaged piezoceramic modules with a heterogeneous, multilayer design.

First, the paper introduces the methods and the new developed test stands. Furthermore, measurement results characterizing commercial material samples are presented. Secondly, a new algorithm is acquired to apply the measurement methods and the test stands for the evaluation of production processes. As a real-world example the multi-stage procedure is applied to the above mentioned manufacturing process of thermoplastic composite structures with embedded TPMs. Finally, the measurement results characterizing this specific process are shown.

1. Motivation

Fiber-reinforced composites with new **T**hermoplastic-compatible **P**iezoceramic **M**odules (TPM) enable the development of a new generation of active lightweight structures with the application potential in:

- material-integrated structural health monitoring
- energy-harvesting and
- active vibration damping functionalities

Currently, the lack of robust manufacturing technologies is a major obstacle for the intensive use of these new active composites especially in automotive applications. With the new developed continuous process chain, a high volume manufacture of active thermoplastic composites with integrated TPMs becomes possible for the first time. Hence a crucial question concerns the degradation of remanent polarization of the piezoceramics according to the thermal load during the hot pressing process, which is considered in the present paper.

2. State of the Art

In dielectrics, the polarization arises from different physical mechanisms [1], [2]:

- Electronic (displacement of electrons)
- Ionic (displacement of ions)
- Orientation (permanent dipoles)

The first two mechanisms are intrinsic properties of the material itself and are dominated by the

material composition. Their contribution to the macroscopic polarization of piezoceramics is minor. The macroscopic polarization of piezoceramics is dominated by the orientation of permanent dipoles. The dipoles originate from a separation of the positive and negative charge centers in the crystal lattice. Macroscopically the material consists of distributed regions with uniform crystal orientation, so called domains. Due to the random distributed orientation of the domains after the production process piezoceramics show no macroscopic polarization. But because piezoceramics are ferroelectric materials the orientation polarization can be changed by an external electric field. The alignment of the domains is achieved by an additional polarization step. In the polarization step an external electric field is applied to the piezoceramic element and the piezoceramic coupling of the material is activated. After the removal of the field the resulting polarization (P_r) is remanent. The minimum electric field strength needed to reverse the polarization is called the remanent electric field strength E_C. [3]

The symmetry and the lattice parameters of the crystal and therefore the polarization depend on the temperature. Above the Curie temperature (T_C) the lattice becomes cubic and the ferroelectric order disappears. This phase change is accompanied by the release of the previously bounded charge [1]. A usual method to determine T_C is the measurement of the temperature characteristic (or temperature coefficient) of the small signal capacity (TkC). At T_C the C(T)-curve shows a global maximum.

A wide spread method to determine the total switchable polarization of piezoceramics is to apply an alternating electric field with a field strength above E_C and to simultaneously measure the occurring charge flow. This method is often implemented by the Sawyer-Tower-Circuit [4], [5]. This method changes the polarization state of the specimen and can therefore not be used for a monitoring or in-situ determination of polarization states.

The pyroelectric coefficient at constant stress is the sum of the pyroelectric coefficient at constant strain (primary effect) and the piezoelectric effect due to thermal strain (secondary effect) [6]. This provides the capability of poling procedure control by means of thermal wave methods. In the case of PZT, the primary effect of PZT is opposite in sign compared to the much smaller secondary one [7]. In relaxor ferroelectrics, like PMN-PT, the piezoelectric effect due to thermal strain provides a significant contribution to pyroelectric response [8]. Recently, the thermal square wave method at constant frequency was proposed for the characterization of ferroelectric ceramics [9]. The thermal square wave method determines the pyroelectric coefficient depth profile (the polarization distribution) of ferroelectrics from the time dependence of the pyroelectric current at a certain heat pulse modulation frequency. It assumes a constant heating rate during pulse time and a constant wave velocity and consists of constraints related to the penetration depth of the thermal wave.

Especially looking at thermally stimulated processes the so called **t**hermo-**s**timulated **c**urrent spectroscopy (TSC) is often used to examine material characteristics during temperature change. As the name implies the method is based on the measurement of the electrical current corresponding to processes in the specimen during a temperature change. The interpretation of the obtained curves with respect to time and temperature depends on the evaluated material, the (micro)structure, the morphology and the absolute temperature (range). TSC has been used for many different kinds of insulating materials. [10] In [11] for instance TSC was used to characterize phase transitions and to determine the remanent polarization of a doped PZT material.

3. Measurement Setup

The new developed measurement setup and the measurement signal flow is shown in Figure 1. The specimen is placed on a planar ceramic heater. The resistive heater (Bach Resistor Ceramics GmbH) is made of silicon nitride. The heating area of the present implementation and therefore the largest specimen size that can be measured is 14 x 14 mm^2. The maximum heating rate is 150K/min up to a temperature of 500°C. The temperature profile is programmed by a PC via a remote controlled power supply (EA-PS 3065-05) powering the heater.

As shown in Figure 1 the specimen is electrically contacted from the top by two isolated electrodes. For the current measurement an electrometer (Keithley 6514) is used. The data recording is realized by an AD-converter connected to the analogous output of the electrometer. The AD-converter is USB-connected to the PC. To simultaneously record the heater temperature the therefore used Type-K temperature sensor is connected to a special

input connector of the AD-converter. The control of the measurement procedure and data acquisition is done by a PC.

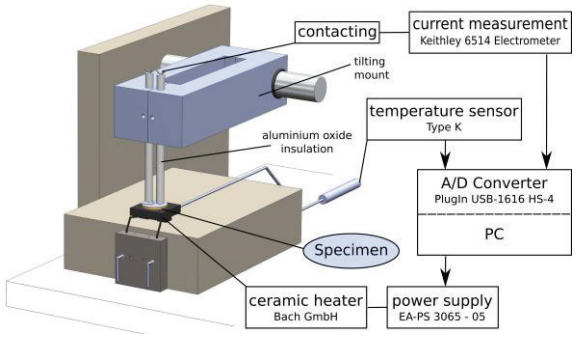

Fig. 1: *Measurement setup and signal flow diagram*

The aim of the measurement is to determine the amount of charge that is released by the specimen in dependence of the temperature profile that is applied. Therefore the following measurement procedure was set up.

The temperature profile is applied to the specimen. The current due to the heating is measured with respect to temperature and time. Simultaneously the temperature is recorded. The measured data are used to calculate the released charge over temperature. By measuring the entire thermal cycle the amount of the charge is related to the polarization of the specimen and the resulting polarization state is determined.

4. Measurement System Analysis

This section presents test measurements on commercially available disc specimens. The aim of the measurements is to show that the measurement system works properly and to determine the accuracy and stability of the derived charge curves. For the tests two kinds of specimens were used and are listed in table 1.

Table 1: *List of specimen for the measurement system analysis*

Material	***disc geometry***	***Number of samplest***
PIC151 (PI Ceramic)	*diameter: 10 mm thickness: 1 mm*	*2*
PIC255 (PI Ceramic)	*diameter: 10 mm thickness: 1mm*	*3*

Each specimen was measured five times. The measurement cycle started with a poled specimen. Than the temperature profile was applied. After the measurement the sample was repoled by applying 2 kV/mm for about 10 minutes at room temperature. After a pause of at least 18 hours the next measurement started.

The temperature profile for these measurements is a simple ramp signal starting at room temperature rising up to about 400°C which is well above the Curie temperature (T_C) of the used materials. The temperature - time curve of the specimen is shown in figure 2 (red line).

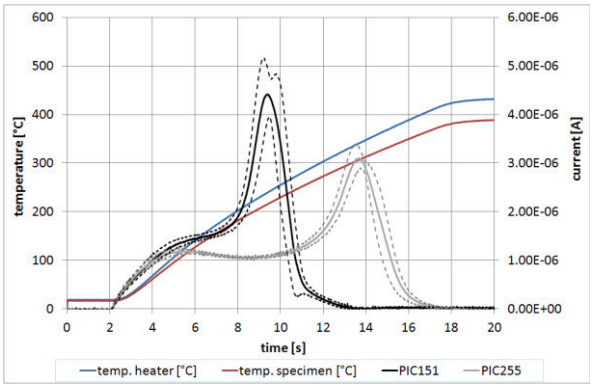

Fig. 2: *Measurement results for the two materials, solid line depicts the mean value, dashed lines show the variance*

Figure 2 also shows the measured current over time. As the temperature rises the current is increasing as well. Once the temperature approaches T_C there is a large increase of the current which climaxes around T_C. Above T_C the current decreases fast toward zero. Using these curves the charge over temperature released from the specimen was calculated as shown in figure 3.

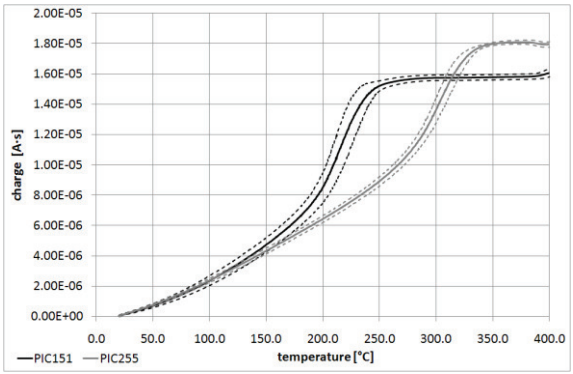

Fig. 3: *Charge-temperature curve, solid line depicts the mean value, dashed lines show the variance*

The comparison of the measured T_C values (temperature of phase change) with the values from the data sheet show very good accordance. Furthermore the measurement results reveal that the PIC 255 material has first local maximum of the thermally induced current around 120°C. This indicates passing through the phase coexistence region (rhombohedral - tetragonal) which needs to be proved by further investigations. The results show clearly that the measurement system works properly, delivers stable results

and can be used to measure the charge transfer during temperature changes. The results show clearly that the measurement system works properly, delivers stable results and can be used to measure the charge transfer during temperature changes.

5. Measurement - Hot Pressing Process

As stated above, the aim of the presented work is to characterize the polarization state of Thermoplastic-compatible Piezoceramic Modules during the embedding process in fiber-reinforced composites. A TPM consists in principle of a piezoceramic layer embedded between two thermoplastic layers with integrated electrode structures. Further information on the production process, the design, and the characteristics of TPMs (Figure 4) are given in [12] and [13].

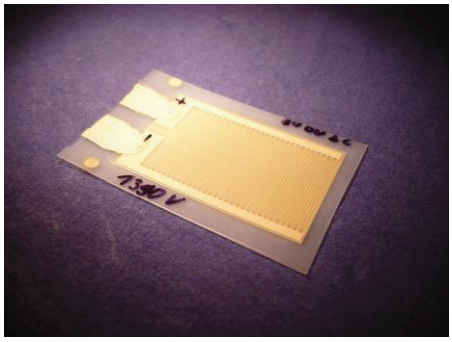

Fig. 4: *Thermoplastic-compatible piezoceramic module (TPM)*

The new production technology to embed the TPMs in fiber-reinforced thermoplastic structures bases on a hot pressing process. Therefore, the TPM and the conductors are assembled and fixed on a thermoplastic film. For the hot pressing process this film is positioned in the pressing die and preheated up to 140°C. At the same time a structural fiber-reinforced thermoplastic part is melted in a preheating station, transferred to the pressing die, and the part is consolidated. A detailed description of the new developed process chain is given in [14].

The hot pressing step is crucial with respect to the polarization of the piezoceramics embedded in the TPM. Figure 5 shows a typical temperature profile of the hot pressing process used in present studies. The depicted temperature was measured during the consolidation in the pressing tool.

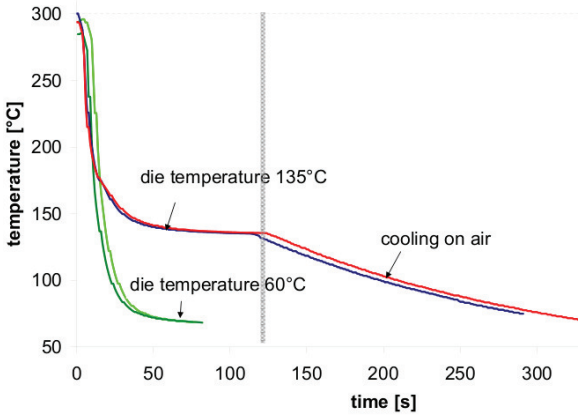

Fig. 5: *Temperature profile of the hot pressing process step. The gray line marks the opening of the pressing tool.*

To simulate the influence of the temperature change on the TPM the new developed test stand is used and an equal temperature profile is applied. In pilot tests was shown that the thin polymer packaging foil does not have a significant influence on the temperature change of the embedded piezoceramic. Therefore only the piezoceramic foil without packaging was placed on the heater. For the measurements shown in figure 6 specimens with a size of 7 by 10 mm^2 and a thickness of 200 µm were used.

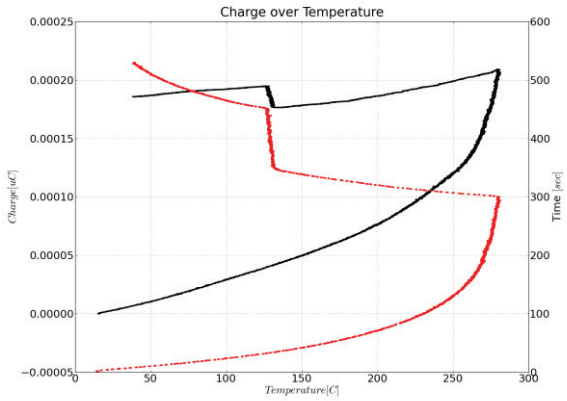

Fig. 6: *Used temperature profile to simulate the hot pressing process (red), derived charge-temperature curve (black)*

Figure 6 shows exemplarily the measurement result for one temperature profile (red line). The temperature rises within the first 300 seconds from room temperature to 280°C. Than the piezoceramic is cooled down to 130°C within 50 seconds and held at that temperature for 100 seconds. Subsequently the specimen is further cooled down to almost room temperature in 80 seconds. The charge released from the piezoceramic foil over temperature is displayed by the black line. The remanently released amount of charge is given by the charge value at the end of the temperature loop.

Following this approach it is possible to compare different temperature profiles with respect to the change in polarization of the piezoceramic material.

6. Thermal Wave Methods

Another innovative approach to evaluate the polarization state of PZT plates embedded into polymers is to measure the pyroelectric response after applying a thermal wave. This is possible because in many piezoelectric materials the pyroelectric properties are strongly coupled to the piezoelectric ones.

Considering a thermal wave generated by a square wave modulated laser beam with a given modulation frequency hitting the surface of a TPM, the thermal wave becomes sinusoidal due to filtering effects when the TPM thickness exceeds the wave penetration depth at fundamental frequency. Therefore the integrated piezoceramic can be modeled as a piezoelectric plate which is harmonically heated and exhibits thermal losses to the environment characterized by a thermal relaxation time. The derivation of the corresponding equation to calculate the periodically induced charge due to the pyroelectric coefficient is presented in [15]. So far this method was successfully used to characterize the polarization of LTCC/PZT modules (Fraunhofer IKTS) and of commercial Macro-Fiber Composites (MFC, Smart Material Corp.). We expect the usability of thermal wave methods also for the characterization of TPMs. Further details on this topic are given in the present proceeding by [16].

7. Conclusion

Concerning a highly productive manufacture of active thermoplastic components short cycle times have to be realized. Therefore, the temperature profile of the hot pressing process to embed TPMs has to be optimized. The new measurement method offers a useful tool to assist the optimization with respect to the polarization state of the piezoceramic modules under the influence of hot pressing. Further work focuses on the use of the test system for not only modules but for the analysis of structural components with embedded piezoceramic modules. In addition the results will be compared to direct polarization measurements (ferroelectric hysteresis measurement) [17] to gain a closer understanding of the physical effects occurring during temperature changes.

8. Acknowledgement

The financial support of the Deutsche Forschungsgemeinschaft (DFG) in the program CRC / Transregio 39 ("PT-PIESA") is gratefully acknowledged.

Literature

[1] Kittel, C.: Introduction to Solid State Physics. Wile, 8th Edition, 2005.

[2] Heilig, C.: Transiente Vorgänge in piezo-elektrischen Keramiken für Aktoranwen-dungen, Fortschritt-Bericht VDI, Reihe 5, Nr. 618

[3] Jaffe et al.: "Piezoelectric Ceramics ", 1971

[4] Sawyer, C. B.; Tower, C. H.; Rochelle Salt as a Dielectric. Phys. Rev. 35 (1930) 3, pp. 269-273.

[5] Singh, K.: PC Based Ferroelectric Analyzer Using Modified Sawyer and Tower Circuit. Ferroelectrics 189 (1996), p. 9.

[6] Nye, J.F.: Physical properties of crystals: their representation by tensors and matrices, Oxford: Clarendon Press, 1960

[7] Cook, W.R.: Berlincourt, D.A.; Scholz, F.J.; Thermal expansion and pyroelectricity in lead titanate zirconate and barium titanate. In: J. Appl. Phys., 34, (1963) 5, pp. 1392-1398

[8] Movchikova, A.; Suchaneck, G.; Malyshkina, O.V.; Pedko, B.B.; Gerlach, G.: Thermal wave study of piezoelectric coefficient distribution in PMN-PT single crystals. In: Adv. Appl. Ceram., 109, (2010) 3, pp. 131-134

[9] Malyshkina, O.V.; Movchikova, A.A.; Suchaneck, G.: A new method for determining the coordinate dependences of the pyroelectric current in ferroelectric materials. In: Physics of the Solid State, 49 (2007) 11, pp. 2144-2147

[10] Lavergne, C; Lacabanne,C.: A Review of Thermo-Stimulated Current, IEEE Electrical Insulation Magazine, March/April 1993-Vol.9, No.2, pp. 9-21

[11] Jankowska-Sumara, I.; Osak, A.: Physica B 404 (2009), pp. 3698-3702

[12] Hufenbach, W.; Gude, M.; Heber, T.: Embedding versus adhesive bonding of adapted piezoceramic modules for function-integrative thermoplastic composite structures. In: Composites Science and Technology 71 (2011), pp. 1132-1137

[13] Hufenbach, W.; Gude, M.; Heber, T.: Development of novel piezoceramic modules for adaptive thermoplastic composite structures capable for series production. In: Sensors and Actuators A 156 (2009), pp. 22-27

[14] Hufenbach, W.; Modler, N.; Gude, M.; Heber, T.; Winkler, A.; Friedrich, J.: Processing studies for the development of a robust manufacture process for active composite structures with matrix adapted piezoceramic modules. Composites 9:2 (2009) pp. 133-137

[15] Suchaneck, G.; Hu, W.; Gerlach, G.: Evaluation of polarization of embedded piezoelectrics by the thermal wave method. In: Applications of Ferroelectrics (ISAF/PFM), 2011 International Symposium on and 2011 International Symposium on Piezoresponse Force Microscopy and Nanoscale Phenomena in Polar Materials, 24-27 July 2011, pp.1-4. DOI: 10.1109/ISAF.2011.6014120

[16] Suchanek, G.: Thermal wave evaluation of the polarization state of embedded piezocermics, CRC / Transregio 39 - 3rd Scientific Symposium, 12.-13. Oct. 2011, Chemnitz

[17] Nicolai, M. et al.: 2008, Advances in Science and Technology, 56, 105